Universidade Federal de Minas Gerais
Instituto de Geociências
Programa de Pós-Graduação em Geologia

DISSERTAÇÃO DE MESTRADO

PETROGRAFIA, GEOQUÍMICA, GEOLOGIA ISOTÓPICA E GEOCRONOLOGIA DOS DIQUES MÁFICOS DO SUL DO ESTADO DO ESPÍRITO SANTO, ORÓGENO ARAÇUAÍ.

Autora: Raíssa Santiago Mendes

Orientação: Prof. Dr. Fabrício de Andrade Caxito
Coorientação: Profª. Drª. Mirna Aparecida Neves

Nº: 177

BELO HORIZONTE
DATA (19/10/2017)

Universidade Federal de Minas Gerais
Instituto de Geociências
Programa de Pós-Graduação em Geologia

DISSERTAÇÃO DE MESTRADO

PETROGRAFIA, GEOQUÍMICA, GEOLOGIA ISOTÓPICA E GEOCRONOLOGIA DOS DIQUES MÁFICOS DO SUL DO ESTADO DO ESPÍRITO SANTO, ORÓGENO ARAÇUAÍ.

AUTORA: Raíssa Santiago Mendes

Dissertação apresentada ao programa de Pós- Graduação em Geologia do Instituto de Geociências da Universidade Federal de Minas Gerais como requisito para a obtenção do título de Mestre em Geologia.

Área de Concentração: Geologia Regional.
Orientação: Prof. Dr. Fabrício de Andrade Caxito.
Coorientação: Profª. Drª. Mirna Aparecida Neves.

Belo Horizonte - MG
2017

M538p Mendes, Raíssa Santiago.

2017 Petrografia, geoquímica, geologia isotópica e geocronologia dos diques máficos do sul do estado do Espírito Santo, orógeno Araçuaí [manuscrito] / Raíssa Santiago Mendes – 2017.

82 f., enc. (principalmente color.)

Orientador: Fabrício de Andrade Caxito.

Coorientadora: Mirna Aparecida Neves.

Dissertação (mestrado) – Universidade Federal de Minas Gerais, Instituto de Geociências, 2017.

Área de concentração: Geologia Regional.

Bibliografia: f. 65-73.

Inclui anexos.

1. Geoquímica – Teses. 2. Tempo geológico – Teses. 3. Petrologia – Teses. 4. Espírito Santo (Estado) – Teses. I. Caxito, Fabrício de Andrade. II. Neves, Mirna Aparecida. III. Universidade Federal de Minas Gerais. Instituto de Geociências. IV. Título.

CDU: 550.4 (815.2)

Ficha catalográfica elaborada por Graciane A. de Paula – CRB6 3404

UNIVERSIDADE FEDERAL DE MINAS GERAIS

PROGRAMA DE PÓS-GRADUAÇÃO EM GEOLOGIA

FOLHA DE APROVAÇÃO

Petrografia, geoquímica, geologia isotópica e geocronologia dos diques máficos do sul do estado do Espírito Santo, Orógeno Araçuaí.

RAISSA SANTIAGO MENDES

Dissertação submetida à Banca Examinadora designada pelo Colegiado do Programa de Pós-Graduação em GEOLOGIA, como requisito para obtenção do grau de Mestre em GEOLOGIA, área de concentração GEOLOGIA REGIONAL.

Aprovada em 19 de outubro de 2017, pela banca constituída pelos membros:

Prof. Fabricio de Andrade Caxito - Orientador
UFMG

Prof. Antonio Carlos Pedrosa Soares
UFMG

Profa. Glaucia Nascimento Queiroga
UFOP

Belo Horizonte, 19 de outubro de 2017.

AGRADECIMENTOS

Agradeço à Universidade Federal de Minas Gerais - UFMG e o ao Instituto de Geociências - ICG pela oportunidade de ampliar meus estudos. E aos professores do Programa de Pós-Graduação em Geologia.

Ao orientador, professor Dr. Fabrício Caxito, pelo apoio e confiança. Sua dedicação, paciência e incentivos constantes, além dos conhecimentos transmitidos, foram essenciais para a realização desta pesquisa. E por me apresentar, sempre com entusiasmo, novos caminhos desta encantadora ciência.

À coorientadora, professora Drª. Mirna Neves, pela atenção e companheirismo. Pelas nossas longas conversas acompanhadas de sugestões e ideias para a pesquisa. E pelos momentos de descontração e amizade; alegria dar continuidade ao projeto.

Ao professor Dr. Edgar Medeiros Júnior, pelo apoio e incentivo com novas discussões dos resultados. Aos professores Drs. Elton Dantas e Gláucia Queiroga pelo suporte e significativa contribuição para o trabalho.

Ao Programa de Capacitação de Recursos Humanos da Petrobras (PFRH) da Petróleo Brasileiro S.A. - PETROBRAS pela disponibilização da bolsa de mestrado. Ao Laboratório de Geocronologia da Universidade de Brasília (UnB) pela análise isotópica; e ao Laboratório de Microanálise da Universidade Federal de Ouro Preto (UFOP) que integra a Rede RMIc, Microscopia e Microanálises de Minas Gerais - FAPEMIG pela análise de química mineral.

Aos amigos Gabriella Andrade, Guilherme Potratz, Salomão Calegari e Victor Mateus Fernandes, por mais uma vez estarem presente com suas valiosas discussões geológicas e sobre a vida. Pelo apoio, incentivo e amizade.

Aos familiares de Ouro Preto que me acolheram nestes últimos anos proporcionando muitos momentos de carinho e felicidade. E àqueles que me hospedaram ao longo deste estudo: Tia Izabel Santiago, Tio Júlio e Tia Mônica Peixoto, Júlia França, Ana Clara Legora, República Arapongas e Carolina Hupp.

À minha família, em especial aos principais responsáveis para a concretização deste trabalho, meu pais, José e Fátima. Por tudo que me ensinam e proporcionam, sempre apoiando minhas decisões e me motivando a continuar. Por todo amor, carinho, dedicação e pela maneira que veem o próximo e a vida. Meus exemplos de caráter e determinação! E ao meu melhor parceiro de campo, José Mendes!

“As novas opiniões são sempre suspeitas e geralmente opostas, por nenhum outro motivo além do fato de ainda não serem comuns”

John Locke

“Lutam melhor os que têm belos sonhos”

Che Guevara

SUMÁRIO

LISTA DE FIGURAS

CAPÍTULO I

CAPÍTULO II

CAPÍTULO III

LISTA DE TABELAS

CAPÍTULO III

CAPÍTULO IV

RESUMO

Na costa do sudeste do Brasil, enxames de diques máficos intrudiram o embasamento pré-cambriano, colocados em importantes estruturas regionais de tendências NW-SE, como os lineamentos de Alegre e Piúma. Durante muito tempo, a maioria desses diques foi relacionada com a ruptura do Gondwana Ocidental e com os derrames basálticos da província ígnea Paraná-Etendeka. Recentemente, no entanto, datações U-Pb sugeriram que pelo menos alguns desses diques teriam sido colocados em ca. de 500-490 Ma, durante o colapso gravitacional do Orógeno Araçuaí. Para esclarecer esta questão, apresenta-se aqui o primeiro estudo sistemático de diques máficos no sul do estado do Espírito Santo. Os resultados indicam que os diques colocados nos mesmos lineamentos estruturais podem, de fato, ser separados em dois grupos, de acordo com distintas características petrográficas, geoquímicas, isotópicas e geocronológicas. Os diques do Grupo 1 são toleíticos, mostram REE moderadamente fraccionado, $^{87}Sr/^{86}Sr_{(i)}$ de 0,7041 - 0,7065, $\varepsilon Nd_{(t)}$ de -3,4 a -5,5 e TDM entre 0,8 e 1,5 Ga. As fontes do manto são, provavelmente, representadas por SCLM (manto litosférico subcontinental) enriquecido no campo de estabilidade do espinélio (<40 km). Os diques do grupo 2 são alcalinos, mostram REE altamente fracionado, maior $^{87}Sr/^{86}Sr_{(i)}$ de 0,7064 - 0,7088, $\varepsilon Nd_{(t)}$ mais negativo $\varepsilon Nd_{(t)}$ <-12 e TDM mais antigo em torno de 1,7-1,9 Ga. As fontes do manto eram profundas (> 40 km), no campo de estabilidade da granada, e foram diferenciados por cristalização fracionada com assimilação crustal muito importante. Os zircões mais novos recuperados dos diques do Grupo 1 apresentaram uma idade Concordia de 141,9 ± 1,9 Ma, vinculando esse grupo com a evolução das bacias Fanerozóicas da costa brasileira. Por outro lado, os zircões mais jovens dos diques do Grupo 2 forneceram uma idade Concordia de 504,7 ± 6,9 Ma, indicando que esses diques são contemporâneos com os complexos intrusivos da Supersuite G5. Este grupo provavelmente está relacionado com a delaminação da crosta e *slab break-off* após a fase de colapso gravitacional do Orógeno Araçuaí. Os resultados sugerem que os lineamentos estruturais foram ativos em pelo menos três episódios distintos: primeiro, no Cambriano, durante o colapso do Orógeno Araçuaí, quando serviram de condutos tanto para os plutons da Supersuite G5 quanto para os diques alcalinos do Grupo 2; segundo, durante o rifte do Gondwana no Jurássico Superior-Cretáceo Inferior, quando serviram como condutos para os diques toleíticos do Grupo 1; e terceiro, durante o Cenozóico, quando foram reativados como falhas normais. Este estudo demonstra a importância da análise geoquímica, isotópica e geocronológica para a compreensão da evolução e do contexto

geodinâmico dos enxames de diques máficos, especialmente em áreas com episódios de magmatismo máfico desenvolvidos em diferentes contextos tectônicos, provenientes de fontes distintas e diferenciados através de processos distintos no tempo e espaço.

Palavras-chave: Enxame de dique; geoquímica isotópica; magmatismo alcalino e toleítico; reativação de estruturas.

ABSTRACT

In the Southeastern Brazilian Coast, mafic dyke swarms crosscut the Precambrian basement, emplaced in important regional NW-SE trending structures such as the Alegre and Piúma lineaments. For a long time, the majority of those dykes were related to West Gondwana break-up and basalt flows of the Paraná-Etendeka igneous province. Recently, however, U-Pb dating suggested that at least some of those dykes were emplaced around 500-490 Ma ago, during the collapse of the Araçuaí Orogen. In order to clarify this issue, we present the first systematic study of mafic dykes in the Southern Espírito Santo State. Our results indicate that dykes emplaced in the same structural lineaments can, in effect, be separated in two groups, according to distinct petrographic, geochemical, isotopic and geochronological characteristics. Group 1 dykes are tholeiitic, show moderately fractionated REE, $^{87}Sr/^{86}Sr_{(i)}$ of 0.7041 – 0.7065, $\varepsilon Nd_{(t)}$ of -3.4 to -5.5 and T_{DM} between 0.8 and 1.5 Ga. Their mantle sources were shallow (<40 km in depth), probably represented by enriched SCLM (subcontinental lithospheric mantle) in the spinel stability field. Group 2 dykes are alkaline, show highly fractionated REE, higher $^{87}Sr/^{86}Sr_{(i)}$ of 0.7064 – 0.7088, more negative $\varepsilon Nd_{(t)} < -12$ and older T_{DM} around 1.7-1.9 Ga. The mantle sources were deep (>40 km), in the garnet stability field, and they were differentiated through fractional crystallization with very important crustal assimilation. The youngest zircons recovered from the Group 1 dykes yielded a Concordia age of 141.9 ± 1.9 Ma, linking this group with syn-rift evolution of the Phanerozoic Brazilian Coast Basins. On the other hand, the youngest zircons from the Group 2 dykes yielded a Concordia age of 504.7 ± 6.9 Ma, thus indicating that those alkaline dykes are coeval with the intrusive complexes of the G5 Supersuite. This Group is probably related to crustal delamination and slab break-off following the gravitational collapse phase of the Araçuaí Orogen. Our results suggest that the structural lineaments were active in at least three distinct episodes: first, in the Cambrian, during the Araçuaí Orogen collapse, when they served as conduits for both the G5 Supersuite plutons and alkaline dykes of Group 2; second, during the Upper Jurassic – Lower Cretaceous rifting of Gondwana, when they served as conduits for the tholeiitic dykes from Group 1; and third, during the Cenozoic, when they were reactivated as normal faults. This study demonstrates the power of geochemical, isotope and geochronological analysis for understanding the evolution and geodynamic context of mafic dyke swarms, especially in areas with overlapping mafic magmatism episodes developed in distinct tectonic settings, coming from distinct sources and differentiated through distinct processes in time and space.

CAPÍTULO I: INTRODUÇÃO

1.1 ESTRUTURA DA DISSERTAÇÃO

Esta dissertação de mestrado é apresentada em formato de artigo científico, composta por quatro capítulos e referências bibliográficas. O capítulo I apresenta o tema principal da dissertação, os objetivos, localização da área de estudo e materiais e métodos. O capítulo II compõe-se de um breve contexto geológico da região estudada e uma compilação dos estudos sobre o magmatismo máfico presente na Costa Sul e Sudeste do Brasil. O capítulo III consiste no artigo intitulado "*Two generations of mafic dyke swarms in the Southeastern Brazilian Coast: implications for the gravitational collapse phase of the Araçuaí-Ribeira Orogen (500 Ma) and for West Gondwana breakup (140 Ma)*". Este artigo apresenta os principais resultados e discussões obtidos na pesquisa e foi submetido ao periódico internacional Lithos. O capítulo IV sumariza as conclusões do estudo e sugestões para trabalhos futuros.

1.2 APRESENTAÇÃO

Este trabalho busca ampliar o conhecimento existente sobre os processos geológicos que atuaram no sul do Estado do Espírito Santo. Expõe um estudo minucioso sobre os diques máficos da região, dando ênfase em dados de petrografia, química mineral, litoquímica, geologia isotópica e geocronologia, que auxiliam no entendimento da filiação magmática dos diques e implicações na evolução geológica da área.

Diques máficos ocorrem em uma ampla variedade de configurações geológicas e tectônicas e seu estudo detalhado através do espaço e tempo é imprescindível para a compreensão de diversos eventos geológicos. Frequentemente, marcam eventos de extensão crustal e são indicadores importantes de eventos de estabilização da crosta terrestre, reconstrução e dispersão de supercontinentes e interação crosta-manto. Além disto, desempenham um papel significativo no processo de delimitação das províncias basálticas da crosta terrestre e fornecem chaves para decifrar eventos de evolução crustal (Srivastava., 2011).

Os diques tendem a ser paralelos ou a se encaixarem em estruturas rúpteis como falhas e juntas, que se manifestam regionalmente na área continental como grandes lineamentos geomorfológicos. Tais lineamentos são importantes na estruturação geológica regional, controlando o arcabouço do embasamento pré-cambriano e a formação das

bacias sedimentares costeiras, podendo atuar como marcadores na datação relativa de estruturas geológicas.

No Brasil, um dos eventos marcados por intenso magmatismo máfico é o tectonismo mesozóico relacionado ao processo de reativação da Plataforma Sul-Americana, responsável pela fragmentação do Supercontinente Gondwana. Este magmatismo é representado por derrames basálticos da Formação Serra Geral na Bacia do Paraná e por enxames de diques básicos, no Sudeste do Brasil (Renne et al.,1996).

Atualmente, no estado do Espírito Santo, a questão da idade, controle estrutural e fonte dos magmas básicos relacionados aos diques é um ponto em discussão, uma vez que dados geocronológicos obtidos por métodos distintos revelaram idades diferentes para diques máficos encaixados no lineamento Colatina, no norte do estado, e consequentemente, foram relacionados a distintos eventos geológicos. Os dados geocronológicos Ar-Ar apontaram idade de 128±1,4 Ma (Teixeira & Rodarte 2003), indicando que estes diques são resultado de atividade magmática do Cretáceo, possivelmente associada à fragmentação do Gondwana. Por outro lado, os dados geocronológicos U-Pb (Belém., 2014) mostraram idades cambrianas, de aproximadamente 500 Ma, sugerindo que parte destes diques pode estar relacionada à fase de colapso do Orógeno Araçuaí.

Assim, o estudo dos diques máficos no sul do estado do Espírito Santo expõe resultados que auxiliam no entendimento dos processos geológicos que atuaram na região. A pesquisa relata a existência de pelo menos duas famílias de diques muito distintas colocadas ao longo dos lineamentos estruturais Alegre e Piúma, evidenciando aspectos relevantes de áreas com episódios de magmatismo máfico desenvolvidos em diferentes contextos tectônicos, provenientes de fontes distintas e diferenciados através de processos no tempo e espaço.

1.3 OBJETIVO

O trabalho tem como objetivo principal estudar os diques máficos da região, com o intuído de proporcionar informações para o melhor entendimento da evolução geológica regional, a partir do estudo petrográfico, químico mineral, geoquímico, isotópico e geocronológico dos diques máficos encontrados no Sul do Estado do Espírito Santo, Região Sudeste do Brasil. Para isso, foi necessária a organização e análise qualitativa e quantitativa dos dados, enfocando a caracterização petrogenética e a comparação com outras unidades máficas regionais. Tais informações, em conjunto, contribuíram para a

elaboração do modelo evolutivo, considerando o desenvolvimento dos principais lineamentos estruturais regionais.

1.4 LOCALIZAÇÃO E VIAS DE ACESSOS

Localizada na porção Sudoeste do Estado do Espírito Santo até a divisa com o Estado de Minas Gerais, a região estudada está a uma distância de aproximadamente 200 km de Vitória, capital do estado capixaba. A área de estudo abrange os municípios de Castelo, Muqui, Jerônimo Monteiro, Iúna (ES) e Lajinha (MG) e os distritos de Itaoca Pedra, Santa Angélica e Itaici pertencentes aos municípios de Cachoeiro de Itapemirim, Alegre e Muniz Freire, respectivamente. Em relação à Vitória, o acesso se dá pela BR-101 sul e ES-482. Já o acesso à área, partindo da cidade de Alegre (ES), é possível pela rodovia ES-482 rumo às localidades de ocorrência dos diques. Também podem ser utilizadas rodovias adjacentes a estas, como para Castelo, onde se chega pela rodovia ES-166 e para Muqui, pela rodovia ES-177. Para as cidades Iúna e Lajinha, utiliza-se a ES-185 (Figura 1-1).

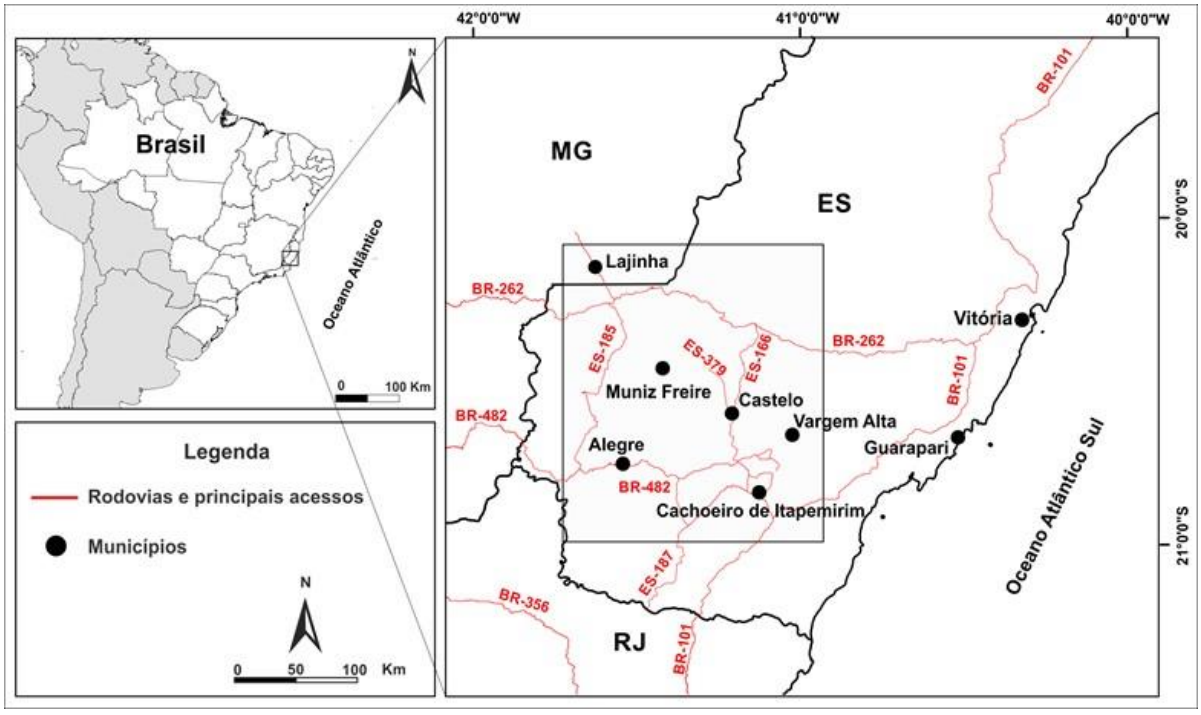

Figura 1-1: Mapa de localização e acesso a área de estudo pelas principais vias.

1.5 MATERIAIS E MÉTODOS

1.5.1 Coleta e preparação de amostras

Treze diques máficos foram identificados e estudados (Figura 1-3); eles são nomeados de acordo com as localidades onde afloram. As amostras de cada dique foram coletadas nas bordas e porção central dos diques com o intuito de observar variações de textura e composição (Figura 1-2). A partir destas amostras, 29 lâminas foram confeccionadas para auxiliar na descrição mineralógica, textural e estrutural das rochas (Tabela 1-1). Apenas amostras de rocha sã, sem sinais de intemperismo e heterogeneidades como veios, foram selecionadas para análises litoquímicas e isotópicas.

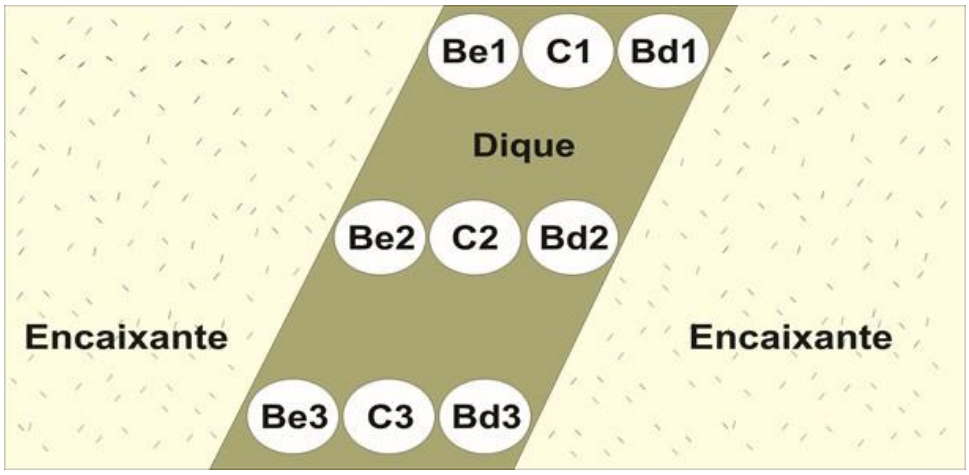

Figura 1-2: Metodologia de amostragem utilizada. Sempre que possível foram coletadas amostras das bordas e do centro de cada dique. Be – Borda esquerda (repetição 1, 2 e 3); Bd – Borda direita (repetição 1, 2 e 3); C – Centro (repetição 1, 2 e 3).

1.5.2 Química mineral

As análises de química mineral foram realizadas em amostras dos diques Cobiça, Lajinha e Santa Angélica (Tabela 1-1).

As microanálises de olivina, clinopiroxênio, plagioclásio, anfibólio, biotita e minerais opacos foram realizadas em uma microssonda eletrônica JEOL JXA-8230 no Laboratório de Microanálises da Universidade Federal de Ouro Preto. O feixe de elétrons foi ajustado a 15 kV, 20 nA, 2-5 μm e as correções de matriz comum ZAF foram aplicadas. Os padrões naturais e sintéticos apropriados da coleção de laboratório foram utilizados para calibração. Os tempos de contagem nos picos/fundo foram 10/5s para todos os elementos (Na, Si, Al, Mg, Fe, Cr, Ti, Ca, Ni, K, Mn, F, Cl). Os erros analíticos estão dentro de 0,29 e 1,06%. Os

minerais foram caracterizados por análises de núcleos e bordas. As fórmulas minerais foram calculadas com base em 4 oxigênios para olivina, 6 para piroxênios, 8 para os cristais de plagioclásio, 22 oxigênios para biotita e para anfibólio as fórmulas foram baseadas em 23 oxigênios e o método de Leake et al., (1997) utilizado foi a média entre 15eNK e 13eCNK (cátions) correspondente aos anfibólios cálcicos. O teor total de ferro obtido pela microssonda foi considerado como FeO. Os diagramas binários e ternários utilizados para caracterizar os minerais principais foram obtidos utilizando-se os *softwares* Excel e Origin 6.1, respectivamente. Também foram obtidos mapas químicos de olivina, clinopiroxênio e plagioclásio para ilustrar as zonas minerais. As condições de operação foram aceleração de 15 kV, corrente de feixe de 20-nA e tempo de espera de 20 ms por ponto (modo de estágio). Todos os elementos considerados aqui (Fe, Mg, Na, Ca) foram analisados por espectroscopia de dispersão de comprimento de onda (WDS). Os mapas mostram distribuições de elementos quantitativos. A termometria foi realizada de acordo com os parâmetros de Lindsley (1983) para os cristais de piroxênio e a partir do princípio de Deer et al., (1992) para o plagioclásio, ambos para um ambiente de pressão de 5 Kbar (hipoabissal).

1.5.3 Análises litoquímicas

A análise litoquímica foi realizada tanto no ACME Analytical Laboratories LTD. (Canadá), e na SGS Geosol Ltda (Brasil) (Tabela 1-1). Os teores dos elementos foram analisados via ICP-MS após fusão com metaborato/tetraborato de lítio e digestão com ácido nítrico diluído. Os erros analíticos estão dentro de 2% para óxidos principais e 5% para elementos traços. O limite de detecção para os principais elementos está acima de 0,01%. Para os elementos secundários e traços, os limites estão acima de 10 ppm (Ba, Sr, Zr), 5 ppm (Zn, V, Cu, Ni), 0,5 ppm (Co), 0,3 ppm (Sn), 0,2 ppm (Rb), 0,1 ppm (Ce, Ga, La, Nd, Sm, Th, W, Yb) e 0,05 ppm (Cs, Dy, Er, Eu, Gd, Hf, Ho, Lu, Nb, Pr, Ta, Tb, Tm, U, Y). Os teores de metais-base e preciosos foram determinados por digestão em ”água régia”, seguidas da análise por ICP-MS. A perda por ignição (LOI) foi determinada pela diferença de peso após ignição a 1000 °C.

1.5.4 Análises Sm-Nd, Sr e U-Pb

As análises dos isótopos Sm-Nd, Sr e U-Pb foram realizadas no Laboratório de Geocronologia da Universidade de Brasília (UnB) (Tabela 1-1). As amostras foram

dissolvidas em uma mistura de HF-HNO_3 em vasos de teflon de alta pressão. Foi adicionado um marcador ^{150}Nd-^{149}Sm para determinar as concentrações de Nd e Sm. O REE foi então purificado por cromatografia de permuta catiônica, e Sm e Nd foram subsequentemente separados seguindo o procedimento de Gioia e Pimentel (2000). As análises de Sm e Nd usaram um conjunto de duplo filamento em um espectrômetro de massa Thermenticientífico Triton Plus operando em modo estático. As concentrações Sm e Nd e as relações ^{147}Sm/^{144}Nd possuem uma precisão de 0,5% que corresponde a um erro médio no valor εNd inicial de ± 0,5 unidades epsilon, com base em medidas repetidas de padrões JNdi e BCR-1. O Sr foi separado usando o procedimento convencional de troca de cátions de acordo com Pankhurst e O'Nions (1973). As amostras foram medidas a 1250-1300 °C no modo multi-coleção dinâmico, juntamente com o padrão NBS 987 Sr. Os valores ^{87}Sr/^{86}Sr das amostras foram corrigidos para o deslocamento em relação ao valor NIST SRM 987 certificado de 0,710250. Os brancos processuais totais são menores do que 100 pg.

Para a análise de U-Pb, duas amostras foram moídas e pulverizadas para a faixa de tamanho de 50-500 μm e os cristais de zircão foram separados através de técnicas magnéticas e de escolha manual (Tabela 1-1). Os grãos de zircão foram então montados em uma resina epóxi, moída e polida, e foram criadas imagens por microscopia eletrônica de varredura (MEV) em um microscópio FEI Quanta 450, utilizando a técnica de backscattering (BSE); também foram obtidas imagens por catodoluminescência. As imagens resultantes mostram a estrutura interna dos grãos de zircão (zoneamento, fraturamento, etc.) e auxiliam na localização dos pontos de incisão a laser nas porções mais homogêneas dos grãos de zircão (evidenciando, por exemplo, se estão livres de fraturas e inclusões). As razões isotópicas de U e Pb foram determinadas em um espectrômetro de massa Finnigan Neptune acoplado a um sistema de ablação a laser Nd-YAG 213 nm. As análises U-Pb seguem os procedimentos de Bühn et al. (2009). A ablação foi realizada usando *spots* de 25-30 mm no modo *raster*, em uma frequência de 9-13 Hz e intensidade de 0.19-1.02 J/cm^2. O material ablacionado foi carreado por Ar (~0.90 L/min) e He (~0.40 L/min) em 40 ciclos de 1 s cada, seguindo uma intercalação padrão-amostra de três amostras entre um branco e um padrão de zircão GJ-1. A acurácia foi controlada usando o padrão TEMORA-2. Os dados brutos foram reduzidos usando uma planilha interna e correções para *background*, viés de massa do instrumento e chumbo comum. As idades U-Pb foram calculadas usando o programa Isoplot 3.7 (Ludwig., 2008).

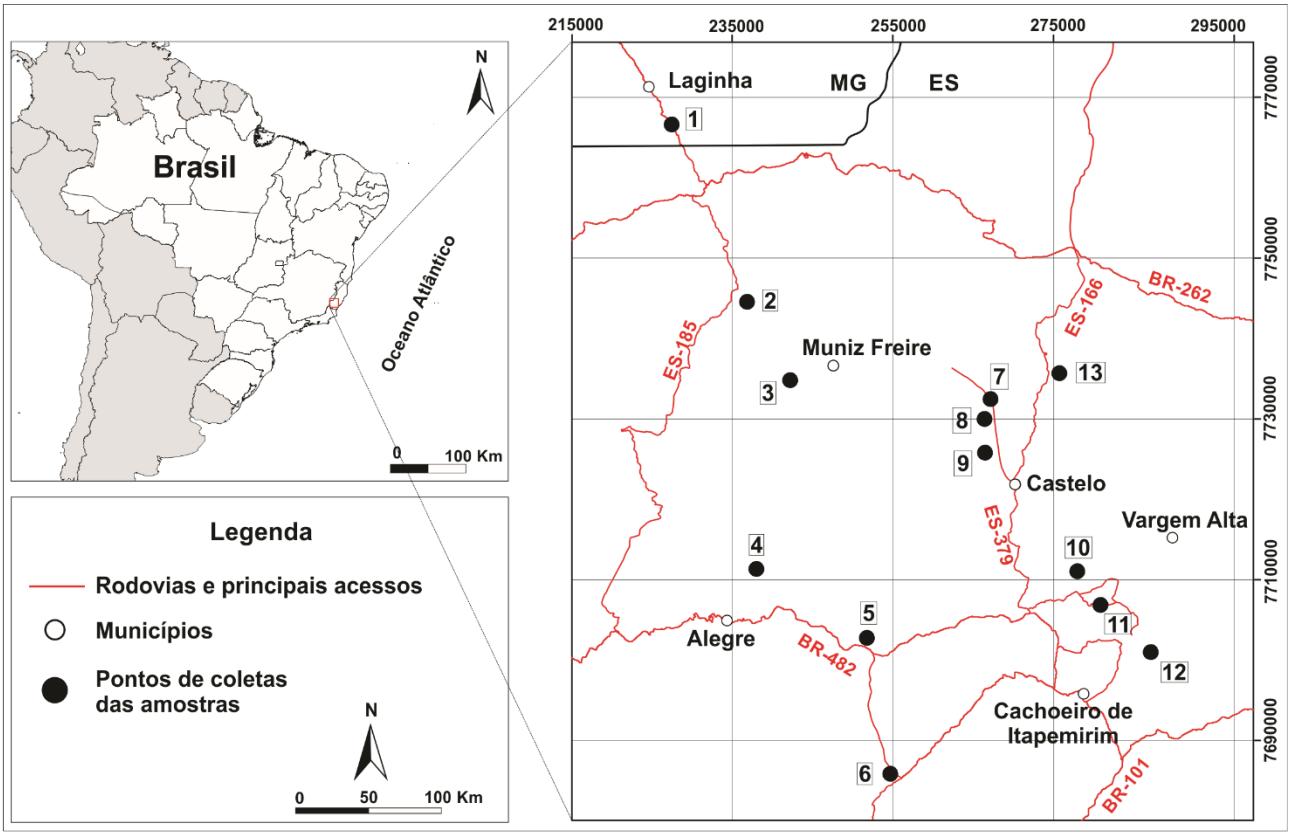

PONTOS	AMOSTRAS	COORDENADAS E	COORDENADAS N	DIREÇÃO	ANÁLISES
1	Dique Lajinha	226974	7766747	NW-SE	Petrografia, química mineral, geoquímica e Sm-Nd
2	Dique Iúna	237652	7743636	NW-SE	Petrografia e geoquímica
3	Dique Itaici	242064	7734872	NW-SE	Petrografia, geoquímica e Sm-Nd
4	Dique Santa Angelica	240061	7709191	NW-SE	Petrografia, química mineral, geoquímica, Sm-Nd e U-Pb
5	Dique Jerônimo Monteiro	251707	7702624	NW-SE	Petrografia, geoquímica e Sm-Nd
6	Dique Muqui	254740	7685683	NE-SW	Petrografia, geoquímica e Sm-Nd
7	Dique São Manoel	267379	7730281	NW-SE	Petrografia e geoquímica
8	Dique Nogueira	266939	7731590	NW-SE	Petrografia e geoquímica
9	Dique Castelo	265497	7725225	NW-SE	Petrografia, geoquímica e Sm-Nd
10	Dique Cantagalo	279477	7710204	NW-SE	Petrografia e geoquímica
11	Dique Itaoca	280664	7707154	NNE-SSW	Petrografia, geoquímica e Sm-Nd
12	Dique Cobiça	287006	7700787	NW-SE	Petrografia, química mineral, geoquímica, Sm-Nd e U-Pb
13	Dique Caxixe	276542	7733149	NW-SE	Petrografia, geoquímica e Sm-Nd

Figura 1-3: Mapa de localização das coletas das amostras e relação das análises realizadas nas amostras de cada ponto.

CAPÍTULO II

2.1 CONTEXTO GEOLÓGICO

A área de trabalho está inserida na porção interna do Orógeno Araçuaí (Figura 2-1), que representa o segmento setentrional da Província Mantiqueira Neoproterozóica (Heilbron et al., 2004). Um conjunto de componentes geotectônicos o caracterizam como um Orógeno colisional sucessor de um orógeno acrescionário de margem continental ativa, tais como depósitos de margem passiva, lascas ofiolíticas, zona de sutura, arco magmático, granitos sin-colisionais e plutonismo pós-colisional (Pedrosa-Soares et al., 2007).

Segundo Pedrosa-Soares et al., (2011), o Orógeno Araçuaí compreende quatro estágios evolutivos: pré-colisional (630-585 Ma), sin-colisional (585-565 Ma), tardi-colisional (565-535 Ma) e pós-colisional (530-490 Ma), sendo que esta última fase dá lugar a um regime tectônico extensional ligado ao colapso orogênico, com processos deformacionais e plutonismo.

Ocorrem, na região, vários corpos graníticos da fase pós-colisional atribuídos à suíte granítica G5 (Heilbron et al., 2004), caracterizada por diápiros inversamente zonados de composição gabroica a granítica (Pedrosa-Soares et al., 2011). Durante toda a orogenia, zonas de cisalhamento de alto ângulo estiveram ativas, inclusive durante o empilhamento de blocos em colisão, sincrônicos à acomodação regional (Pedrosa Soares e Wiedemann-Leonardos., 2000). A zona de cisalhamento mais importante da região corresponde ao Lineamento Guaçuí, de direção NE-SW, que parece representar uma continuação do norte da Zona de cisalhamento Paraíba do Sul, dividindo os estados de Minas Gerais e Rio de Janeiro. Outro conjunto de estruturas de alto ângulo trunca aquelas zonas de cisalhamento e é constituído por sistemas de juntas e fraturas orientadas para NW-SE e NNW-SSE (Silva et al., 2004; Vieira et al., 2014). Entre essas, uma das estruturas mais importantes é o Lineamento Alegre, de direção NNW-SSE (Calegari et al., 2016). Essa estrutura provavelmente foi gerada no Cambriano, pois parece controlar a colocação de grandes plútons do tipo G5, como o maciço de Santa Angélica. Também foi uma estrutura importante na evolução da bacia costeira de Campos, tanto no Cretáceo Inferior como no Paleoceno/Oligoceno, quando fraturas que compõem este lineamento foram reativadas como falhas normais (Calegari et al., 2016). O Lineamento Piúma, de direção geral NW-SE e mergulho para SW, provavelmente foi desenvolvido em resposta à distensão NNE-SSW após a Orogenia Brasiliana, mas também foi mais tarde reativado por esforço dextral

transtensional, provavelmente relacionado à abertura do Oceano Atlântico Sul no início do Cretáceo (Lourenço et al., 2016).

A unidade litológica que constitui o embasamento pré-cambriano da área de trabalho é o Grupo Paraíba do Sul, que se estende descontinuamente desde o Orógeno Ribeira até o Araçuaí (Heilbron et al., 2004). Compreende uma sucessão de rochas metapsamíticas e metapelíticas intercaladas por rochas calciossilicáticas, gonditos,quartzitos, mármores e rochas metamáficas. A ocorrência de mármores distingue esta unidade dos domínios Andrelândia e Juiz de Fora, os quais incluem quartzitos e, mais raramente, calciossilicáticas (Silva., 1993; Heilbron et al., 2004) (Figura 2-1).

2.2 MAGMATISMO BÁSICO

2.2.1 Suíte Fundão

Segundo Belém (2014), diques máficos toleíticos, constituídos por diabásios, basaltos e gabros de baixo-TiO_2 pertencentes à Suíte Fundão encontram-se alojados no Feixe de Fraturas Colatina com direções NNW-SSE, no Norte do Espírito Santo.

O embasamento, localizado na região de *back-arc* do Orógeno Araçuaí, inclui paragnaisses do Complexo Nova Venécia, granitos das supersuítes G2 e G3 e plútons pós-colisionais da supersuíte G5. O contato dos diques com estas rochas é abrupto, com presença de bordas de resfriamento rápido (*chilledmargins*).

Dados litogeoquímicos apontam para a existência de mais de uma suíte de baixo-TiO_2 que teriam sido geradas por diferentes quantidades de assimilação crustal, indicando AFC (Assimilação concomitante a cristalização fracionada) sem mudança de assembleia fracionante.

Dados de U-Pb (SHRIMP e LA-MC-ICP-MS) em zircão e em titanita registram idade de cristalização magmática entre 490 Ma e 520 Ma para os diques da Suíte Fundão e concordam com uma evolução conjunta com a supersuíte G5, que representa um evento magmático pós-colisional (tardi orogênico) relacionado ao colapso gravitacional do Orógeno Araçuaí. Desta forma, Belém (2014) interpreta a Suíte Fundão como contemporânea à supersuíte G5, representando um magmatismo basáltico, raso a intermediário, com contribuição do manto litosférico. A autora também apresenta dados de Ar-Ar em rocha total e plagioclásio que sugerem desequilíbrio isotópico provavelmente relacionado à abertura do Atlântico.

2.2.2 Magmatismo Básico Mesocenozóico

A reativação Sul-Atlantiana (Almeida et al., 1986), responsável pela fragmentação do Gondwana e pela abertura do Oceano Atlântico Sul, iniciou durante o Cretáceo Inferior (137 Ma) como consequência de uma extensão litosférica possivelmente associada à influência da pluma mantélica de Tristão da Cunha (Chang et al., 1992; Mohriak et al., 2002).

Este estágio, correspondente à fase rifte, foi assinalado por abatimentos da crosta com formação de estruturas extensionais, que deram origem às bacias da margem continental brasileira. Além da formação das bacias, o processo de rifteamento foi acompanhado por intenso magmatismo toleítico e alcalino (Almeida et al., 1996).

O magmatismo toleítico, de idade Neojurássica-Eocretácica é caracterizado por uma ampla distribuição de diques de diabásio e derrames basálticos (Almeida et al.,1996). Os diques compõem enxames que registram os movimentos extensionais iniciais da ruptura do Gondwana e estão situados no Estado do Espírito Santo (com direção principalmente NW-SE), entre São Paulo e Rio de Janeiro (com direção principal NE-SW), em Florianópolis (principalmente nas direções NE-SW) e no Arco de Ponta Grossa (orientados principalmente a NW-SE) (Deckart et al., 1998) (Figura 2-1).

A Bacia do Paraná no Sul e Sudeste do Brasil é caracterizada por intenso magmatismo basáltico (Northfleet et al., 1969), e é considerada como uma das maiores províncias ígneas do mundo (LIP) (Deckart et al., 1998). Além da província ígnea, autores como Renne et al., (1996) estudaram, no Paraná, o enxame de diques básicos (Enxame de Diques de Ponta Grossa) que inclui centenas de diques. São predominantemente basálticos e raramente andesíticos e riolíticos. Concentram-se em uma zona de tendência NW-SE coincidente com o Arco de Ponta Grossa, cujo desenvolvimento começou no Paleozóico e continuou até o início Jurássico. Infere-se que o Enxame de Diques de Ponta Grossa represente uma zona de extensão NE-SW relacionada ao estresse gerado pela rotação no sentido horário da Placa Sul-americana em relação à Placa Africana durante a assimétrica abertura do Atlântico Sul, que progrediu de sul para norte (Renne et al., 1996). Segundo Piccirillo et al., (1990), o alojamento destes diques ocorreu durante as fases iniciais de rifteamento e/ou flexura, cortando os derrames basálticos mais antigos. Dados químicos e isotópicos revelaram que estes diques não sofreram significativos processos de contaminação crustal, com razões $^{87}Sr/^{86}Sr_i < 0,7060$ (Piccirillo et al., 1990). Através de dados geocronológicos e químico-estratigráficos, identificaram que o pulso magmático é distintamente mais jovem do que o vulcanismo sul da Bacia do Paraná datado em 133 ± 1

Ma e quase contemporâneo com fluxos do centro da Bacia do Paraná, bem como as inundações vulcânicas de Etendeka na Namíbia, que se inserem no faixa de 133-131 Ma (Renne et al.,1996).

Renne et al., (1996) mencionam, ainda, que muitos autores notaram que o Enxame de Diques de Ponta Grossa se assemelha a um componente de uma junção tríplice relacionada ao início da abertura do Atlântico Sul, sendo esta interpretação favorecida pela existência de enxames que ocorrem ao nordeste (Enxame de Diques Santos-Rio de Janeiro) e ao sul (Enxame de Diques de Florianópolis) da região por eles estudada. Porém, conforme Coutinho (2008), a junção tríplice do Paraná não representa uma junção tríplice clássica. Para este autor, o rifte já estava se propagando de sul para norte quando atingiu o ponto de articulação dos três enxames de diques, provavelmente após a fase principal de formação da Província Magmática do Paraná. Ao atingir este ponto, o rifte criou um padrão de rupturas que se assemelha a uma junção tríplice.

O Enxame de Dique de Florianópolis está exposto ao longo da região costeira de Santa Catarina, sendo a maioria dos diques de orientação NNE-SSW (Marques et al., 2003; Tomazzoli e Lima., 2006). Os diques intrudem granitos pós-colisionais neoproterozóicos relacionados com tectonismo de caráter transcorrente. Os contatos entre os diques máficos e os granitos hospedeiros são geralmente abruptos e regulares, mas podem ser localmente irregulares e difusos. Estudos geoquímicos mostram que o Enxame de Diques de Florianópolis é composto principalmente por basaltos (Marques et al., 1993), em grande maioria de alto-TiO_2 (TiO_2 > 3%) (Marques., 2001). Foi identificado um pequeno grupo de diques semelhantes aos derrames de alto-TiO_2 da subprovíncia norte da Província do Paraná, mas com maior enriquecimento em LILE, indicando que os magmas que o originaram podem ter sido afetados por contaminação crustal mascarando, assim, as características geoquímicas originais (Marques e Ernesto., 2004). Foram identificadas idades Ar/Ar no intervalo entre 131-127 Ma e 123-121 Ma. No entanto, dados obtidos a partir de estudos paleomagnéticos mostram que idades inferiores a 127 Ma seriam predominantes (Raposo et al., 1998). Isso levou alguns autores a interpretar esses diques como representantes do episódio magmático mais novo da Província Magmática do Paraná–Etendeka, relacionada com a extensão da crosta continental pouco antes da formação da crosta oceânica (Raposo et al., 1998; Marques et al., 2003). Enquanto, Florisbal et al., (2014), a partir de dados de isótopos U-Pb, interpretaram que o principal período de colocação dos diques é de curta duração e ocorreu em aproximadamente 134 Ma.

O Enxame de Diques da Serra do Mar ocorre ao longo da região costeira dos Estados de São Paulo, Rio de Janeiro e uma parte do Estado do Espírito Santo. Estes diques estão orientados predominantemente a N40-50°E (Almeida., 1996). O enxame compreende essencialmente uma suíte de alto-TiO_2 (Ti/Y>310; Valente et al., 1998) e uma suíte subordinada de baixo-TiO_2 (Ti/Y<310; Monteiro e Valente., 2003). Dados geoquímicos de rocha total e isotópicos indicaram que os diques alto-TiO_2 evoluíram essencialmente por AFC (Assimilação concomitante a cristalização fracionada) em diferentes graus de contaminação (Marques e Ernesto., 2004; Corval., 2005) e também que estes magmas estão associados a uma fonte predominantemente astenosférica e composicionalmente similar à pluma de Tristão da Cunha (Valente et al., 2007).

Guedes et al., (2016) relatam o Enxame de Diques de Resende-Ilha Grande (RIGDS), localizado no sul do Rio de Janeiro. Relaciona-se ao desmembramento do Gondwana e é composto de diques/sills intrudidos em gnaisses pré-cambrianos. Os diques têm três orientações distintas NNW-SSE, NS a NNE-SSW e NE-SW, coincidentes com lineamentos estruturais pré-cambrianos. O enxame compreende basaltos de alto-TiO_2 divididos em três suítes com base em dados de ETR e isotópicos Sr e Nd. As suítes de Resende e Volta Redonda apresentam maiores proporções iniciais de $^{87}Sr/^{86}Sr$ entre 0,7077 e 0,7065, enquanto a suíte de Angra dos Reis apresenta valores de 0,7066 a 0,7057. Dados geoquímicos e isotópicos sustentam o Manto Litosférico Sub-Continental (SCLM) como a principal fonte para os basaltos. As heterogeneidades das suítes são explicadas por diferentes composições de SCLM em terrenos pré-cambrianos e/ou diferentes graus de fusão parcial e fracionada. Os dados de Ar/Ar indicam intervalo de idade entre ca. 156 a 144 Ma para o enxame, mais velho do que a média para a separação do Gondwana (aproximadamente 130-120 Ma). O intervalo de idade coloca o RIGDS entre o magmatismo Karoo (181-178 Ma) e o magmatismo Paraná-Etendeka (133 e 134 Ma), indicando que o processo extensional afetou o supercontinente antes do desmembramento.

Novais et al. (2004) destacam que, na Bacia do Espírito Santo, sequências sedimentares se alinham ao longo de falhas normais N-S e NNW-SSE, coincidentes com as direções dos diques básicos que ocorrem nas proximidades e a NNW da cidade de Vitória (ES). A estes elementos estruturais associam-se falhas secundárias que são verdadeiras zonas de alívio de tensão e falhas transcorrentes ou transversais de direções NW-SE e E-W, que se comportam como dutos de migração de hidrocarbonetos. Os diabásios da região foram classificados como basaltos e andesito-basaltos segundo a litoquímica, enquanto os dados geocronológicos (Ar-Ar) apresentados por Teixeira e

Rodarte (2003) indicaram idade de 128 ± 1,4 Ma, situando a atividade magmática no Cretáceo.

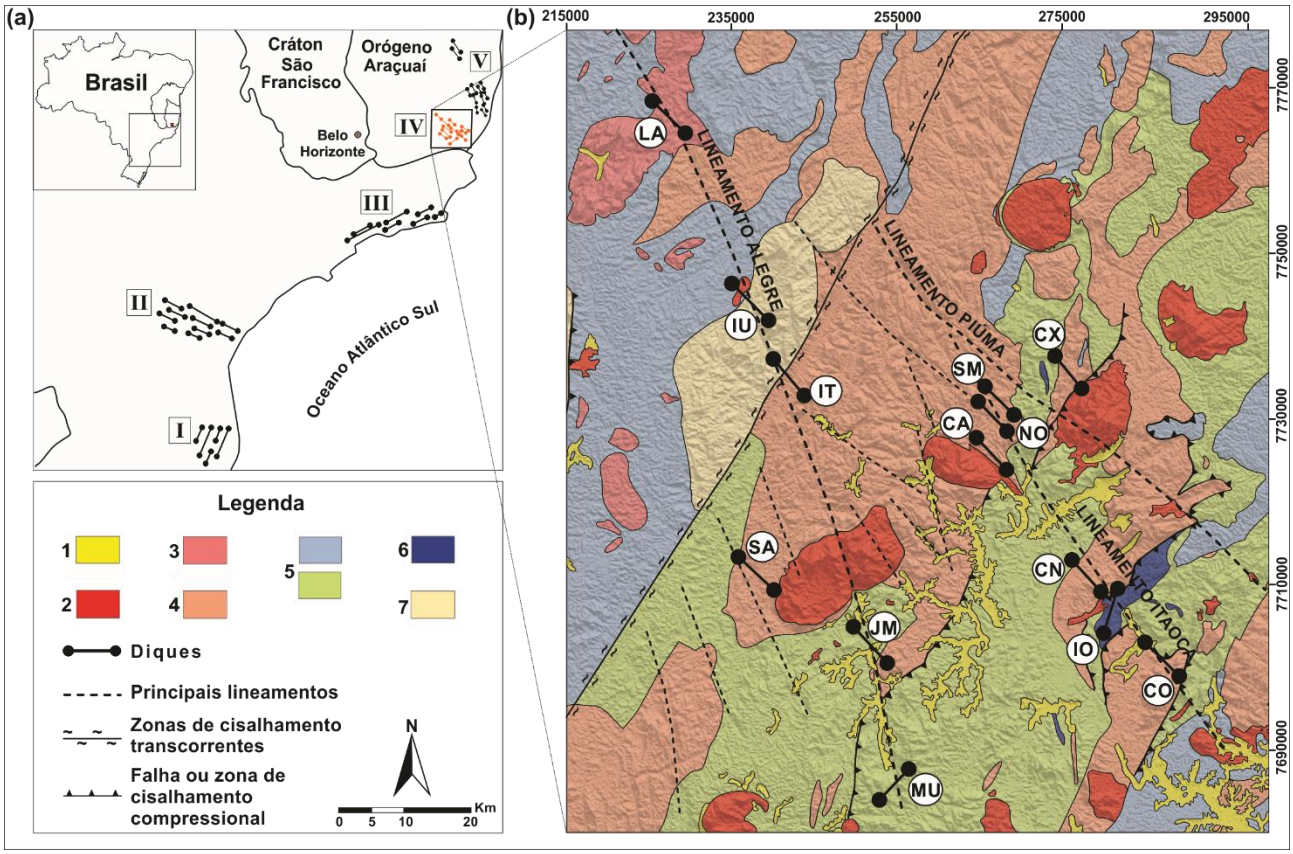

Figura 2-1: (a) Principais enxames de diques máficos na costa do Sul e Sudeste do Brasil: (I) Enxame de dique de Florianópolis; (II) Enxame de dique do Arco de Ponta Grossa; (III) Enxame de dique Serra do Mar; (IV) diques máficos no sul do Espírito Santo; (V) Enxame de dique da Suíte Fundão. (b) Mapa geológico simplificado do embasamento Pré-Cambriano na área estudada (destacado na Figura (a)). Modificado de Silva (1993). (1) Cobertura sedimentar - depósitos aluviais não consolidados (Cenozóico); (2) Supérstite G5 - granitoides intrusivos ácidos, intermediários e básicos (Cambriano, tardio a pós-colisonal); (3) Granitóides do tipo S pouco foliados, peraluminosos, cálcio-alcalinos, alto K (Ediacarano, sin a tarde-colisional); (4) Supérstite G1 - Granitoides foliados a gnaisses metaluminosos, cálcio-alcalinos, tipo I (Ediacarano, pré a sin-colisonal); (5) Grupo Rio Doce - Formação Palmital do Sul: biotita xisto com intercalações metavulcânicas; Grupo Italva - metavulcano-sedimentar grupo Bom Jesus do Itabapoana (Ediacarano, pré-colisional); (6) Lentes de mármore (Ediacarano); (7) Compleco Serra do Valentim - Noritos, enderbitos, charnockitos e charno-enderbitos (Rhyaciano). Diques: LA - Lajinha; IU - Iúna; TI - Itaici; SA - Santa Angélica; JM - Jerônimo Monteiro; MU - Muqui; SM - São Manoel; NÃO - Nogueira; CA - Castelo; CN - Cantagalo; IO - Itaoca; CO - Cobiça; CX – Caxixe.

CAPÍTULO III: DIQUES MÁFICOS NO SUL DO ESTADO DO ESPÍRITO SANTO

Os principais resultados da dissertação de mestrado serão aqui apresentados e discutidos em forma de artigo submetido ao periódico internacional Lithos.

3. TWO GENERATIONS OF MAFIC DYKE SWARMS IN THE SOUTHEASTERN BRAZILIAN COAST: IMPLICATIONS FOR THE GRAVITATIONAL COLLAPSE PHASE OF THE ARAÇUAÍ-RIBEIRA OROGEN (500 Ma) AND FOR WEST GONDWANA BREAKUP (140 Ma)

3.1. INTRODUCTION

Mafic dykes occur in a wide variety of tectonic configurations and their detailed study is essential for understanding the succession of diverse geological events through space and time. Most frequently, mafic dyke swarms are markers of crustal extension and important indicators of stabilization, reconstruction and dispersion of paleocontinents and crust-mantle interaction. Besides, mafic dyke swarms play a meaningful role in the delimitation of large basalt provinces of the Earth's crust, as well as in the deciphering crustal evolution events (e.g. Srivastava, 2011).

Individual dykes within swarms tend to be parallel or emplaced in major linear structures such as faults, shear zones and joints that mark the continental area as long geomorphological lineaments. Such structural lineaments often control both the basement and the sedimentary basins that overlie it, and thus the dykes emplaced along those structures can be used as markers in the relative dating of geologic units.

In southeastern and southern Brazil, one of the main events accompanied by intense mafic magmatism was the Mesozoic tectonism related to the reactivation of the South American Platform, which is responsible for the fragmentation of West Gondwana and separation of South America from Africa. This magmatism is represented by the extensive basalt flows of the Serra Geral Formation of the Paraná Basin, dated around 140-135 Ma, and various mafic dyke swarms in southeastern and southern Brazil (Renne et al.,1996).

In the northern Espírito Santo State, mafic dykes emplaced in the NW-SE 250 km long Colatina lineament were described (Novais et al., 2004; Valente et al., 2009) and dated at 128 ± 1.4 Ma using the Ar-Ar method (Teixeira and Rodarte, 2003), thus suggesting a link between the development of this structure and the fragmentation of Gondwana during the Early Cretaceous. This is very important because if this interpretation is correct, the Colatina

lineament and other similar lineaments in that region might have controlled the development of Phanerozoic coastal basins off the Brazilian continental margin, such as the oil-producing basins of Espírito Santo and Campos. However, recent robust geochronological data suggest that at least part of those dykes are instead related to the collapse phase of the Edicaran-Cambrian Araçuaí-Ribeira Orogen, presenting Cambrian ages of ca. 500 Ma (U-Pb in zircon and titanite; Belém, 2014). Thus, there is presently a great debate on the age and tectonic meaning of mafic dykes related to major lineaments in the Espírito Santo state and in the southeastern Brazilian coast in general. At one hand, the Cambrian U-Pb ages can be interpreted as crystallization ages of the dykes, while the Ar-Ar ages would be due to thermal resetting during Gondwana breakup; but at the other hand, Cambrian zircons and titanite can be interpreted as inherited from the Brasiliano basement of the Araçuaí Orogen and the Ar-Ar ages would then represent the real crystallization age of the dykes.

In this paper, we present the first field, petrographic, mineral chemistry, geochemical, isotopic and geochronological results of a systematic study on mafic dykes of the southern Espírito Santo state. Our results suggest that, in fact, there are at least two very distinct families of dykes in this region: one with a Cambrian age (ca. 500 Ma), related to the final stages of the Araçuaí-Ribeira Orogen collapse; and another developed at the Early Cretaceous (ca. 140 Ma, as dated for the first time using the U-Pb method on zircons), related to the breakup of Gondwana and opening of the South Atlantic Ocean. Our results emphasize the importance of reactivation of ancient structures during distinct tectonic events, e.g. the Alegre lineament which seems to have been active in distinct times and under distinct tectonic conditions: (i) during the Cambrian Araçuaí-Ribeira Orogen collapse; (ii) during the Early Cretaceous extension, playing a major role in the development of the oil-producing Campos basin; and (iii) during the Cenozoic, when this structure was also reactivated as a brittle fault (Calegari et al., 2016).

3.2. GEOLOGICAL CONTEXT

The studied area is located in the southern portion of the Espírito Santo state (Figure 3-1b), in the internal domain of the Araçuaí-Ribeira Orogen, belonging to the northern segment of the Neoproterozoic Mantiqueira Province (Heilbron et al., 2004). According to Pedrosa-Soares et al. (2011), magmatism in the Araçuaí Orogen comprehends four evolutionary stages: (i) pre-collisional, represented by the Rio Doce magmatic arc (G1 Supersuite) and related volcanic rocks in syn-orogenic basins (630-585 Ma); (ii) syn-collisional, represented by the G2 Supersuite garnet-bearing leucogranites (585-565 Ma);

(iii) late-collisional, represented by the G3 Supersuite leucogranites (565-535 Ma); and (iv) post-collisional, represented by the G4 and G5 Supersuite intrusions (530-490 Ma), which are generally undeformed. This last phase is related to the gravitational collapse of the orogenic wedge, leading to an extensional regime at the end of the Brasiliano Orogeny.

The Precambrian basement in the studied area is represented by the Paraíba do Sul Group (Figure 3-1b), a medium-to-high-grade gneissic unit composed of metapsammitic and metapelitic rocks interleaved with calc-silicate lenses, gondites, quartzites, marbles and metamafic rocks (Silva, 1993; Heilbron et al., 2004). This unit is extended through the Ribeira and Araçuaí orogens and little is known about its subdivision, age and tectonic significance. Intruded in the paragneiss sequence, a variety of igneous bodies of the post-collisional phase of the Araçuaí Orogen, mainly attributed to the G5 Supersuite, occur in the studied area (Heilbron et al., 2004). Those are characterized by inversely zoned diapirs of gabbroic and granitic composition, sometimes forming hybrid rocks in the contact zone of distinct magma types (Pedrosa-Soares et al., 2001).

Extensive high-angle shear zones were active during the whole Ediacaran and Early Cambrian, including during block stacking in the collisional phase (Pedrosa Soares and Wiedemann-Leonardos, 2000). The most important shear zone system in the region is the NE-SW trending Guaçuí Lineament (Figure 3-1b), which seems to represent a northwards continuation of the Paraíba do Sul Shear Zone dividing the Minas Gerais and Rio de Janeiro states further SW. Those shear zones follow the regional trend of the Brasiliano Orogeny in the area. Another set of structures truncates those shear zones at a high angle, and is constituted of systems of joints and fractures oriented at NW-SE and NNW-SSE (Silva et al., 2004; Vieira et al., 2014). Among those, one of the most important structures is the NNW-SSE Alegre Lineament (Calegari et al., 2016). This structure was probably generated in the Cambrian, as it seems to control the emplacement of major G5 plutons such as the Santa Angélica massif; but it was also a very important structure that controlled the sedimentation of the coastal Campos basin during both the Early Cretaceous rift phase and later during the Paleocene/Oligocene, when its subsidiary fractures were reactivated as normal brittle faults (Calegari et al., 2016). The Piúma Lineament further north, trending N50W and dipping to the SW was probably developed in response to NNE-SSW distension after the Brasiliano Orogeny, but was also later reactivated as a transtensional dextral zone, probably related to the South Atlantic Ocean opening in the Early Cretaceous (Lourenço et al., 2016).

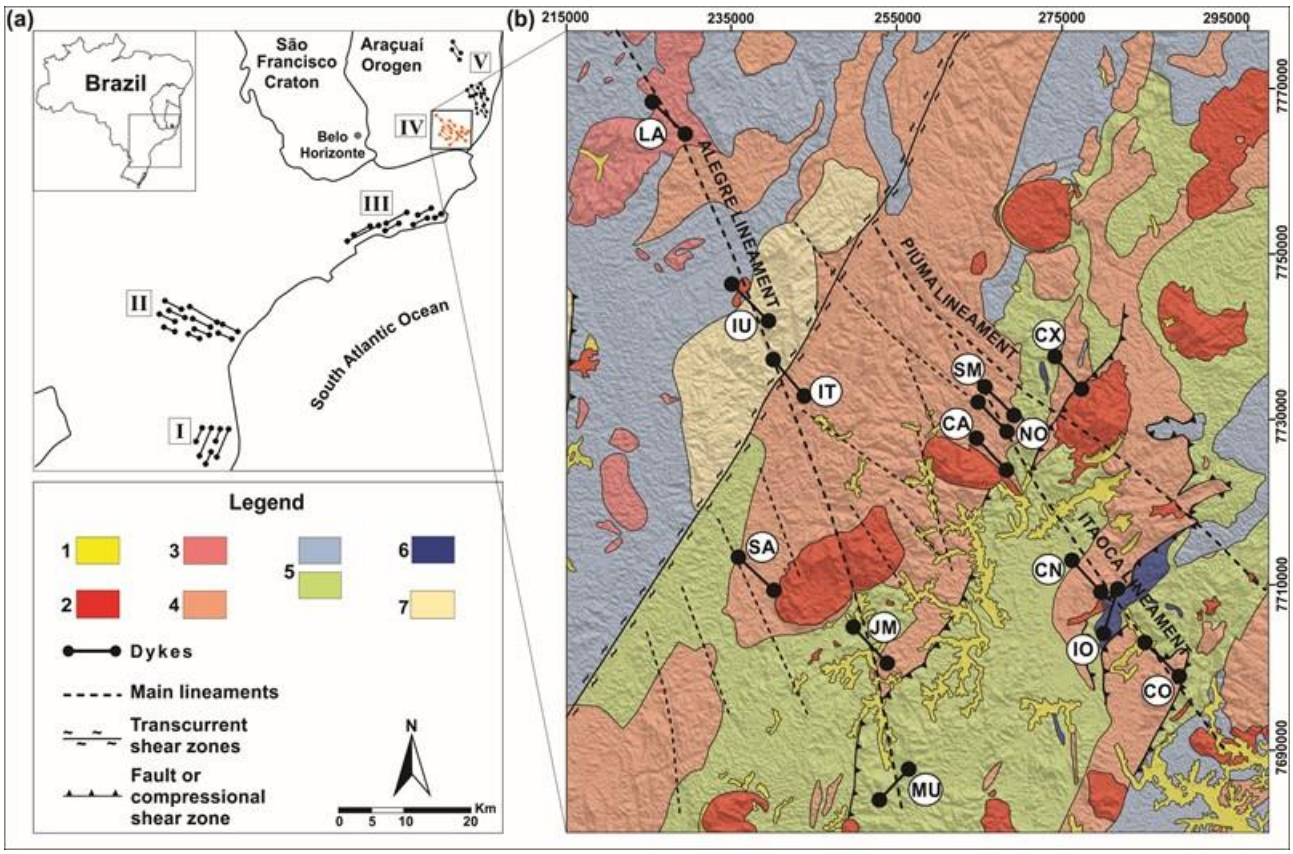

Figure 3-1: (a) Main mafic dyke swarms throughout the Southern and Southeastern Brazilian coast: (I) Florianópolis dyke swarm; (II) Ponta Grossa Arc dyke swarm; (III) Serra do Mar dyke swarm; (IV) Mafic dykes in Southern Espírito Santo; (V) Fundão Suite dyke swarm. (b) Simplified geological map of the Precambrian basement in the studied area (highlighted in Figure a). Modified from Silva (1993). (1) Sedimentary cover - unconsolidated alluvial deposits (Cenozoic); (2) G5 Supersuite - acid, intermediate and basic intrusive granitoids (Cambrian, late- to post- collisional); (3) Poorly foliated, peraluminous, calc-alkaline, high K, S type granitoids (Ediacaran, syn- to late- collisional); (4) G1 Supersuite - Foliated granitoids to metaluminous gneisses, calc-alkaline, type I (Ediacaran, pre- to syn- collisional); (5) Rio Doce Group- Palmital do Sul Formation: biotite schist with metavolcanic intercalations; Italva Group - metavolcano-sedimentary Bom Jesus do Itabapoana Group (Ediacaran, pre-collisional); (6) Lenses of marble (Ediacaran); (7) Serra do Valentim Complex - Norites, enderbites, charnockites and charno-enderbites (Rhyacian). Dykes: LA - Lajinha; IU - Iúna; IT - Itaici; SA - Santa Angélica; JM - Jerônimo Monteiro; MU - Muqui; SM - São Manoel; NO - Nogueira; CA - Castelo; CN - Cantagalo; IO - Itaoca; CO - Cobiça; CX - Caxixe.

3.3. MATERIALS AND METHODS

Thirteen mafic dykes were identified and studied in this work; those are named according to the localities where they outcrop (Figure 3-1b). Samples from each dyke were collected from both borders and center portions in order to observe textural and compositional variations. From those samples, 29 thin sections were made to aid in mineralogical, textural and structural description. Only fresh samples, i.e. with no signs of weathering and heterogeneities such as veins, where selected for the lithochemical and isotope analysis.

Microanalyses of olivine, clinopyroxene, plagioclase, amphibole, biotite and opaque minerals were performed with a JEOL JXA-8230 electron microprobe at the Microanalysis Laboratory of the *Universidade Federal de Ouro Preto* (Federal University of Ouro Preto), Brazil. The electron beam was set at 15 kV, 20 nA, 2-5 μm and the common matrix ZAF corrections were applied. Appropriate natural and synthetic standards from the laboratory collection were used for calibration. Counting times on the peaks/background were 10/5 s for all elements (Na, Si, Al, Mg, Fe, Cr, Ti, Ca, Ni, K, Mn). Analytical errors are within 0.29 and 1.06%. Minerals were characterized by analyses from cores and rims. The mineral formulas were calculated based on 4 oxygens for olivine, 6 for pyroxene, 8 for plagioclase crystals, 22 oxygens for biotite and for amphibole was based on 23 oxygens and the method used by Leake et al., (1997) was the average between 15eNK and 13eCNK (cations) corresponding to calcic amphiboles. Ilmenite was the opaque mineral identified. The total iron content obtained by the microprobe was considered as FeO. The binary and ternary diagrams used to characterize the main minerals were obtained by Excel and Origin 6.1 softwares, respectively. Chemical maps of olivine, clinopyroxene and plagioclase were also obtained in order to illustrate the mineral zonations. Operating conditions were 15-kV acceleration, 20-nA beam current, and 20-ms dwell time per spot (stage mode). All the elements considered here (Fe, Mg, Na, Ca) were analyzed by wavelength dispersion spectroscopy (WDS). Maps show quantitative element distributions. The thermometry was performed according to the parameters of Lindsley (1983) for pyroxene crystals and from the principle of Deer et al. (1992) for plagioclase, both in a 5 kbar (hypoabissal) pressure environment.

Lithochemical analyses of fifteen samples (one for each dyke and two second samples collected in distinct outcrops of the Itaoca and Jerônimo Monteiro dykes, identified as A and B in Table 1) were conducted both at the ACME Analytical Laboratories (Canada), and at SGS Geosol (Brazil). Element grades were analyzed via ICP-MS after fusion with

lithium metaborate/tetraborate and digestion with diluted nitric acid. Analytical errors are within 2% for major oxides and 5% for trace elements. The detection limit for major elements is above 0.01%. For the minor and trace elements, the limits are above 10 ppm (Ba, Sr, Zr), 5 ppm (Zn, V, Cu, Ni), 0.5 ppm (Co), 0.3 ppm (Sn), 0.2 ppm (Rb), 0.1 ppm (Ce, Ga, La, Nd, Sm, Th, W, Yb) and 0.05 ppm (Cs, Dy, Er, Eu, Gd, Hf, Ho, Lu, Nb, Pr, Ta, Tb, Tm, U, Y). Base and precious metal grades were determined by digestion in Aqua Regia followed by ICP-MS analysis. The Loss On Ignition (LOI) was determined by the weighing difference after ignition at 1000 °C.

The Sm-Nd and Rb-Sr isotope analyses were conducted at the Laboratório de Geocronologia (Laboratory of Geochronology) of the Universidade de Brasília, Brazil. Samples were dissolved in a HF-HNO_3 mixture in high-pressure Teflon vessels. A ^{150}Nd-^{149}Sm tracer was added to determine Nd and Sm concentrations. Rare Earth Elements (REE) were then purified by cation exchange chromatography, and Sm and Nd were subsequently separated following the procedure of Gioia and Pimentel (2000). Sm and Nd analyses used a double filament assembly in a Thermoscientific Triton Plus mass spectrometer operating in static mode. The Sm and Nd concentrations and the ^{147}Sm/^{144}Nd ratios have an accuracy of 0.5% that corresponds to an average error on the initial εNd value of ±0.5 epsilon units, based on repeated measurements of standards JNdi and BCR-1. Sr was separated using the conventional cation exchange procedure according to Pankhurst and O'Nions (1973). Samples were measured at 1250–1300 °C in dynamic multi-collection mode, along with the NBS 987 Sr standard. The ^{87}Sr/^{86}Sr values of the samples were corrected for the offset relative to the certified NIST SRM 987 value of 0.710250. Procedural blanks for Sr are less than 100 pg.

For the U-Pb analysis also conducted at Laboratório de Geocronologia, Universidade de Brasília, two samples were crushed and powdered to the 50-500 μm size range and zircon crystals were separated through standard magnetic and hand-picking techniques. Zircon grains were then mounted in an epoxy resin, ground and polished, and imaged by Scanning Electron Microscopy (SEM) in a FEI Quanta 450 microscope through the backscattering technique (BKS) and cathodoluminescence images were also obtained. The resulting images emphasize the internal structure of zircon grains (zoning, fracturing, etc.) and aided in the location of laser spots in the most homogeneous portions of zircon grains (e.g. free of fractures and inclusions). Zircon grains were analyzed by laser ablation using a Finnigan Neptune ICP-MS coupled to a Nd-YAG 213 nm laser ablation system. The U-Pb analysis follows the procedures outlined in Bühn et al. (2009). Ablation was done using 25-30 μm spots in raster mode, at a frequency of 9-13 Hz and intensity of 0.19 - 1.02 J/cm^2.

The ablated material was carried by Ar (w0.90 L/min) and He (w0.40 L/min) in 40 cycles of 1 s each, following a standard-sample bracketing of three sample analysis between a blank and a GJ-1 zircon standard. Accuracy was controlled using the TEMORA-2 standard. Raw data were reduced using an in-house program and corrections were done for background, instrumental mass bias and common Pb. U-Pb ages were calculated using Isoplot 3.6 (Ludwig, 2008).

3.4. RESULTS

3.4.1. Field description of the mafic dykes

The studied mafic dykes are composed by massive holocrystalline aphanitic dark grey to black diabase, locally with red or brown hues when weathered. The dykes vary from circa one to four meters thick. All of the dykes are oriented in a NW-SE to NNW-SSE trend, except for Itaoca (NNE-SSW) and Muqui (NE-SW) dykes. The general NW-SE trend is also supported by local scale magnetometric studies (Gomes et al., 2016).

The contact between the Castelo, Itaoca, Jerônimo Monteiro, Lajinha, Nogueira and Muqui dykes with the host rocks is abrupt, with no sign of igneous interaction (Figures 3-2a and 3-2b). Those dykes are densely jointed and show fracture sets with diverse orientation trends, such as subvertical NE-SW, NW-SE and WNW-ESE (Figure 3-2f). Cooling joints occur near the contacts with the host rock (Figure 3-2c).

The Caxixe, Itaici and Santa Angélica dykes differ from the others by the sinuous contacts with the host rocks and absence of cooling joints or fractures. Although there is no sign of magmatic interaction with the host rocks, the dykes diverge from their main direction following the foliation trend of the host paragneisses (Figure 3-2d and 3-2e). In the Itaici dyke, there is a xenolith of the host mylonitic gneiss.

The host rocks are mainly paragneiss and mylonitic gneisses. Locally, however, the dykes are intruded in granitic rocks, which only show an incipient foliation. The main trend of mylonitic foliation and gneissic banding is NE-SW, steeply dipping to SE. There is also a crenulated foliation trending NW-SE, with a steep dip to SW. Joints in the host rocks are grouped in two main families, one trending NE-SW and another WNW-ESE, both subvertical. Subordinately, a N-S trending family and a less frequent E-W family occur (Figure 3-2g and 3-2h).

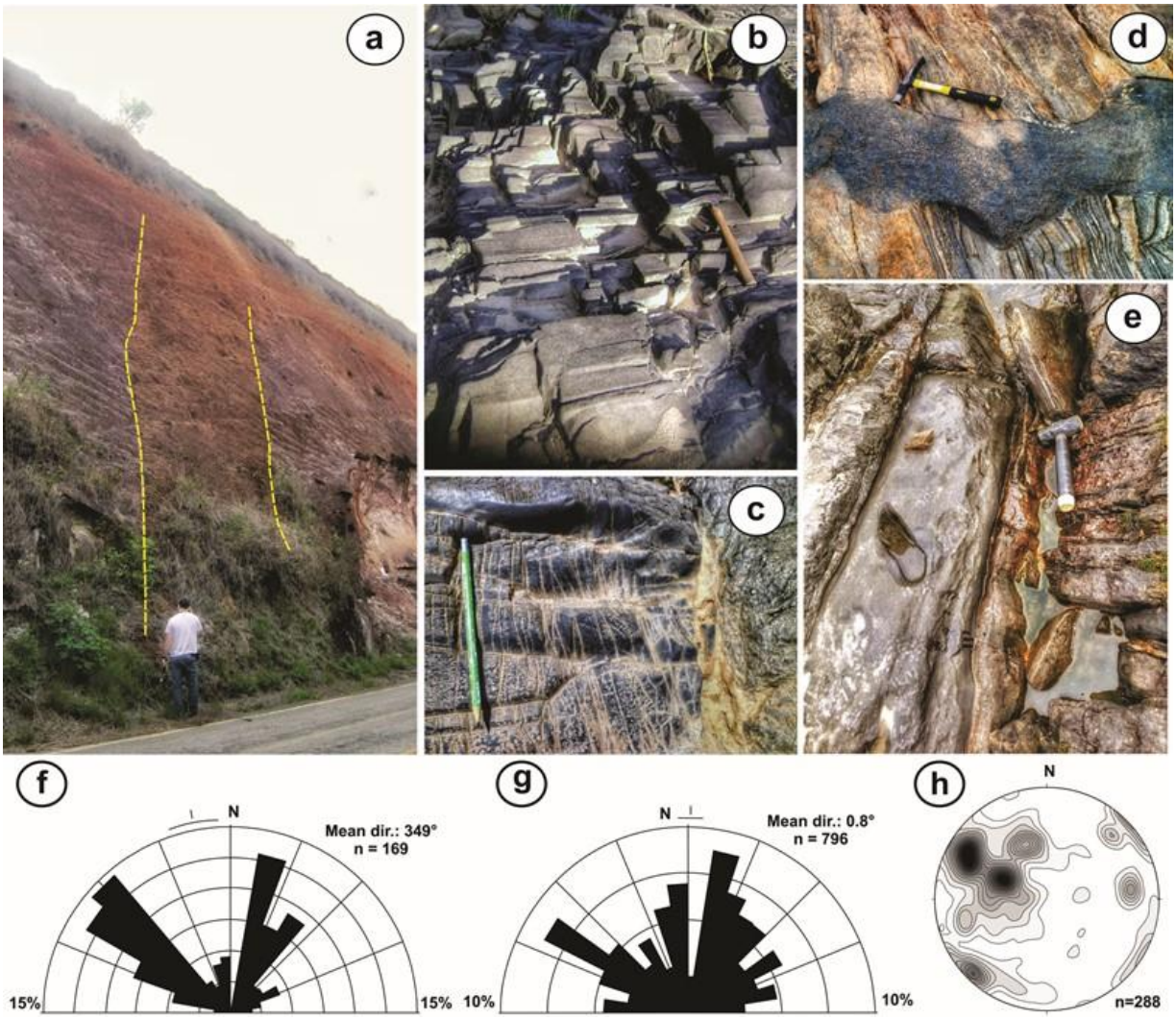

Figure 3-2: (a) Lajinha dyke; (b) Castelo dyke with fractures and (c) cooling joints; (d) Santa Angélica dyke presenting sinuous contact with the host mylonitic rock; (e) massive Itaici dyke (without fractures or cooling joints); (f) rose diagram represent the orientation of joints in the dykes; (g) rose diagram of the joints in the basement and (h) equal-area projection of the poles to the basement foliation.

3.4.2. Petrography and mineral chemistry

The dykes can be distinguished into two main groups according to their mineralogical and textural characteristics. The first petrographic group (Group 1) is composed by the Castelo, Muqui, Itaoca, Lajinha, Cobiça, Nogueira, Iúna, Cantagalo, São Manoel and Jerônimo Monteiro dykes; and the second group (Group 2) is represented by the Santa Angélica, Caxixe and Itaici dykes. Each dyke is petrographically homogeneous, as attested by the similarity between samples collected in the borders and centers of the dykes. Mineral chemistry analyses were performed in two dykes of the Group 1 (Cobiça and Lajinha) and in one dyke of the Group 2 (Santa Angélica). The cores and rims of plagioclase,

clinopyroxene, olivine, amphibole, biotite and opaque mineral crystals were analyzed (see results on the Supplementary Material).

Group 1 samples are inequigranular and porphyritic and subordinately subophitic. Plagioclase, clinopyroxene and, eventually, olivine (varietal mineral) phenocrystals float in a fine-grained matrix of the same composition, with opaque accessory minerals. The plagioclase varies from labradorite to bytownite, between $An_{53}Ab_{44}Or_3$ and $An_{83}Ab_{17}Or_1$ (Figure 3-3e and Figure 3-4a). The crystals are dispersed or compose the subophitic texture, are hipiodomorphic with tabular habit, and are fine to medium-grained (0.1 to 1.0 mm). Some crystals show Carslbad and also polysynthetic twinning, and sometimes irregular twinning. Clinopyroxene crystals are predominantly augite, both in core and rim, ranging from $Wo_{0.35}En_{0.35}Fs_{0.30}$ to $En_{0.56}Fs_{0.18}Wo_{0.26}$ (Figure 3-3g and Figure 3-4d). Some analyzes show depletion in CaO, plotting into the pigeonite field, emphasizing the hypoabyssal characteristic of Group 1. A crystal zoning is defined by depletion of MgO and CaO, followed by enrichment in FeO, from core to rim. The grains are hypidiomorphic, prismatic and fine to medium-grained (0.1 to 0.6 mm). Some of them are twinned and dispersed in the rock groundmass, but essentially compose the subophitic texture. Olivine has an average content of Fo_{85} to Fo_{80}. There is noticeable subtle zoning in some grains, with slight increase of FeO at the rim and composition change from Fo_{76} to Fo_{74} (Figure 3-3f). The olivine crystals are euhedral to subhedral, with an approximate size of 0.1 to 0.5 mm. They sometimes occur as crystals partially or totally substituted by iddingsite. Ilmenite crystals are included in the plagioclase and augite or dispersed in the fine-grained matrix (Figure 3-3a and 3-3b).

Group 2 samples generally show intergranular texture. The essential minerals are plagioclase and clinopyroxene. Secondary minerals such as biotite and amphibole also occur, and the main accessory is ilmenite, but abundant titanite is also an important accessory phase in the Santa Angélica dyke. Apatite occurs along with secondary carbonate and sericite, in addition to some allanite. In Group 2, the plagioclase has a more sodic composition than in Group 1, being essentially classified as andesine with a composition of $An_{34}Ab_{64}Or_2$ to $An_{53}Ab_{47}Or_1$) (Figure 3-3h and Figure 3-4b). The grains are randomly dispersed in the matrix and ca. 0.1 mm long, but when in tabular habit their sizes vary, ranging from 0.3 to 1.0 mm. They are locally sericitized, especially the Itaici dyke samples. The clinopyroxene crystals are predominantly diopside, but there is some augite, which vary between $Wo_{0.48}En_{0.35}Fs_{0.17}$ and $Wo_{0.38}En_{0.40}Fs_{0.21}$ (Figure 3-4e). Clinopyroxene is highly altered and partially or completely replaced by amphibole of endenite to endenite hornblende composition. The grains of amphibole are anhedral, with incolor to light green / deep green pleochroism and low birefringence. Biotite appears with different colors, ranging

from a more reddish to a light brown tone. Biotite crystals partially replace amphibole, and in the Itaici dyke this process is so advanced that biotite is preponderant over amphibole. Ilmenite crystals occur included in the essential minerals or dispersed throughout the groundmass. Idiomorphic acicular apatite crystals are mostly included in idiomorphic plagioclase and allanite crystals (Figure 3-3c and 3-3d).

3.4.3. Lithochemistry

Fifteen samples were selected for geochemical analysis (Table 1), which classify the dykes in two different series, corresponding to the petrographic groups described above: a subalkaline tholeiitic series (Group 1) and an alkaline series (Group 2) (Figure 3-5a and 3-5b).

Group 1 samples show normative (CIPW) hypersthene and no nefeline, supporting their tholeiitic affinity. On the other hand, Group 2 samples are more complex; the Santa Angélica and Caxixe dykes show hypersthene and no nefeline in their norms, but the Itaici dyke reaffirms an alkaline nature by its normative olivine and nefeline (Table 2).

SiO_2 grades in Group 1 vary from 50.00 to 56.05 wt.%, MgO between 2.72 and 7.32 wt.% and Mg# between 27 and 53. In Group 2, SiO_2 grades vary from 49.08 to 54.21 wt.%, MgO between 3.39 and 8.33 wt.% and Mg# between 35 and 62. TiO_2 grades vary between 1.0 and 3.3%, characterizing mainly low TiO_2 mafic rocks (Bellieni et al., 1986; Mantovani et al., 1985), excepting for four dykes (Muqui, Iúna, Santa Angélica and Caxixe).

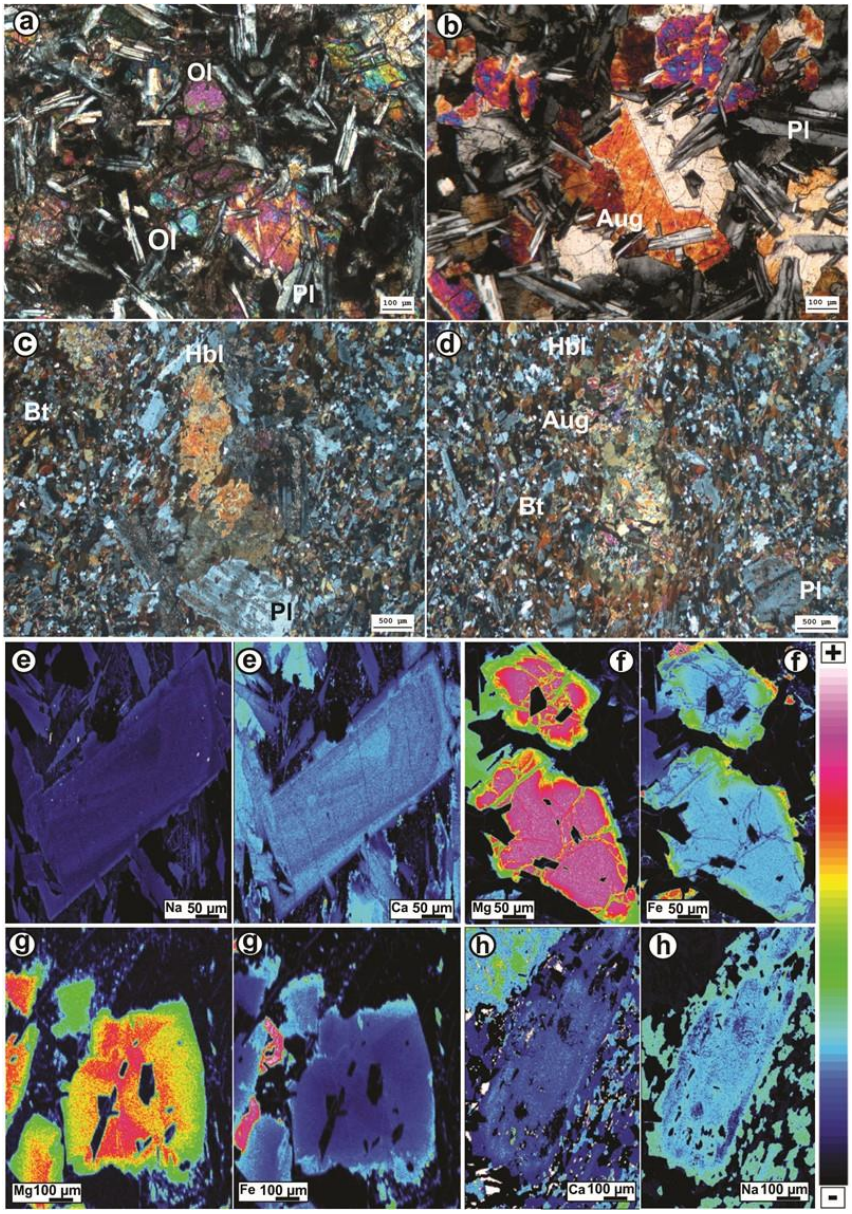

Figure 3-3: Photomicrographs of thin sections under parallel (ppl) and cross-polarized light (cpl), showing (a) olivine and (b) augite in the Cobiça dyke with twinning and subophitic texture (cpl). Photomicrographs (c) and (d) show intergranular texture and secondary processes of augite substitution in the Santa Angélica dyke (ppl). (e) Chemical map of plagioclase from the Cobiça dyke presenting the variation of Na contents from the core (light blue) to the rim (dark blue) and Ca contents from the core (dark blue) to the rim (light blue). (f) Chemical map of olivine from the Cobiça dyke presenting the variation of Mg contents from the core (pink) to the rim (red-green) and Fe contents from the core (light blue) to the rim (green). (g) Chemical map of augite from the Lajinha dyke presenting the variation of Mg contents from the core (red) to the rim (green) and Fe contents from the core (dark blue) to the rim (light blue). (h) Chemical map of plagioclase from the Santa Angélica dyke presenting virtually no variation of Ca and Na contents from the core (light blue) to the rim (lighter blue).

Chondrite-normalized (Sun and McDonough, 1989) REE patterns have three distinct trends, allowing to separate the tholeiitic dykes into Group 1A (Castelo, Cantagalo, Cobiça, Itaoca, Lajinha, Jerônimo Monteiro, Nogueira and São Manoel) and Group 1B (Muqui and Iúna) (Figure 3-6a). These sub-groups show very similar patterns, but Group 1B is slightly more enriched in total REE contents and in light REE (LREE) than Group 1A (mean $La/Yb_{(N)}$= 2.59). Patterns are relatively flat with only a slight Eu anomaly (Eu/Eu* = 0.79-0.91), suggesting plagioclase fractionation. The alkaline dykes of Group 2 are remarkably more enriched in LREE than the others (mean $La/Yb_{(N)}$= 19.62) and show relatively flat patterns (Eu/Eu* = 0.80-0.90) (Figure 3-6a). Group 2 has higher values for $La/Sm_{(N)}$ ratios (4.1-5.0), while Group 1 varies between $La/Sm_{(N)}$ = 2.0 to 2.7. The dykes also have low $Lu/Hf_{(N)}$ ratios (0.73-1.82 for tholeiitic and 0.18-0.41 for alkaline dykes), indicating that they were probably formed by the melting of sources containing variable contents of residual garnet (Piccirillo and Melfi, 1988).

In general, the tholeiitic dykes of Group 1 present a negative correlation of MgO contents with SiO_2, Fe_2O_3, TiO_2, Na_2O, P_2O_5 and K_2O contents, and a positive correlation of MgO, CaO and Al_2O_3. As for the trace elements, there is a positive correlation between MgO, Ni and Sc, but the Rb, Ba, Nb, La, Zr and Y increase with the degree of the magma fractionation (Figure 3-7). Patterns for the alkaline dykes of Group 2 are not easily distinguishable because of the low number of samples.

The patterns of incompatible elements normalized to the primitive mantle of Sun and McDonough (1989) show enrichment in LILE (Large Ion Lithophile Elements), such as Ba and K, but also show negative anomalies of Rb and Th. As for the incompatible HFS (High Field Strenght) elements, they exhibit depletion of Nb, Ta, P, Sr, Ti, Hf and Zr relatively to the primitive mantle (Figure 3-6b).

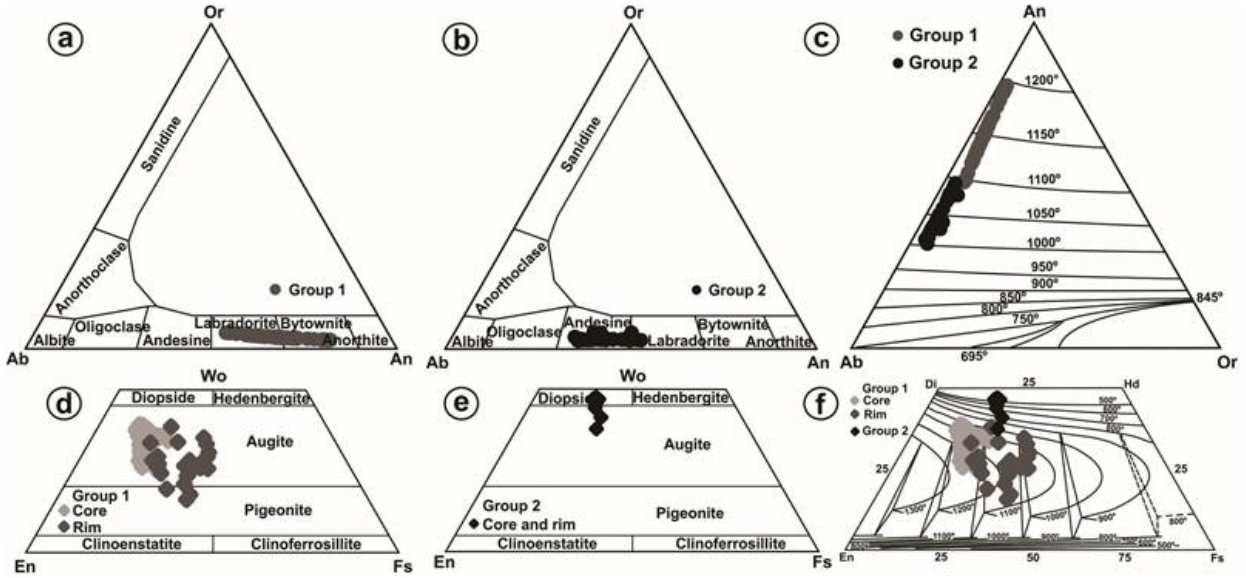

Figure 3-4: Compositional variation of plagioclase (Or-Ab-An diagram, Deer et al., 2003) in (a) Group 1 (Cobiça and Lajinha dykes) and (b) Group 2 (Santa Angélica dyke); and compositional variation of pyroxenes according to the ternary diagram Wo-En-Fs (Morimoto, 1988) in (d) Group 1 and (e) Group 2 dykes. (c) Estimated crystallization temperatures of different plagioclases according to Deer et al. (1992). (f) Variation in crystallization temperatures of pyroxenes in Group 1 and Group 2 dykes in a 5 Kbar environment (Lindsley 1983).

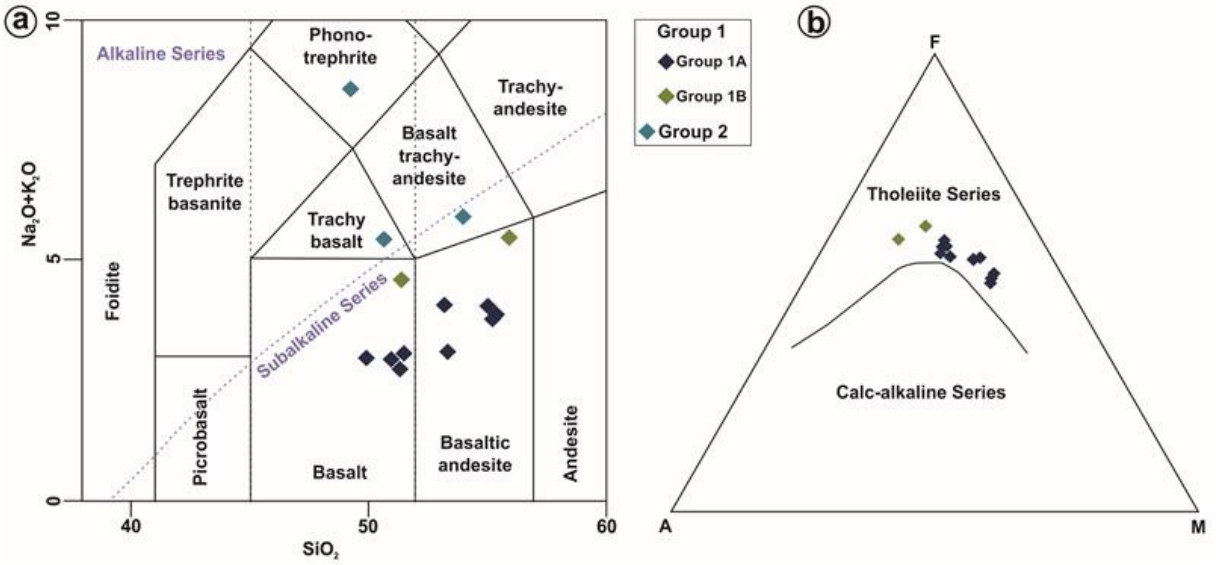

Figure 3-5: (a) Total Alkalis-Silica (TAS) diagram ($Na_2O + K_2O$ versus SiO_2, LeBas et al., 1986) and (b) AFM diagram (Irvine and Baragar, 1971) for the geochemical discrimination of the dyke samples. A = $Na_2O + K_2O$; F = Fe_2O_3; M = MgO.

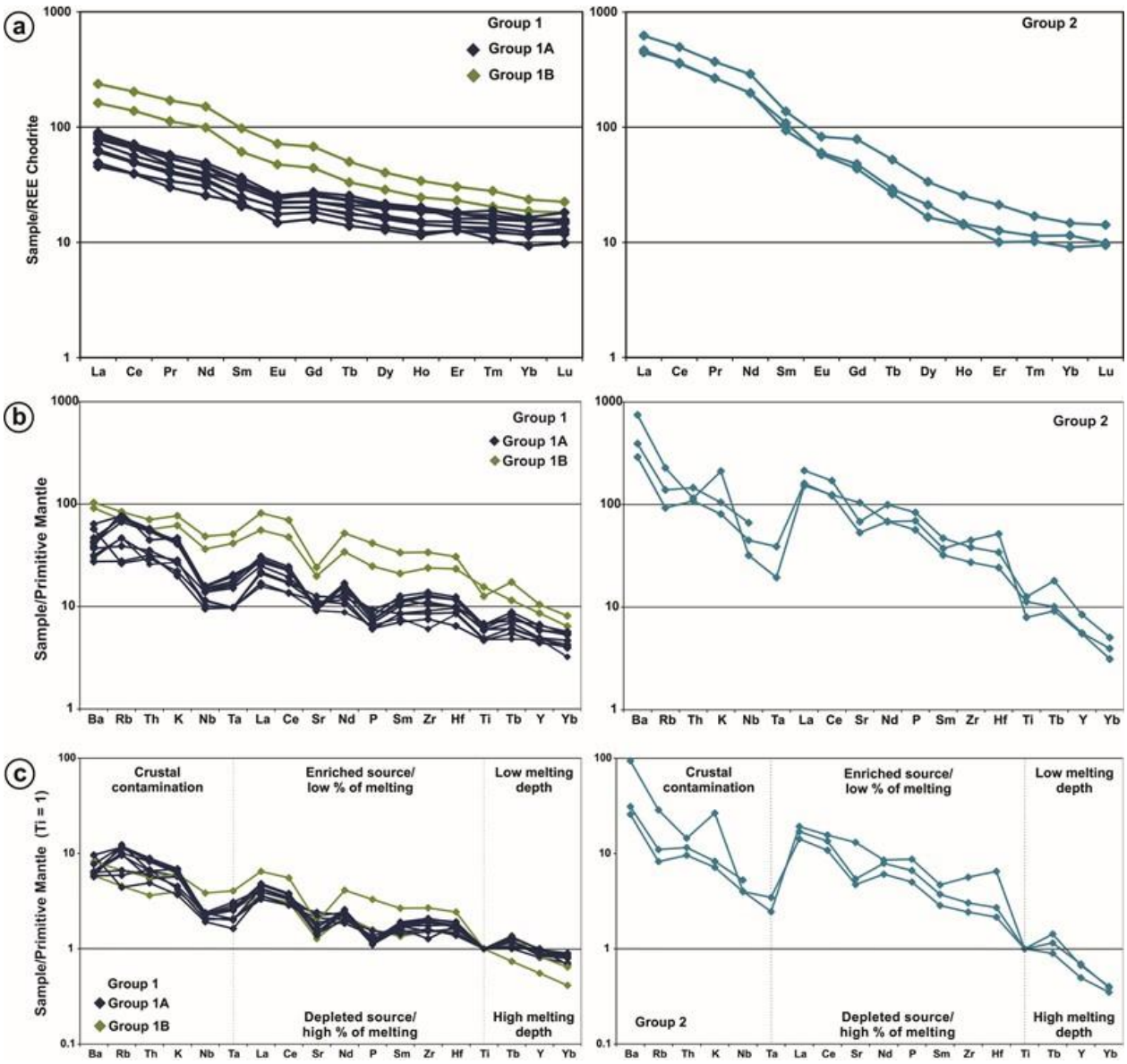

Figure 3-6: (a) Chondrite-normalized REE patterns (Sun and McDonough, 1989); (b) multi-element spidergram normalized to the Primitive Mantle (element ordering after Thompson et al., 1984; normalizing values after McDonough and Sun, 1989) for the dyke samples (c) additional normalization of (b) for Ti = 1.

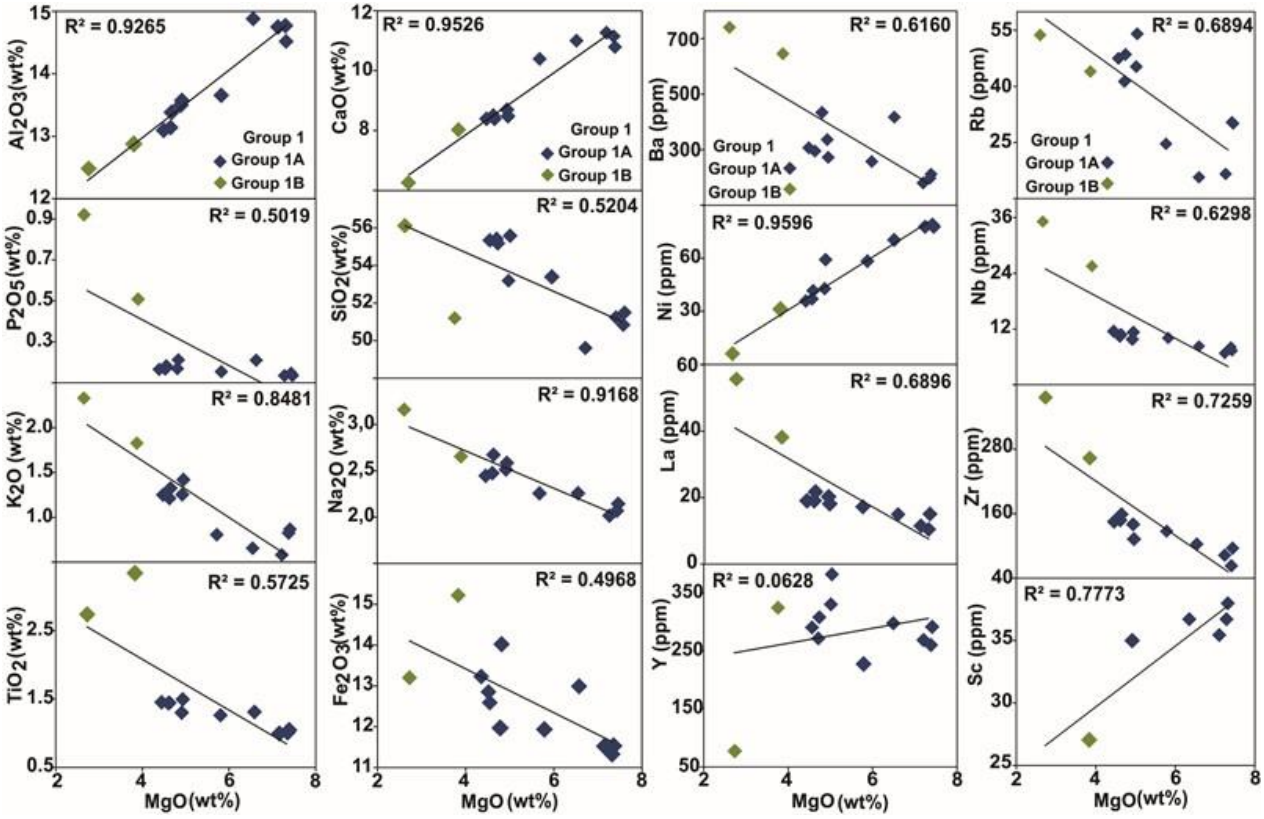

Figure 3-7: Binary diagram displaying MgO (wt.%) versus major and minor elements (wt.%) and trace elements for the tholeiitic dyke samples.

Table 3-1

Lithochemical data of mafic dykes samples from the southern Espírito Santo state. Element ratios at the bottom of the table are normalized to the chondrite of Sun and McDonough (1989). (1) – Samples analyzed at ACME Analytical Laboratories (Canada); (2) – Samples analyzed at SGS Geosol (Brazil).

Group	**Group 1 (tholeiitic)**												**Group 2 (alkaline)**		
Sample	**Muqui** (1)	**Jerônimo Monteiro A**(1)	**Castelo** (1)	**Itaoca A**(1)	**Cobiça** (1)	**Lajinha** (1)	**Iúna** (2)	**Nogueira** (2)	**São Manoel**(2)	**Cantagalo**(2)	**Itaoca B**(2)	**Jeorônimo Monteiro B**(2)	**Santa Angélica**(1)	**Itaici**(1)	**Caxixe**(2)
Major Elements (%)															
SiO_2	50.7	50.5	50.1	52.6	50.5	50.8	54.5	56.5	54.4	55.2	55.0	53.5	49.8	47.7	53.8
TiO_2	3.3	1.2	1.0	1.5	1.0	1.0	2.7	1.5	1.3	1.4	1.4	1.3	2.4	1.7	2.7
Al_2O_3	12.7	14.1	14.5	13.4	14.5	14.3	12.1	13.7	13.2	13.1	13.1	13.7	15.2	13.6	14.2
Fe_2O_3	15.0	12.3	11.3	13.7	11.3	11.2	12.8	13.0	11.8	13.1	12.8	12.0	10.9	8.9	11.4
MnO	0.2	0.2	0.2	0.2	0.2	0.2	0.2	0.2	0.2	0.2	0.2	0.2	0.2	0.1	0.1
MgO	3.8	6.2	7.2	4.9	7.0	7.2	2.7	4.8	4.8	4.5	4.6	5.8	5.5	8.1	3.4
CaO	7.9	10.4	10.9	8.4	11.0	10.6	6.1	8.6	8.5	8.4	8.5	10.4	7.7	7.2	6.1
Na_2O	2.6	2.1	2.0	2.6	2.0	2.1	3.0	2.7	2.5	2.5	2.5	2.2	2.9	2.3	2.6
K_2O	1.8	0.6	0.8	1.4	0.6	0.8	2.3	1.4	1.2	1.3	1.2	0.8	2.4	6.2	3.1
P_2O_5	0.5	0.2	0.1	0.2	0.1	0.1	0.9	0.2	0.2	0.2	0.2	0.2	1.2	1.5	1.8
Cr_2O_3	<0.002	0.01	0.025	0.006	0.025	0.024	<0.01	<0.01	<0.01	<0.01	<0.01	<0.01	0.017	0.094	<0.01
LOI	1.2	2.0	1.7	0.9	1.6	1.3	<0.01	0.4	0.4	0.2	0.2	0.9	1.4	1.7	0.4
TOT/C	<0.02	0.1	0.1	0.0	0.1	<0.02	ND	ND	ND	ND	ND	ND	0.0	0.1	ND
TOT/S	0.1	0.1	<0.02	<0.02	0.0	<0.02	ND	ND	ND	ND	ND	ND	0.2	0.1	ND
Sum	99.7	99.8	99.8	99.8	99.8	99.7	97.1	102.9	98.4	100.2	99.5	101.0	99.5	98.9	100.0
Trace Elements (ppm, except Au in ppb)															
Ba	639	400.0	207.0	271.0	192.0	220.0	722.0	446.0	327.0	301.0	291.0	258.0	2031.0	5228.0	2743.0
Rb	44.9	16.8	29.8	53.4	17.6	29.5	53.4	48.7	45.9	47.8	42.5	24.7	59.0	144.7	88.3
Sr	418.6	265.0	192.8	206.4	239.0	227.3	509.0	207.0	212.0	211.0	193.0	225.0	1126.7	2199.7	1441.0
Ga	20.9	16.4	15.0	17.8	17.0	16.6	28.7	24.0	22.8	22.4	23.3	21.3	18.4	15.8	25.0
Ta	1.7	0.4	0.4	0.8	0.4	0.4	2.1	0.7	0.7	0.8	0.7	0.6	1.6	0.8	<0.05

Nb	26	8.2	8.0	11.2	6.8	7.3	34.6	10.8	9.9	11.4	10.5	9.8	32.0	22.8	47.4
Hf	7.2	3.0	2.6	3.1	2.0	2.7	9.5	3.8	3.6	3.6	3.6	3.1	7.5	16.0	10.6
Zr	266.7	101.8	67.7	117.0	84.3	95.5	379.0	154.0	139.0	143.0	145.0	124.0	306.8	503.0	429.0
Y	39.2	22.1	21.7	30.3	20.2	22.2	47.6	29.7	26.9	26.5	26.9	22.5	25.5	25.1	38.5
Th	4.8	2.5	2.2	3.8	2.7	2.7	6.0	4.7	4.6	4.9	4.6	3.0	9.2	9.8	12.4
U	1	0.5	0.5	1.0	0.6	0.6	1.4	1.3	1.3	1.2	1.2	0.6	1.5	1.4	1.6
Ni	30.0	71.0	78.0	57.0	77.0	77.0	6.0	42.0	43.0	37.0	38.0	58.0	67.0	71.0	30.0
Co	37.3	41.9	36.0	35.8	42.0	43.3	51.1	57.4	53.7	59.8	58.0	59.4	31.5	28.1	67.5
Sc	27.0	37.0	37.0	35.0	36.0	38.0	ND	ND	ND	ND	ND	ND	17.0	27.0	ND
V	331.0	295.0	264.0	380.0	271.0	290.0	75.0	317.0	336.0	302.0	286.0	225.0	169.0	221.0	166.0
Cu	244.4	134.4	118.0	168.5	120.3	120.6	46.0	180.0	160.0	161.0	168.0	139.0	33.1	66.0	38.0
Pb	2.5	2.9	1.2	2.8	2.7	1.8	ND	ND	ND	ND	ND	ND	5.3	4.6	ND
Zn	97.0	62.0	50.0	66.0	49.0	42.0	157.0	117.0	110.0	109.0	116.0	98.0	85.0	61.0	151.0
W	0.5	<0.5	<0.5	0.6	<0.5	<0.5	119.5	68.1	62.2	108.1	89.7	82.9	0.6	<0.5	238.7
Mo	1.1	3.2	1.5	5.2	1.3	0.7	3	<2	<2	<2	<2	<2	2.2	1.8	3
Au	2.6	3.2	1.7	4.2	1.6	3.3	ND	ND	ND	ND	ND	ND	0.9	2.6	ND
As	<0.5	0.8	0.8	1.0	<0.5	<0.5	ND	ND	ND	ND	ND	ND	0.7	<0.5	ND
Rare Earth Elements (ppm)															
La	38.3	15.0	10.8	18.5	11.6	14.4	56.1	21.2	20.1	19.2	19.2	17.1	110.2	105.1	147.4
Ce	84.5	30.6	24.1	39.8	24.1	29.9	124.1	43.4	41.0	41.1	40.6	34.4	217.1	221.0	303.2
Pr	10.7	3.9	2.9	4.5	3.2	3.8	16.2	5.5	5.1	5.2	5.1	4.4	25.2	25.3	35.1
Nd	46.3	16.6	11.9	18.6	14.4	15.9	70.3	22.8	21.2	20.9	21.4	18.2	92.7	92.2	134.9
Sm	9.3	3.8	3.4	5.2	3.1	3.8	14.9	5.6	4.9	4.8	5.1	4.5	14.3	16.6	20.9
Eu	2.8	1.2	0.9	1.3	1.0	1.2	4.2	1.5	1.4	1.4	1.4	1.3	3.5	3.4	4.8
Gd	9.1	4.1	3.3	4.6	3.8	4.1	13.9	5.6	5.4	5.4	5.2	4.6	9.8	9.0	16.1
Tb	1.2	0.7	0.5	0.8	0.6	0.7	1.9	1.0	0.9	0.9	0.9	0.8	1.1	1.0	2.0
Dy	7.3	4.3	3.3	5.0	3.5	4.0	10.2	5.5	5.3	5.0	5.4	4.3	5.4	4.2	8.5
Ho	1.4	0.8	0.7	1.1	0.7	0.8	1.9	1.1	1.0	1.1	1.1	0.9	0.8	0.8	1.4
Er	3.8	2.3	2.1	2.7	2.1	2.3	5.0	3.0	2.9	2.9	3.1	2.5	2.1	1.7	3.5
Tm	0.5	0.3	0.3	0.4	0.3	0.3	0.7	0.5	0.4	0.4	0.4	0.4	0.3	0.3	0.4
Yb	3.2	2.1	1.6	2.7	2.0	2.0	4.0	2.8	2.7	2.7	2.6	2.3	2.0	1.5	2.5

Lu	0.5	0.3	0.3	0.4	0.3	0.3	0.6	0.5	0.4	0.4	0.4	0.4	0.3	0.2	0.4
Mg#	31.0	47.4	53.0	38.7	52.5	53.4	26.9	39.7	42.1	38.0	39.2	46.4	47.3	62.0	34.5
$\sum_{REE}$	218.8	86.0	65.8	105.5	70.7	83.4	323.9	119.9	112.8	111.3	111.7	96.0	484.7	482.2	681.1
Eu/Eu*	0.9	0.9	0.8	0.8	0.9	0.9	0.9	0.8	0.9	0.8	0.9	0.9	0.9	0.8	0.8
$La/Yb_{(N)}$	3.9	2.3	2.2	2.2	1.9	2.4	4.5	2.4	2.4	2.3	2.4	2.4	18.1	21.9	18.9
$La/Sm_{(N)}$	2.7	2.6	2.0	2.3	2.4	2.5	2.4	2.4	2.7	2.6	2.4	2.5	5.0	4.1	4.6
$Lu/Hf_{(N)}$	0.8	0.5	1.0	0.3	1.4	1.3	2.6	0.6	1.6	2.4	1.3	0.4	0.8	0.8	1.2
$Nb/La_{(N)}$	0.7	0.5	0.7	0.6	0.6	0.5	0.6	0.5	0.5	0.6	0.5	0.6	0.3	0.2	0.3
$La/Nb_{(N)}$	1.5	1.9	1.4	1.7	1.8	2.0	1.7	2.0	2.1	1.8	1.9	1.8	3.6	4.8	3.2

Table 3-2

CIPW normative values for the studied samples. All values are expressed in wt%.

Sample	Q	Or	Ab	An	Ne	Di	Hy	Ol	Il	Hm	Tn	Pf	Ru	Ap	Sum
Group 1															
Muqui	11.465	10.992	22.677	17.539	0.000	5.846	6.830	0.000	0.342	15.220	7.831	0.000	0.000	1.279	100.021
Jerônimo Monteiro	6.989	3.959	18.954	28.649	0.000	16.084	8.883	0.000	0.449	12.950	2.611	0.000	0.000	0.474	100.004
Castelo	7.102	4.846	17.600	28.543	0.000	17.615	10.017	0.000	0.385	11.530	2.031	0.000	0.000	0.332	100.000
Itaoca A	12.075	8.333	21.916	21.182	0.000	11.879	6.748	0.000	0.428	13.900	3.080	0.000	0.000	0.474	100.014
Cobiça	8.426	3.546	17.262	29.317	0.000	17.484	9.729	0.000	0.364	11.520	2.034	0.000	0.000	0.308	99.990
Lajinha	7.705	5.023	18.108	27.530	0.000	17.176	10.270	0.000	0.385	11.360	2.105	0.000	0.000	0.308	99.970
Cantagalo	16.034	7.446	20.900	20.963	0.000	12.121	5.614	0.000	0.449	13.130	2.955	0.000	0.000	0.379	99.992
Iúna	16.714	13.651	26.401	13.170	0.000	2.654	5.545	0.000	0.471	13.200	6.094	0.000	0.000	2.132	100.030
Jerônimo Monteiro B	12.398	4.728	18.954	24.828	0.000	17.287	6.482	0.000	0.406	11.970	2.593	0.000	0.000	0.355	100.001
Itaoca B	15.740	7.269	21.154	21.026	0.000	12.416	5.801	0.000	0.428	12.840	2.958	0.000	0.000	0.379	100.012
Nogueira	14.423	7.860	22.508	20.558	0.000	12.301	5.905	0.000	0.406	12.630	2.985	0.000	0.000	0.426	100.002
São Manoel	14.838	7.505	21.408	21.701	0.000	12.776	6.282	0.000	0.406	11.990	2.715	0.000	0.000	0.379	100.001
Group 2															
Santa Angélica	4.642	14.420	24.877	21.780	0.000	0.728	13.636	0.000	0.321	11.140	5.600	0.000	0.000	2.913	100.057
Itaici	0.000	37.704	13.473	8.806	3.336	9.556	0.000	11.435	0.278	9.110	0.000	2.696	0.000	3.577	99.971
Caxixe	13.924	18.616	22.170	17.982	0.000	0.000	8.444	0.000	0.299	11.440	0.555	0.000	2.357	4.311	100.097

3.4.4. U-Pb data

Zircon grains were extracted from two samples, one from each group, for U-Pb analysis. The results are shown in Table 3 and in the Concordia diagrams of Figure 3-8.

3.4.4.1. Group 1: Cobiça dyke

A total of 28 zircon grains were recovered and analyzed from the Cobiça dyke samples. Zircon grains are large (up to 400 μm), mainly alongated prisms with length/width ratios of up to 1:5, colourless and clear (showing no inclusions). CL (cathodoluminescence) images shows well defined internal oscillatory zoning (Figure 3-8a). All zircons show high Th/U ratios between 0.13 and 0.50, typical of igneous zircons (Rubatto, 2002; Hoskin and Schaltegger, 2003). The analyzed zircons show very homogeneous $^{207}Pb/^{235}U$ and $^{206}Pb/^{238}U$ ratios, clustering around the Concordia and yielding three distinguishable Concordia ages of 141.9 ± 1.9 Ma, 146.8 ± 1.1 Ma, and 150.6 ± 0.77 Ma (Figure 3-8a). We consider the Concordia age of 141.9 ± 1.9 Ma as the best estimate for the crystallization age and emplacement of the dyke, while the other two ages are interpreted as remnants from protracted phases of magma development before the final emplacement. A single inherited zircon yielded a $^{206}Pb/^{238}U$ age of 250 ± 2 Ma.

3.4.4.2. Group 2: Santa Angélica dyke

Twenty-nine zircon grains up to 200 μm long, colourless and inclusion-free, were recovered from this dyke. Zircon grains are prismatic with some rounded to sub-rounded grains, and length/width ratios of 1:2 to 1:3. The Th/U ratios vary between 0.20 and 2.16. The youngest zircon grains define the Concordia age of 504.7 ± 6.9 Ma, but abundant inherited zircons in the 500-600 Ma age range occur (Figure 3-8b), broadly corresponding to the age ranges of G1 (630-585 Ma), G2 (585-565 Ma), and G3 (565-535 Ma) Supersuite plutons of the Araçuaí-Ribeira Orogen basement in the area. A single concordant inherited zircon also yielded a $^{207}Pb/^{206}Pb$ age of 1910 ± 32 Ma. Other inherited zircons show discordance above ± 10% and are not considered here.

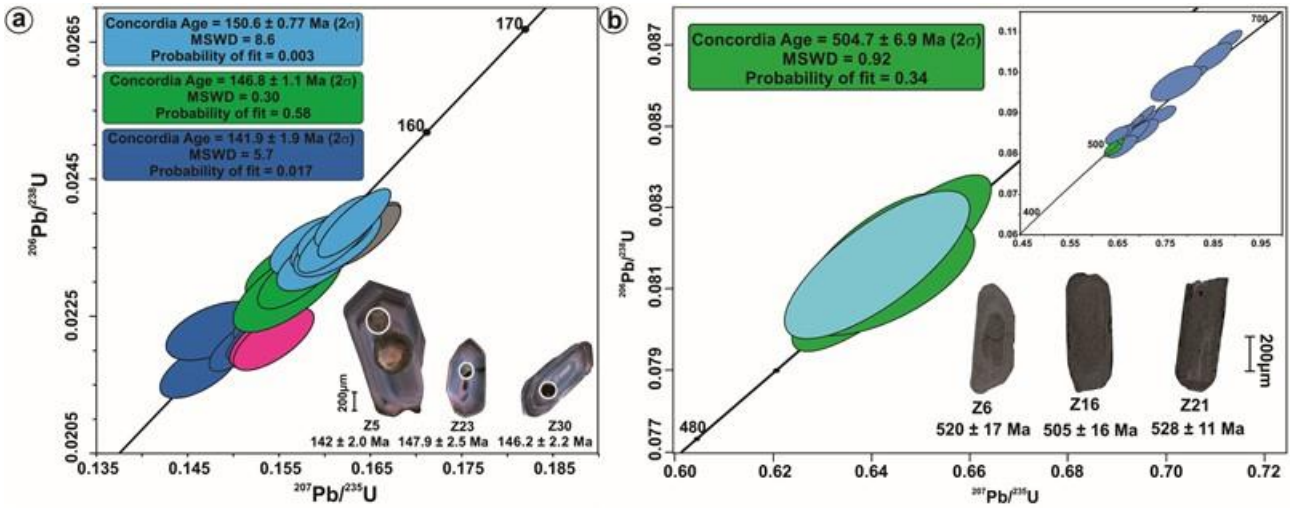

Figure 3-8: (a) Concordia diagram and cathodoluminescence images of the zircon grains from the Cobiça dyke and (b) Concordia diagram and backscattered electron images of the zircon grains from the Santa Angélica dyke.

3.4.5. Sm-Nd and Rb-Sr isotopes

Sm-Nd and Rb-Sr isotope analysis also shows a broad distinction between the tholeiitic dykes of Group 1 and the alkaline dykes of Group 2. According to the U-Pb zircon data, the initial isotopic values were recalculated to 140 Ma for the Group 1 dykes and 500 Ma for the Group 2 dykes (Table 4).

In general, Group 2 dykes show higher concentrations of Sm (>17 ppm) and Nd (>115 ppm), initial $^{143/144}$Nd of ca. 0.5113 corresponding to highly negative εNd(t) of ca. -13 and older T_{DM} model ages (DePaolo, 1981) of 1.7-1.9 Ga, high Rb (>60 ppm) and Sr (>1000 ppm) concentrations, and initial $^{87/86}$Sr of 0.706-0.709. Group 1 dykes, in contrast, show way lower Sm (<11 ppm), Nd (<55 ppm), Rb (<53 ppm) and Sr (<418 ppm) concentrations; initial $^{143/144}$Nd of ca. 0.5121-0.5123 corresponding to less negative $\varepsilon Nd_{(t)}$ of ca. -3 to -4 (with exception of the Lajinha dyke which shows $^{143/144}$Nd of ca. 0.5119 and $\varepsilon Nd_{(t)}$ = -9); younger T_{DM} model ages of 0.8-1.5 Ga; and initial $^{87/86}$Sr of 0.704-0.706.

Thus, the Sm-Nd and Rb-Sr isotope data strongly support the subdivision of the studied dykes into two distinct groups, each with homogeneous isotopic features, as also suggested by field, petrographic, lithochemical and geochronological data. The tholeiitic dykes of Group 1 have younger, Neo to Mesoproterozoic model ages, lower elemental concentrations and isotopic signatures closer to the mantle (lower $^{87/86}$Sr and higher $^{143/144}$Nd), although crustal contamination to some degree is certainly implied by the negative $\varepsilon Nd_{(t)}$ values. The alkaline dykes of Group 2 represent the reworking of much older continental crust (older Paleoproterozoic T_{DM}, higher $^{87/86}$Sr and lower $^{143/144}$Nd).

Table 3-3

U-Pb (LA-ICP-MS) results for magmatic zircon crystals from the Cobiça and Santa Angélica dykes. Colors correspond to zircons used in the Concordias of Fig. 8. N – Analysis in zircon nucleus and B – Analysis in zircon border.

Group 1 - Cobiça dyke																	
	Concentrations	Isotope ratios									Apparent ages (Ma)						
Zircon	Th/U	$^{206}Pb/^{204}Pb$	f_{206}%	$^{207}Pb/^{206}Pb$	1σ (%)	$^{207}Pb/^{205}U$	1σ (%)	$^{206}Pb/^{208}U$	1σ (%)	ρ	$^{207}Pb/^{206}Pb$	1σ (%)	$^{207}Pb/^{205}U$	1σ (%)	$^{206}Pb/^{208}U$	1σ (%)	Conc. (%)
Z1	0.24	11104.3	0.163	0.048772	0.99	0.1463	1.30	0.021757	0.84	0.62	137	23	139	2	139	1	100
Z3	0.29	40938.4	0.045	0.049035	0.63	0.1553	1.08	0.022977	0.87	0.79	149	15	147	1	146	1	100
Z5	0.20	16008.7	0.102	0.049898	0.65	0.1527	0.96	0.022197	0.70	0.69	190	15	144	1	142	1	98
Z6N	0.50	110231.9	0.017	0.051641	0.27	0.2816	0.77	0.039548	0.72	0.92	270	6	252	2	250	2	99
Z7	0.26	41038.3	0.045	0.049228	0.80	0.1570	1.20	0.023128	0.89	0.72	159	19	148	2	147	1	100
Z8	0.14	26687.8	0.062	0.049206	0.59	0.1622	0.90	0.023908	0.68	0.72	158	14	153	1	152	1	100
Z9	0.17	36792.4	0.050	0.049527	0.52	0.1631	1.00	0.023884	0.85	0.84	173	12	153	1	152	1	99
Z10	0.43	19613.8	0.094	0.048034	1.23	0.1477	1.46	0.022295	0.79	0.51	101	29	140	2	142	1	102
Z11	0.23	23082.8	0.080	0.049326	0.90	0.1612	1.15	0.023709	0.72	0.58	163	21	152	2	151	1	100
Z12	0.34	20338.4	0.095	0.049314	0.80	0.1605	1.09	0.023604	0.75	0.65	163	19	151	2	150	1	100
Z14	0.44	23021.4	0.080	0.050161	0.60	0.1641	0.98	0.023733	0.78	0.76	202	14	154	1	151	1	98
Z15	0.24	13177.2	0.140	0.049462	0.87	0.1591	1.17	0.023329	0.78	0.64	170	20	150	2	149	1	99
Z17	0.31	29737.2	0.062	0.049837	0.60	0.1602	0.91	0.023316	0.68	0.71	187	14	151	1	149	1	98
Z18	0.30	18161.3	0.102	0.049403	0.68	0.1613	1.14	0.023679	0.92	0.79	167	16	152	2	151	1	99
Z19	0.30	26142.4	0.075	0.050259	0.55	0.1643	0.95	0.023705	0.78	0.79	207	13	154	1	151	1	98
Z20N	0.14	32621.6	0.057	0.051634	0.50	0.1662	0.98	0.023351	0.84	0.84	269	12	156	1	149	1	95
Z20B	0.18	16007.9	0.115	0.053058	0.75	0.1762	1.02	0.024092	0.68	0.63	331	17	165	2	153	1	93
Z22	0.30	13275.6	0.109	0.049563	0.89	0.1612	1.23	0.023591	0.85	0.67	175	21	152	2	150	1	99
Z23	0.27	18795.5	0.098	0.048637	0.89	0.1558	1.24	0.023226	0.86	0.67	130	21	147	2	148	1	101
Z24	0.21	12746.6	0.145	0.048880	1.03	0.1588	1.30	0.023564	0.80	0.58	142	24	150	2	150	1	100
Z25	0.20	8003.0	0.231	0.049320	1.11	0.1558	1.58	0.022905	1.12	0.70	163	26	147	2	146	2	99
Z26	0.29	17342.3	0.096	0.051315	0.71	0.1683	1.00	0.023790	0.71	0.67	255	16	158	1	152	1	96
Z28	0.28	28863.9	0.064	0.050847	0.59	0.1753	1.16	0.025009	0.99	0.85	234	14	164	2	159	2	97
Z29	0.28	23089.8	0.090	0.050574	0.69	0.1758	1.11	0.025214	0.87	0.76	221	16	164	2	161	1	98

Z30	0.23	31037.4	0.060	0.049174	0.63	0.1554	0.99	0.022919	0.77	0.75	156	15	147	1	146	1	100
Z31	0.23	14381.5	0.129	0.050346	0.82	0.1541	1.17	0.022196	0.84	0.69	211	19	146	2	142	1	97
Z32	0.17	47566.9	0.039	0.049450	0.47	0.1534	1.15	0.022501	1.05	0.91	169	11	145	2	143	1	99
Z33	0.36	13408.4	0.121	0.049332	0.80	0.1533	1.05	0.022539	0.68	0.60	164	19	145	1	144	1	99
Z34	0.22	20653.8	0.090	0.049566	0.69	0.1511	1.05	0.022104	0.80	0.73	175	16	143	1	141	1	99

Group 2 - Santa Angélica dyke

	Concentrations	Isotope ratios									Apparent ages (Ma)						
Zircon	**Th/U**	**$^{206}Pb/^{204}Pb$**	**f_{206}%**	**$^{207}Pb/^{206}Pb$**	**1σ (%)**	**$^{207}Pb/^{205}U$**	**1σ (%)**	**$^{206}Pb/^{208}U$**	**1σ (%)**	**ρ**	**$^{207}Pb/^{206}Pb$**	**2σ abs**	**$^{207}Pb/^{205}U$**	**2σ abs**	**$^{206}Pb/^{208}U$**	**2σ abs**	**Conc (%)**
ZR1	0.22	7019.9	0.222	0.077972	3.21	0.8442	4.57	0.078515	3.23	0.71	1146	125	621	42	487	30	43
ZR2	0.99	12859.3	0.121	0.058723	1.19	0.5598	1.95	0.069129	1.50	0.77	557	51	451	14	431	12	77
ZR3	1.61	336.7	4.624	0.155501	2.90	22.073	3.35	0.102941	1.65	0.49	2407	97	1183	46	632	20	26
ZR4	0.37	8729.7	0.179	0.066564	6.30	0.3862	12.94	0.042077	11.30	0.87	824	252	332	72	266	59	32
ZR5	0.28	15567.3	0.100	0.058737	2.14	0.6635	3.10	0.081923	2.21	0.71	557	92	517	25	508	22	91
ZR6	0.32	2441.1	0.638	0.055723	1.75	0.6512	2.46	0.084750	1.69	0.69	441	77	509	20	524	17	119
ZR7	0.45	38125.6	0.041	0.056296	1.79	0.6581	2.67	0.084772	1.94	0.73	464	78	513	21	525	20	113
ZR8	0.40	8527.4	0.183	0.073366	3.57	0.7562	6.02	0.074748	4.84	0.80	1024	141	572	52	465	43	45
ZR9	0.50	27539.7	0.057	0.059499	1.23	0.8871	1.97	0.108130	1.50	0.76	585	53	645	19	662	19	113
ZR10	0.57	24928.5	0.062	0.059428	2.05	0.8532	3.11	0.104120	2.31	0.74	583	88	626	29	639	28	110
ZR11	1.04	46.1	33.743	0.301131	13.44	41.356	15.99	0.099598	8.67	0.54	3476	388	1661	246	612	101	18
ZR12	1.07	3146.3	0.495	0.057412	1.41	0.6433	1.86	0.081255	1.15	0.62	507	62	504	15	504	11	99
ZR13	1.20	4289.2	0.363	0.059429	2.53	0.7011	3.57	0.085562	2.50	0.70	583	108	539	30	529	25	91
ZR14	1.24	14448.2	0.108	0.058759	1.48	0.6836	3.35	0.084374	2.98	0.89	558	64	529	27	522	30	94
ZR15	1.16	41698.1	0.037	0.055071	2.35	0.6170	2.64	0.081255	1.14	0.43	415	103	488	20	504	11	121
ZR16	0.46	114527.7	0.014	0.057220	1.06	0.6441	2.08	0.081634	1.76	0.84	500	46	505	17	506	17	101
ZR17	1.19	2171.4	0.718	0.061539	0.96	0.7163	1.92	0.084411	1.62	0.84	658	41	548	16	522	16	79
ZR18	0.26	22504.7	0.069	0.057744	3.46	0.7759	4.57	0.097452	2.97	0.65	520	148	583	40	599	34	115
ZR19	0.44	63798.0	0.024	0.057425	0.92	0.7096	2.02	0.089616	1.76	0.87	508	40	545	17	553	19	109
ZR20	0.57	159092.6	0.010	0.056693	0.83	0.6404	1.46	0.081918	1.15	0.78	480	36	503	12	508	11	106
ZR21	0.36	148876.1	0.010	0.056575	0.82	0.6729	1.49	0.086251	1.18	0.79	475	36	522	12	533	12	112

ZR22	0.30	123165.0	0.013	0.056994	0.69	0.6932	1.31	0.088205	1.05	0.80	491	30	535	11	545	11	111
ZR23	0.77	14516.2	0.107	0.060405	1.77	0.7477	2.42	0.089767	1.60	0.66	618	76	567	21	554	17	90
ZR24	0.62	53682.7	0.028	0.112957	1.21	55.608	1.88	0.357020	1.39	0.74	1848	43	1910	32	1968	47	107
ZR25	0.37	7906.4	0.197	0.058357	0.70	0.7190	1.28	0.089348	1.00	0.79	543	30	550	11	552	11	102
ZR26	0.21	14213.3	0.110	0.060567	7.42	0.7368	8.34	0.088221	3.79	0.45	624	305	561	71	545	40	87
ZR27	0.92	43792.3	0.036	0.059525	1.01	0.8219	1.49	0.100130	1.03	0.69	586	44	609	14	615	12	105
ZR28	0.46	75836.1	0.021	0.059042	0.75	0.7897	1.15	0.097000	0.79	0.69	569	33	591	10	597	9	105
ZR29	2.16	37.7	41.189	0.506194	19.89	89.983	27.74	0.128917	19.33	0.70	4259	530	2338	453	782	282	18

Table 3-4

Sm–Nd and Rb-Sr isotope data of dyke samples from the southern Espírito Santo state. Initial isotope ratios are calculated for t = 140 Ma for Group 1 for t = 500 Ma for Group 2. (m) – measured; (i) – initial (calculated). T_{DM} model ages after DePaolo (1981).

Group 1

Sample	Sm (ppm)	Nd (ppm)	$^{147}Sm/^{144}Nd$	$^{143}Nd/^{143}Nd_{(m)}$ ± 2σ (abs)	$\varepsilon Nd_{(0)}$	$^{143}Nd/^{143}Nd_{(i)}$	$\varepsilon Nd_{(i)}$	T_{DM} (Ga)	Rb (ppm)	Sr (ppm)	$^{87}Rb/^{86}Sr_{(m)}$	$^{87}Sr/^{86}Sr_{(m)}$	$\varepsilon Sr_{(0)}$	$^{87}Sr/^{86}Sr_{(i)}$	$\varepsilon Sr_{(i)}$
Cobiça	2.25	15.24	0.0894	0.512368 ± 16	-5.3	0.512286	-3.4	0.83	17.6	239.0	0.198189	0.708870	62.0	0.708446	58.4
Muqui	11.80	55.53	0.1285	0.512426 ± 20	-4.1	0.512308	-2.9	1.10	44.9	418.6	0.310305	0.706670	30.8	0.706053	24.4
Lajinha	5.68	32.37	0.1061	0.512069 ± 27	-11.1	0.511972	-9.5	1.37	29.5	227.3	0.349290	0.708760	60.5	0.708013	52.2
Jerônimo Monteiro A	4.59	19.89	0.1394	0.512346 ± 10	-5.7	0.512218	-4.7	1.41	16.8	265.0	0.183428	0.708080	50.8	0.707715	48.0
Itaoca A	5.89	25.67	0.1388	0.512337 ± 30	-5.9	0.512210	-4.8	1.42	53.4	206.4	0.748740	0.710360	83.2	0.708870	64.4
Castelo	3.80	16.40	0.1400	0.512300 ±12	-6.6	0.512172	-5.6	1.52	29.8	192.8	0.447259	0.709190	66.6	0.708300	56.3

Group 2

Sample	Sm (ppm)	Nd (ppm)	$^{147}Sm/^{144}Nd$	$^{143}Nd/^{143}Nd_{(m)}$ ± 2σ (abs)	$\varepsilon Nd_{(0)}$	$^{143}Nd/^{143}Nd_{(i)}$	$\varepsilon Nd_{(i)}$	T_{DM} (Ga)	Rb (ppm)	Sr (ppm)	$^{87}Rb/^{86}Sr_{(m)}$	$^{87}Sr/^{86}Sr_{(m)}$	$\varepsilon Sr_{(0)}$	$^{87}Sr/^{86}Sr_{(i)}$	$\varepsilon Sr_{(i)}$
Itaici	18.46	124.14	0.0899	0.511643 ± 13	-19.4	0.511354	-12.7	1.71	144.7	2199.7	0.190329	0.708010	49.8	0.706681	39.2
Santa Angélica	17.53	115.16	0.0920	0.511605 ± 15	-20.2	0.511310	-13.6	1.79	59.0	1126.7	0.151514	0.708240	53.1	0.707182	46.3
Caxixe	21.49	129.99	0.0999	0.511623 ± 10	-19.8	0.511302	-13.8	1.89	88.3	1441.0	0.177330	0.710020	78.4	0.708782	69.0

Table 3-5

Variation of chondrite-normalized elemental ratios considering the concentrations in the most primary and most evolved samples of each group. Normalizing values after Sun and McDonough (1989).

	$Zr/Y_{(N)}$	$Zr/Nb_{(N)}$	$Y/Nb_{(N)}$	$La/Yb_{(N)}$	$La/Nb_{(N)}$
Group 1					
Lajinha dyke (primary sample)	1.75	0.83	0.87	2.37	2.05
Iúna dyke (evolved sample)	3.24	0.70	0.37	4.49	1.68
Variation of ratio (%)	**85**	19	**131**	**90**	22
Group 2					
Itaici dyke (primary sample)	8.14	1.40	0.22	21.85	4.78
Caxixe dyke (evolved sample)	4.53	0.58	0.17	18.89	3.23
Variation of ratio (%)	**80**	**144**	28	16	48

3.5. DISCUSSION

3.5.1 Petrogenesis

3.5.1.1. Fractional Crystallization

With exception of major elements CaO, Al_2O_3, and trace elements Ni, Sc and Y, which show positive correlations, most other elements of Group 1 samples show a strong negative correlation with MgO, forming a continuous evolutionary trend that is consistent with fractional crystallization (Bellieni et al., 1984; Picardillo and Melfi, 1988; Peate et al., 1992). The diminishing of CaO and Al_2O_3 indicates that fractionation was controlled by the crystallization of Ca-rich plagioclase and a Ca-rich pyroxene (e.g. augite) (Cox et al., 1979). The Ni contents decrease suggests the crystallization of olivine (Figure 3-7), as observed in the petrographic analysis and confirmed by the mineral chemistry. Subtle Eu anomalies also indicate plagioclase fractionation, and the LREE-enriched patterns might indicate pyroxene fractionation. Group 2 samples are too few to indicate any possible evolutionary trend.

Microanalysis-based thermometry suggest that the pyroxene crystals were crystallized between 1200 °C to 1000 °C, ranging from the core to the grain boundaries of Group 1 dykes. Pyroxenes of dykes from Group 2 crystallized in a larger range, but at lower temperatures, from 1100 °C to < 500 °C. Group 1 plagioclase crystallized at temperatures ranging from 1200 °C to 1100 °C and again, Group 2 reports a lower temperature for the crystallization of plagioclase crystals, between 1100 °C and 1000 °C (Figure 3-4c and 3-4f).

According to Cox et al. (1979), either the Fractional Crystallization (FC) or As similation and Fractional Crystallization (AFC) processes can be inferred from normalized incompatible trace element ratios ($Zr/Y_{(N)}$, $Zr/Nb_{(N)}$, $Y/Nb_{(N)}$, $La/Yb_{(N)}$ and $La/Nb_{(N)}$). Those ratios usually do not vary above 50% for FC, as they do for AFC. The studied samples, however, do not present a well-defined pattern for these ratios, as some of them show variations above 50% while others do not (Table 5). To better constrain if crustal contamination was responsible for the development of the variations in the trace elements and isotopic compositions, a diagram comparing Sr concentrations with the initial $^{87}Sr/^{86}Sr$ ratios can be used (Ngonge et al., 2016). In such diagram, the initial $^{87}Sr/^{86}Sr$ ratios show a typical trend of FC, especially for Group 1 samples (Figure 3-9a).

3.5.1.2. Crustal Assimilation

The gathered data suggest a variable degree of crustal contamination, which was higher in alkaline dykes of Group 2 than in tholeiitic dykes of Group 1. This continental signature can be introduced either by contamination during magma uprising through the crust or, alternatively, it might reflect the character of a metasomatized mantle source (Liu et al., 2008).

For Group 2 alkaline dykes, the high contents of Ba, Th, and LREE, besides the lower contents of Nb, Ta, Ti, Y, and HREE, suggest the assimilation of variable contents of felsic crustal rocks (Puchtel et al., 1998). Crustal contamination of the alkaline dykes is also suggested by the isotope data, with higher Initial $^{87}Sr/^{86}Sr$ (0.7064 – 0.7088), more negative $\varepsilon Nd_{(t)} < -12$ and older T_{DM} around 1.7-1.9 Ga. The presence of xenoliths of the country gneiss in the Itaici dyke also supports crustal assimilation. Group 1 tholeiitic dykes, on the other hand, show less expressive, but yet important, crustal assimilation with Initial $^{87}Sr/^{86}Sr$ of 0.7041 – 0.7065, $\varepsilon Nd_{(t)}$ of -3.4 to -5.5 (with an abnormal value of -9.5 for the Lajinha dyke), and younger T_{DM} of 0.8-1.5 Ga. It is important to notice that both Sr and Nd isotope ratios and factors do not overlap, in general, between groups 1 and 2, characterizing two very distinct groups.

A possible indicator of contamination by intermediate to felsic crust is the P_2O_5/K_2O ratio (Carlson and Hart, 1987; Hart et al., 1997), as silica-rich crustal rocks show P_2O_5/K_2O generally below 0.1 while mantle-derived magmas show higher P_2O_5/K_2O. The diminishing of P_2O_5/K_2O with rising $^{87}Sr/^{86}Sr_{(i)}$ is thus expected for basic magmas mixed with crustal materials. This fact, observed in Group 1 dykes, suggests that crustal contamination occurred during their emplacement. Group 2 samples are too few to indicate clear trends (Figure 3-9). Another proxy that can be used to assess crustal contamination is the Ce/Pb ratio, which according to Muzio et al. (2012), is lower than 25 when crustal contamination is important. This is the value shown by most of the samples.

The negative correlation between MgO and $^{87}Sr/^{86}Sr_{(i)}$ is evident, as well as the positive correlation between $^{87}Sr/^{86}Sr_{(i)}$ and SiO_2, thus characterizing contamination by upper continental crust (Figure 3-9). This is also evident in the $Th/Ta_{(N)}$ and $La/Nb_{(N)}$ ratios above 1 (Figure 3-10) (Neal et al., 2002), suggesting contamination with crustal material similar to that of the upper crust.

Zirconium in general is not saturated in mafic magmas (Watson and Harrison, 1983). Thus, besides the enriched geochemical and isotope proxies, the massive presence of inherited zircons in the Santa Angélica dyke sample (Figure 3-8) is another expressive

evidence for assimilation of the crustal country rocks, especially ca. 600-535 Ma granites related to the G1-G2-G3 Supersuites of the Araçuaí Orogen.

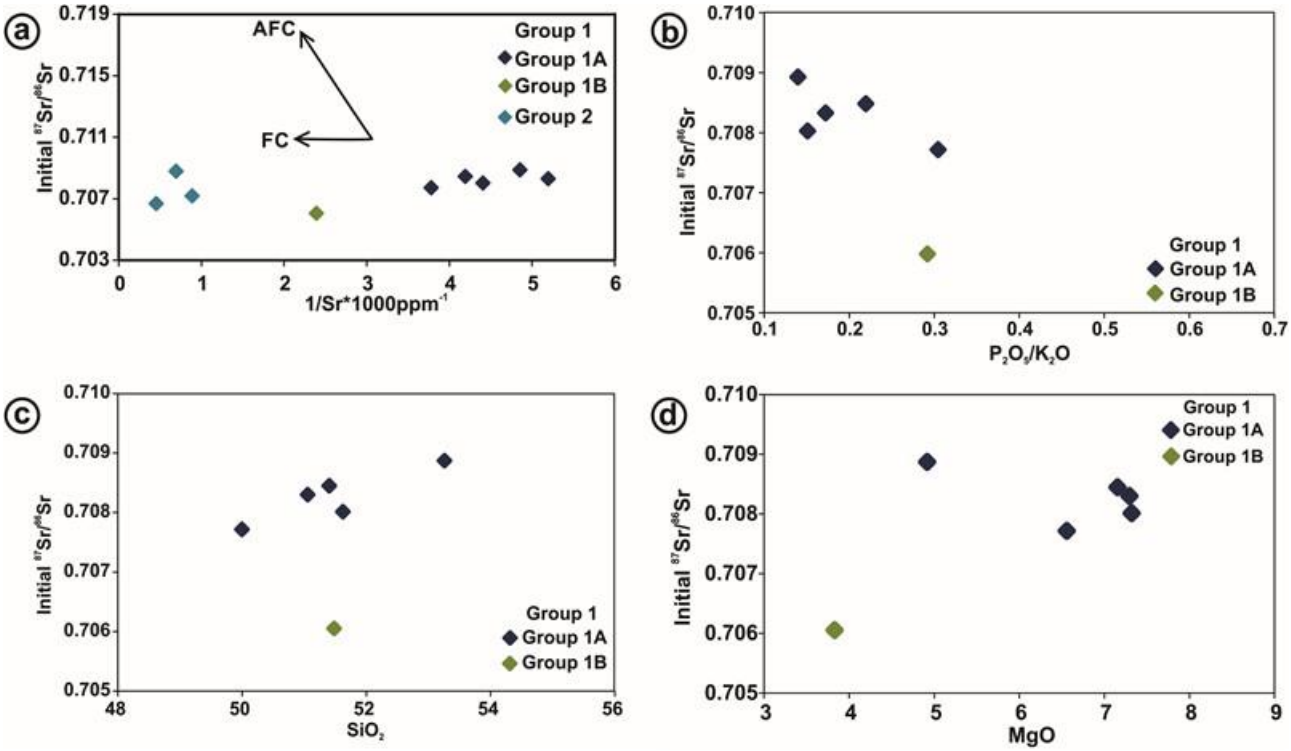

Figure 3-9: (a) Initial $^{87}Sr/^{86}Sr$ *versus* 1/Sr*1000 used to evaluate crustal contamination level in the mafic magmas; (b) initial $^{87}Sr/^{86}Sr$ versus P_2O_5/K_2O; (c) initial $^{87}Sr/^{86}Sr$ versus SiO_2 and (d) initial $^{87}Sr/^{86}Sr$ versus MgO for the mafic dyke samples.

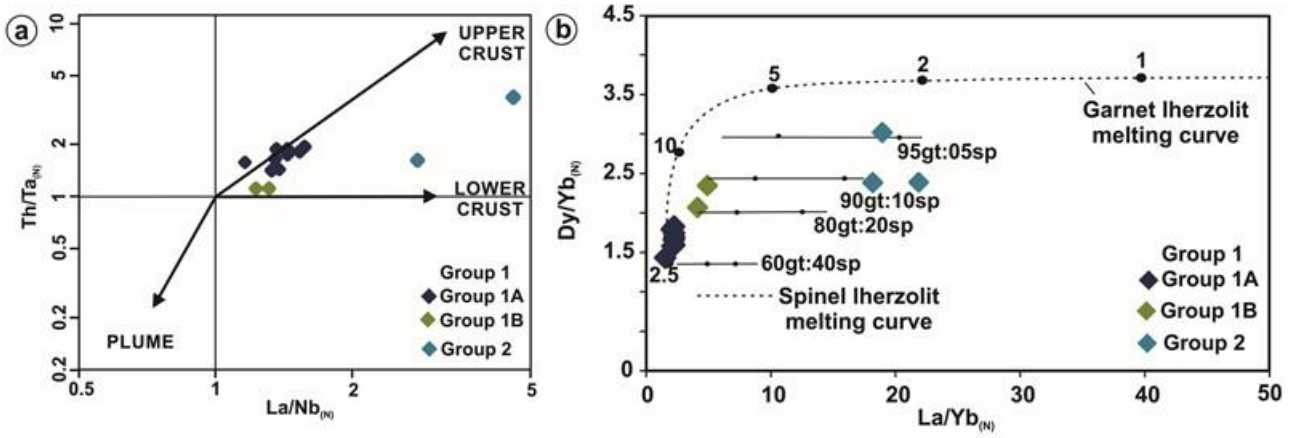

Figure 3-10: (a) $Th/Ta_{(N)}$ *versus* $La/Nb_{(N)}$ normalized to the Primitive Mantle (McDonough and Sun, 1989 after Neal et al., 2002); (b) mixing model curves of spinel and garnet lherzolites using $Dy/Yb_{(N)}$ versus $La/Yb_{(N)}$ ratios to estimate the partial melting ratios and magma source for the dykes (after Ngonge et al., 2016).

3.5.1.3. Nature of the sources and tectonic setting

Pearce (2008) proposed an additional incompatible elements normalization of mafic magmas to Ti = 1, in order to identify the effects of crustal contamination, partial melting degree, source composition and depth of melting on the composition of mafic rocks. In this normalization, the left-hand segment (Ba-Ta) is mainly controlled by crustal contamination, the central segment (La-Hf) is controlled by the degree of partial melting and source composition and the right-hand segment (Tb-Yb) is controlled by the depth of melting. In our study, all samples show significant crustal assimilation, as discussed above, and the alkaline dykes of Group 2 show significantly higher Ba-Ta normalized values (above 10 times the primitive mantle values) (Figure 3-6c). All of the samples are situated above the Primitive Mantle values in the central segment (La-Hf), suggesting the involvement of enriched sources and / or a low melting degree, once again with significantly higher values for the alkaline dykes of Group 2. For the right-hand (Ti-Yb) segment, the alkaline dykes show values way below the Primitive Mantle, thus suggesting high depths of melt generation. For Group 1 tholeiitic dykes, however, the interpretation is more contentious, as they plot near the Primitive Mantle line. The relatively higher HREE contents of Group 1 dykes indicates that they probably derived from a garnetless source, as this mineral entraps HREE such as Tb, Yb and Y in its structure. Thus, partial melting of a mantle source within the spinel stability field, in depths greater than 40 km, probably composed the primary magma source of the tholeiitic dykes. The alkaline dykes of Group 2, on the other hand, were originated in deeper sources (> 40 km), where garnet becomes stable.

$Dy/Yb_{(N)}$ and $La/Yb_{(N)}$ ratios can be used to model the levels of magma generation, at the same time providing an estimate of the melting degree and magma fractionating (Thirwall et al., 1994) (Figure 3-10). Melting of a spinel lherzolite mantle source results in minimal variations of the Dy/Yb ratios, while melting of a garnet lherzolitic mantle generates higher Dy/Yb and more significate HREE depletions. This plot evidences that the tholeiitic dykes of Group 1 are more influenced by spinel lherzolitic sources, though concentrated in the transition zone between the two mantle types. The alkaline dykes, on the other hand, are clearly generated in the garnet lherzolite zone. Thus, the tholeiitic dykes probably were generated by a mixing of shallow (spinel-rich) and deep (garnet-rich) mantle sources, while the alkaline dykes were generated strictly by a deep mantle source (Figure 3-6c and 3-10).

The low $^{143}Nd/^{144}Nd$ ratios and elevated $^{87}Sr/^{86}Sr$ ratios plots the dyke samples between the EMI (Enriched Mantle I) and EMII (Enriched Mantle II) enriched mantle fields. This could be due to a possible enriched oceanic or sublithospheric source, characterized

by the enrichment in Rb and LREE resulting in non-radiogenic Sr and Nd ratios (Allègre, 2008). According to Ernst (2014), EMII might represent the influence of subducted sediments, reflecting a continental crust signature.

Total REE contents of the alkaline dykes of Group 2 are extremely high ($\sum_{REE}$> 100 ppm) suggesting that the source is not purely mantellic (Table 1). Tholeiitic dykes of Group 1, on the other hand, show total REE contents mostly below 100 (Jerônimo Monteiro, Castelo, Cobiça and Lajinha dykes) similar to the enriched MORB (Mid-Ocean Ridge Basalt) reservoir. All of the dykes, however, show a typical negative Nb-Ta anomaly, characteristic of the continental crust. Those anomalies, along with the isotope signatures, are attributed to a Subcontinental Lithospheric Mantle (SCLM) (Piccirillo and Melfi, 1988; Hawkesworth et al., 1992; Marques et al., 1999; Liu et al., 2008). This is supported by $La/Nb_{(N)}$>1 and $La/Yb_{(N)}$> 1, typical of enriched sources, which, in various basaltic provinces around the world, have been associated with melting of the SCLM (Marques et al., 1999; Corval et al., 2009). Sun and McDonough (1989) also point out that volcanic rocks with MORB and OIB signatures do not show negative HFS anomalies, thus distinct from the studied dykes.

The $La/Nb_{(N)}$ (1.4-4.8) and $Ba/Nb_{(N)}$ (2.1-23.4) ratios of the dykes are similar to most of intraplate volcanic rocks (Liu et al., 2008), as well as the $Nb/Th_{(N)}$ (0.20-0.90) and $Nb/La_{(N)}$ (0.20-0.70) ratios which are similar to those of OIB (Oceanic Island Basalts) generated from EMI (e.g., Eisele et al., 2002). Low $Nb/La_{(N)}$ (<1) are characteristic of subduction-related magmatism (McCullouch and Gamble, 1991) and sublithospheric melts show Nb/La around 0.5 (Peate and Hawkesworth, 1996) (Table 1).

To summarize, the tholeiitic dykes of Group 1 were generated through a low degree of partial melting of an enriched mantle sourced in shallow depths (below 40 km), probably similar to the Subcontinental Lithospheric Mantle (SCLM), which was previously chemically altered by metasomatization processes as shown by negative Nb-Ta anomalies. The mantle source had a composition similar to EMI – EMII, but the magmas were slightly contaminated by the continental crust during their ascent. On the other hand, alkaline dykes of Group 2 show very distinct geochemical and isotopic patterns, suggesting a low degree of partial melting of a deeper enriched mantle source (>40 km), also similar to SCLM and previously metasomatized, but expressively more contaminated by continental crust as demonstrated by the higher $^{87}Sr/^{86}Sr_{(i)}$ ratios, lower negative $\varepsilon Nd_{(t)}$, and older T_{DM}.

3.5.2. Comparison with other regional mafic units, evolutionary model and geodynamic implications

We here present a comparison of Group 1 and Group 2 dykes with other regional mafic units with similar ages and geochemical/isotopic features (Figure 3-11 and Figure 3-12), which allows us to draw an evolutionary model (Figure 3-13) for each of those groups.

Widespread Eocretaceous magmatism generated diabase dykes and sills and basaltic flows in the Paraná-Etendeka Province of South and Southeastern Brazil and Western Africa (Almeida et al., 1996). Throughout the Brazilian Coast, diverse dyke swarms are interpreted as evidence of the extensional movements that led to West Gondwana breakup followed by the opening of the South Atlantic Ocean. Those dykes are mainly concentrated in a NE-SW trend in São Paulo and Rio de Janeiro states (Resende - Ilha Grande or RIGDS and Serra do Mar dyke swarms) and in the Florianópolis dyke swarm, in a NW-SE trend in the Ponta Grossa Arc (Deckart et al., 1998) (Figure 3-1a).

The Paraná-Etendeka province is considered as one of the major Large Igneous Provinces (LIPs) on the world (Northfleet et al., 1969; Deckart et al., 1998), composed predominantly of basaltic rocks of the Serra Geral Formation (Courtillot and Renne, 2003) in Brazil and parts of Paraguay, Uruguay and Argentina (Marques and Ernesto, 2004). Some authors suggest the separation of those basalts in high-Ti (Urubici, Pitanga and Paranapanema subtypes) and low-Ti (Gramado, Esmeralda and Ribeira) subtypes; in Namibia, the latter correspond to the Tafelberg and Tafelkop subtypes (Peate et al., 1992, 1997; Turner et al., 1999; Rocha-Júnior et al., 2013).

Group 1 dykes of the Southern Espírito Santo State are characterized by overall low Ti contents. When comparing the $Ti/Zr_{(N)}$ versus $Ti/Y_{(N)}$ ratios of Group 1 dykes with the Paraná-Etendeka basalts, those are most similar to the Esmeralda, Gramado, Tafelberg and Tafelkop subtypes. Alkaline dykes of Group 2 do not correspond to any of those subtypes, reinforcing their distinct character (Figure 3-11a). Still comparing the Group 1 dykes to the high and low Ti basalts of the Paraná basin and to the RIGDS (Guedes et al., 2016), clear similarities are perceived between the patterns of incompatible trace elements, highlighting common negative anomalies of Nb, Ti and P among them. The differences consist of a Sr negative anomaly and a Nd positive anomaly in the dyke samples of Southern Espírito Santo in relation to the RIGDS, besides the fact the former are slightly enriched in HFSE comparing to the latter (Figure 3-11b).

Both RIGDS and other dykes of the Serra do Mar tholeiitic dyke swarms show high Ti (ca. 3.65% TiO_2 for RIGDS; Guedes et al., 2005). However, isotopic data is available only

for RIGDS (Guedes et al., 2016) and for the high-Ti basalts of the Serra Geral Formation (Rocha-Júnior et al., 2013) and so we will compare it with Group 1 tholeiitic dykes. The tholeiitic dykes from Group 1 show very similar Nd isotope signatures as compared to those suites, however showing slightly higher $^{87}Sr/^{86}Sr_{(i)}$ (Figure 3-12a). As interpreted for Group 1, both the RIGDS and Serra do Mar dyke swarm and the high-Ti basalts of the Serra Geral Formation are also interpreted as sourced from SCLM (subcontinental lithospheric mantle) and evolving mainly through FC (RIGDS) and AFC (Serra do Mar).

We present here, for the first time, U-Pb zircon data indicating that tholeiitic dykes were emplaced in the Southern Espírito Santo State around 140 Ma ago. The tholeiitic NNW-SSE trending dykes of the RIGDS yielded Ar-Ar ages between 148.3 ± 3 to 133.9 ± 0.5 Ma (Guedes et al., 2005), thus indicating a very plausible correlation with Group 1 dykes. Those ages are consistent with a Late Jurassic / Eocretaceous magmatic episode described in other parts of South America, such as Amambay (ca. 150 Ma) and Alto Paraguay (ca. 140 Ma; Gibson et al., 2006). The age of extrusion of the Serra Geral basalts is constrained to have started around 135 Ma and lasted for about 1-2 Ma through Ar-Ar data (Renne et al., 1992; Thiede and Vasconcelos, 2010; Baksi, 2017), which are corroborated by recent zircon and baddeleyite U-Pb dating of about 135 Ma (Pinto et al., 2011; Janasi et al., 2011). Although Ar-Ar geochronological data for the Florianopolis dyke swarm aren't consistent, U-Pb baddeleyite/zircon dating of dykes representative of the main activity reveals a restricted age range between 134.7 ± 0.3 and 133.9 ± 0.7 Ma (Florisbal et al., 2014). The Ponta Grossa dyke swarm is slightly younger than the basalts of the Serra Geral Formation, with U-Pb ages between 134.5 and 133.4 Ma (Almeida et al., 2017).

The alkaline dykes of Group 2 are radically distinct from the tholeiitic dykes of Group 1 regarding to petrographic, geochemical, geochronological and isotopic features. In Northern Espírito Santo State, dykes of the Fundão Suite are emplaced in the NNW-SSE trending Colatina Lineament and were interpreted by Belém (2014) as contemporaneous to the Cambrian G5 Supersuite, which would represent the late post-collisional bimodal magmatism related to the gravitational collapse stage of the Edicaran/Cambrian Araçuaí-Ribeira Orogen (Pedrosa-Soares et al., 2001). In effect, major plutons of the G5 Supersuite are found in the area, such as the bimodal Santa Angélica Intrusive Complex (SAIC) (Figure 3-1b). Comparing to isotopic data from this complex (De Campos et al., 2004), Group 2 dykes plot within the same field or very close to it. They are similar to the SAIC in showing low $\varepsilon Nd_{(t)} < -13$, high Sr and Ba values, and similar $^{87}Sr/^{86}Sr_{(i)}$ ratios (Figure 3-12b). De Campos et al. (2004) interpreted those characteristics as due to an abnormal enrichment of the local mantle, probably due to lower crustal delamination following slab break-off.

According to the available geochronological data, the G5 Supersuite plutons were intruded between 530 and 480 Ma, but the climax of magma generation was at 500 Ma (De Campos et al., 2004; 2016). The SAIC, belonging to the G5 set, revealed ages between 513 and 490 Ma, from U-Pb zircon data of granite facies obtained by Sollner et al. (1991). These authors also encountered zircon cores older than 2.0 Ga, and Nd isotope data that suggest assimilation of older crust, which was mixed with a basaltic mass coming from the uprising mantle after crustal delamination. Both the Caxixe and Santa Angélica dykes, situated near G5 plutons, present isotope composition and age very similar to SAIC, indicating that their formation was coeval with the mafic phases of these plutons.

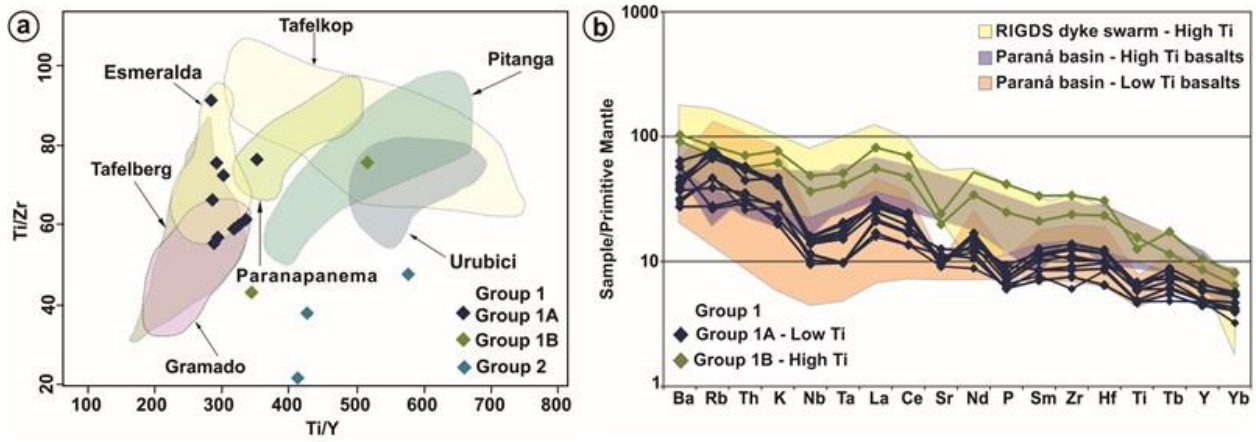

Figure 3-11: (a) Ti/Zr versus Ti/Y plot of the studied dykes. Fields of low-Ti and high-Ti basalt magma types of the Serra Geral Formation, Paraná basin (Peate et al., 1992, 1997; Turner et al., 1999) and of low-Ti basalts of the Etendeka province (Ewart et al., 1984; Milner et al., 1994) are shown for comparison (after Sarmento et al., 2017). (b) Primitive Mantle-normalized multi-element spidergram (Sun and McDonough, 1989) comparing the Espírito Santo dyke samples with basalts of high Ti (Rocha-Júnior et al., 2013) and low Ti (Peate et al., 1997) of the Paraná Basin, and high Ti dykes of the RIGDS (Guedes et al., 2016).

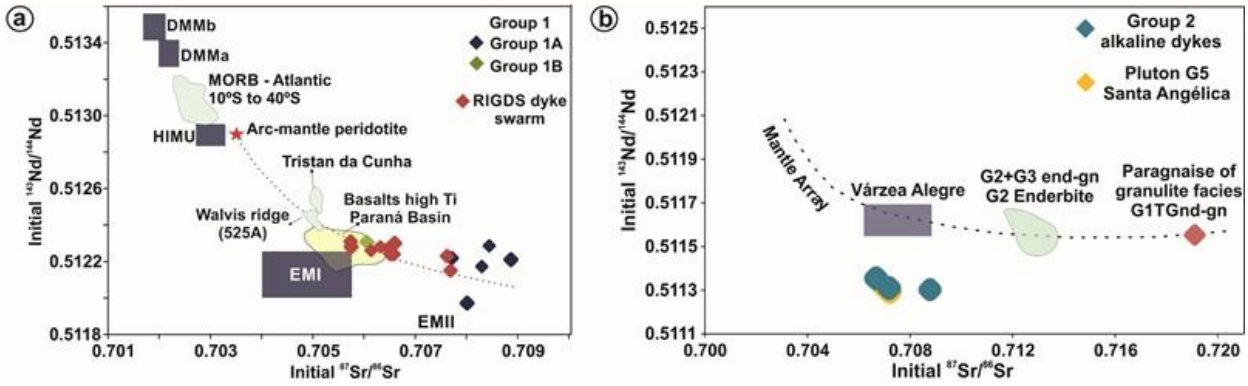

Figure 3-12: (a) Initial $^{87}Sr/^{86}Sr$ versus $^{143}Nd/^{144}Nd$ of the studied mafic dykes of Group 1 compared to basalts of the Paraná Basin (Rocha Junior et al., 2013) and of the RIGDS

(Guedes et al., 2016). Initial values recalculated to 140 Ma. (b) Initial $^{87}Sr/^{86}Sr$ versus $^{143}Nd/^{144}Nd$ of the studied mafic dykes of Group 2 compared to the G5 plutons of the Araçuaí Orogen basement (De Campos et al., 2004). Initial values recalculated to 500 Ma.

3.5.3. Implications for the evolution of the Alegre and Piúma structural lineaments

Both Group 1 and Group 2 dykes are emplaced in continental-scale structural lineaments trending NW-SE and NNW-SSE, such as the Alegre (Calegari et al., 2016), Piúma (Lourenço et al., 2016), and the Itaoca lineaments which control striking topographic breaks. Group 1 tholeiitic dykes (Muqui, Jerônimo Monteiro, Iúna, and Lajinha) and Group 2 alkaline dyke Itaici are emplaced in the Alegre Lineament system. The Group 2 Caxixe dyke is associated with the Piúma Lineament and the Group 1 Cobiça, Itaoca, Cantagalo and Castelo dykes are emplaced in the Itaoca Lineament (Figure 3-1b).

Those lineaments are interpreted as shear zones that developed during the Ediacaran and Cambrian collisional and strike-slip phases of the Araçuaí – Ribeira Orogens, controlling the emplacement of the G5 Supersuite plutons; however, very important reactivations of those lineaments occurred during the Lower Cretaceous and Cenozoic. Calegari et al. (2016) demonstrates that the Alegre Lineament controls both the emplacement of Cambrian G5 plutons and the structure and local depocenters in the offshore Campos basin. Our geochronological data supports this interpretation, as those lineaments control the emplacement of both syn-G5 alkaline dykes (Group 2 at ca. 500 Ma) and the dykes related to West Gondwana breakup and the development of Early Cretaceous syn-rift basins (Group 1 at ca. 140 Ma). Then, the Alegre, Piúma and Itaoca structural lineaments in the area acted as very important structural features that controlled both the evolution of the basement and the development of the marginal oil-producing basins of Southeastern Brazilian Coast.

3.6. CONCLUSIONS

Two distinct groups of mafic dykes were identified in the southern Espírito Santo state, southeastern Brazil, with well-defined petrographic, geochemical, isotopic and geochronological characteristics that clearly distinguish one group from another. The Group 1 tholeiitic dykes were emplaced at ca. 140 Ma, and the Group 2 alkaline dykes at ca. 500 Ma. Both dyke families are controlled by NNW-SSE and NW-SE structural lineaments such

as the Piúma, Alegre, and Itaoca lineaments, which extend for tenths of kilometers along the onshore and offshore areas.

Group 1 tholeiitic dykes (ca. 140 Ma) show moderately fractionated REE (mean $La/Yb_{(N)} = 2.6$), $^{87}Sr/^{86}Sr_{(i)}$ of 0.7041 – 0.7065, $\varepsilon Nd_{(t)}$ of -3.4 to -5.5 and T_{DM} between 0.8 and 1.5 Ga. Their mantle sources were shallow (< 40 km), probably represented by enriched SCLM in the spinel stability field, and their differentiation was mainly controlled by fractional crystallization. Those characteristics are similar to other Late Jurassic / Early Cretaceous dyke swarms of the Brazilian coast and to the expressive basalt flows of the Paraná-Etendeka Province, thus suggesting a link with West Gondwana breakup and the installment of syn-rift basins that ultimately led to the opening of the South Atlantic Ocean.

Group 2 alkaline dykes (ca. 500 Ma) show highly fractionated REE (mean $La/Yb_{(N)} = 19.6$), higher $^{87}Sr/^{86}Sr_{(i)}$ of 0.7064 – 0.7088, more negative $\varepsilon Nd_{(t)} < -12$, and older T_{DM} around 1.7-1.9 Ga. The mantle sources were deep (> 40 km), in the garnet stability field, and they were differentiated through fractional crystallization with very important crustal assimilation. This group is coeval to the expressive G5 Supersuite plutonic activity related to the Cambrian collapse of the Neoproterozoic Araçuaí-Ribeira Orogen, which shows very similar age, geochemical and isotopic features.

We propose a model for the evolution of the mafic magmatism in the area (Figure 13), which starts with the gravitational collapse stage of the Araçuaí-Ribeira Orogen during the Cambrian, when a heat source was supplied by the asthenosphere ascent related to slab breakoff followed by delamination of the lithospheric mantle. This event generated the G5 Supersuite plutons and coeval Group 2 dykes, which might have served as feeders to the mafic phases of bimodal plutons such as the Santa Angelica Intrusive Complex. Those plutons and dykes were emplaced in the main structural lineaments developed in the collisional and strike-slip phases of the Brasiliano Orogeny, such as the Piúma and Alegre lineaments, which served as conduits for the uprising magma. In the Early Cretaceous, during West Gondwana breakup, crustal rifting and the development of syn-rift basins which would ultimately lead to the separation of South America from Africa and opening of the South Atlantic Ocean, those lineaments were reactivated, now functioning as conduits for the Group 1 tholeiitic dykes. In this stage, those lineaments also influenced the development of important oil-producing basins off the southeastern Brazilian coast such as the Campos and Espírito Santo basins.

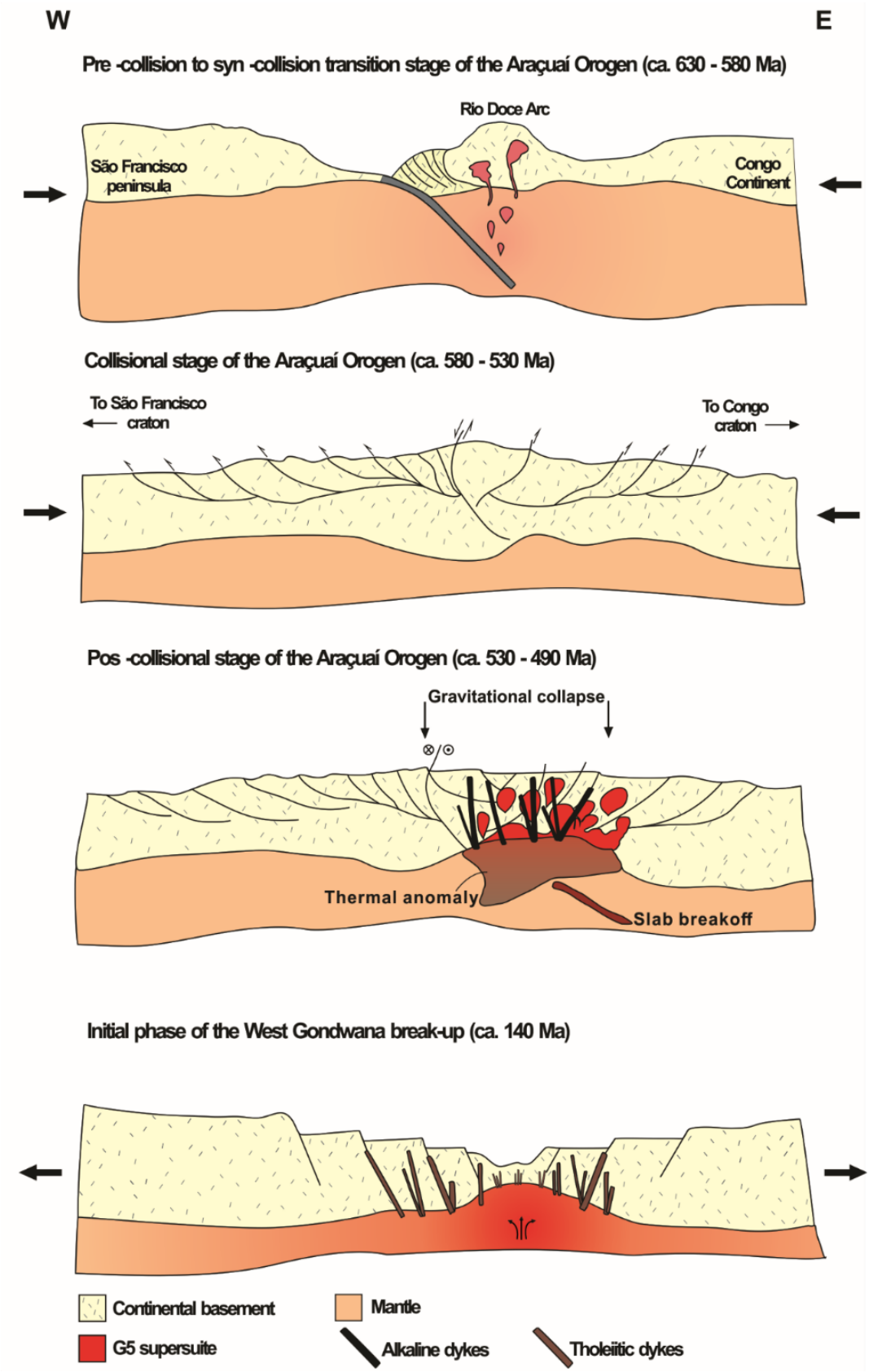

Figure 3-13: Schematic model for the evolution of magmatism and the generation of two groups of mafic dykes in the area. Pre-, syn- and post-collisional phases of the Araçuaí-Ribeira Orogen are based partly on the model by Gradim et al. (2014). See text for discussions.

CAPÍTULO IV: CONSIDERAÇÕES FINAIS

4.1 CONCLUSÕES

A integração e análise dos dados obtidos neste trabalho permitiram tecer as seguintes conclusões (Tabela 4-1):

Os diques máficos do sul do Espírito Santo pertencem a dois grupos de idade, características geoquímicas, isotópicas, geocronológicas e significado tectônico inteiramente distintos. Os grupos são colocados em lineamentos estruturais NNW-SSE e NW-SE, como os lineamentos Piúma, Alegre e Itaoca, que se estendem por dezenas de quilômetros ao longo das áreas *onshore* e *offshore*.

Os diques toleíticos do Grupo-1 (140 Ma) mostram REE moderadamente fraccionado (média $La/Yb_{(N)}$ = 2,6), $^{87}Sr/^{86}Sr$ (i) de 0,7041 - 0,7065, $\varepsilon Nd_{(t)}$ de -3,4 a -5,5 e TDM entre 0,8 e 1,5 Ga. Suas fontes do manto eram rasas (< 40 km), provavelmente representadas por SCLM enriquecido no campo de estabilidade do espinélio, e sua diferenciação foi principalmente controlada por cristalização fracionada. Essas características são semelhantes aos outros enxames de diques do Jurássico Superior/Eocretáceo e aos fluxos expressivos de basalto da província Paraná-Etendeka, sugerindo uma conexão com a separação do Gondwana e a abertura do Oceano Atlântico Sul.

Os diques alcalinos do Grupo-2 (cerca de 500 Ma) mostram REE altamente fracionada (média $La/Yb_{(N)}$ = 19,6), maior $^{87}Sr/^{86}Sr_{(i)}$ (0,7064 - 0,7088), mais negativo $\varepsilon Nd_{(t)}$ < -12, e TDM mais antigo em torno de 1,7-1,9 Ga. As fontes do manto foram profundas (> 40 km), no campo de estabilidade da granada e foram diferenciadas através de cristalização fracionada com assimilação crustal muito importante. Este grupo é contemporâneo com a atividade expressiva dos plútons da Supersuite G5, relacionada ao colapso cambriano do Orógeno Araçuaí, que mostra características muito semelhantes em termos de idade, composição geoquímica e isotópica.

Um modelo para a evolução do magmatismo máfico na área começa com o estágio de colapso do Orógeno Araçuaí durante o Cambriano, quando uma fonte de calor foi criada pela ascensão da astenosfera relacionada à *slab breakoff* e seguida de delaminação do manto litosférico. Este evento gerou os plútons da Supersuite G5 e os diques do Grupo-2, que podem ter servido como alimentadores da fase máfica de plútons bimodais, como o Complexo Intrusivo Santa Angélica. Esses plútons e diques foram colocados nos principais lineamentos estruturais possivelmente ao final da Orogenia Brasiliana, como os

lineamentos Piúma e Alegre, que serviram de condutos para a ascensão do magma. No início do Cretáceo, durante a separação do Gondwana e abertura do Oceano Atlântico Sul, esses lineamentos foram reativados, funcionando agora como condutos para os diques toleíticos do Grupo-1, relacionados ao rifteamento crustal. Nesta fase, estes lineamentos também influenciaram o desenvolvimento das bacias produtoras de petróleo da costa do Sudeste do Brasil, como a Bacia de Campos.

Tabela 4-1: Síntese das conclusões obtidas durante o trabalho.

GRUPO 1 – diques toleíticos	**GRUPO 2 – diques alcalinos**
ca. 140 Ma;	ca. 500 Ma;
REE moderadamente fracionado (média $La/Yb_{(N)}$ = 2,6);	REE altamente fracionado (média $La/Yb_{(N)}$ = 19,6);
$^{87}Sr/^{86}Sr_{(i)}$ = 0,7041 - 0,7065;	$^{87}Sr/^{86}Sr_{(i)}$ = 0,7064 - 0,7088;
$\varepsilon Nd_{(t)}$ = -3,4 a -5,5;	$\varepsilon Nd_{(t)}$ = <-13;
TDM entre 0,8 e 1,5 Ga;	TDM entre 1,7-1,9 Ga;
Fontes do manto menos profunda (<40 km), provavelmente representadas por SCLM enriquecido no campo de estabilidade do espinélio;	Fontes do manto mais profundas (> 40 km), no campo de estabilidade granada;
Diferenciação controlada por cristalização fracionada;	Diferenciados através da cristalização fracionada com assimilação crustal muito importante;
Semelhantes aos outros enxames de diques do Jurássico/ Cretáceo e aos basaltos da Província Paraná-Etendeka, relacionando com a separação do Gondwana Ocidental; a instalação das bacias sin-rifte e a abertura do Oceano Atlântico Sul.	Contemporâneo a Supersuite G5, relacionada ao colapso cambriano do Orógeno Araçuaí, mostrando características muito semelhantes (geoquímicas, isotópicas e de idade).

4.2 SUGESTÃO PARA TRABALHOS FUTUROS

A análise sistemática aqui apresentada revelou a importância dos estudos geoquímicos e isotópicos na compreensão da evolução e do contexto geodinâmico dos enxames de diques máficos. Porém, algumas questões permanecem e existem pontos que carecem de estudos mais específicos. Os seguintes métodos poderiam ser adotados visando ao melhor entendimento da evolução geológica regional:

- Datação dos diques por U-Pb em badeleíta; visto que este é um mineral característico de rochas ígneas máficas, fornecendo maior precisão quanto a idade de cristalização dos diques.

- Realizações de análises Lu-Hf e traços nos zircões, juntamente com o estudo de seu embasamento. Este método e o de U-Pb em zircão revelam muito mais sobre a evolução das rochas em que os diques intrudiram do que propriamente sobre a evolução dos próprios diques, pois, na maioria das vezes, os grãos são herdados das encaixantes.

- Descobertas de novos diques serão sempre importantes para sustentar a diferença dos dois grupos apresentados neste trabalho e para enriquecer a discussão quanto ao processo geotectônico em que estão relacionados.

REFERÊNCIAS BIBLIOGRÁFICAS

Allégre, C. (2008). Isotope Geology. Cambridge University Press, 512 p.

Almeida, F.F.M. (1986). Distribuição regional e relações tectônicas do magmatismo pós-paleozóico no Brasil. Revista Brasileira de Geociências, (16(4)) p. 325-349.

Almeida, F.F.M., Carneiro, C.D.R, Mizusaki, A.M.P., 1996. Correlação do Magmatismo das Bacias da Margem Continental Brasileira com o das Áreas Emersas Adjacentes. Revista Brasileira de Geociências, 26(3): 125-138.

Almeida, V.V., Janasi, V.A., Heaman, L.M., Shaulis, B.J., Hollanda, M. H. B. M., Renne, P.R. (2017). Contemporaneous alkaline and tholeiitic magmatism in the Ponta Grossa Arch, Paraná-Etendeka Magmatic Province: Constraints from U–Pb zircon/baddeleyite and $^{40}Ar/^{39}Ar$ phlogopite dating of the José Fernandes Gabbro and mafic dykes. Journal of Volcanology and Geothermal Research, in press.

Baksi, A.K., (2017). Paraná flood basalt volcanism primarily limited to ~ 1 Myr beginning at 135 Ma: New 40Ar/39Ar ages for rocks from Rio Grande do Sul, and critical evaluation of published radiometric data. Journal of Volcanology and Geothermal Research, in press.

Belém, J. (2014). Geoquímica, geocronologia e contexto geotectônico do magmatismo máfico associado ao Feixe de Fraturas Colatina, estado do Espírito Santo. PhD Thesis, Universidade Federal de Minas Gerais, Minas Gerais, 138 p.

Bellieni, G., Comin-Chiramonti, P., Marques, L.S., Melfi, A.J., Piccirillo, E.M., Nardy, A.J.R. & Rosemberg, A. (1984). High- and Low-TiO2 flood basalts from Paraná plateau (Brazil): petrology ang geochemical aspects bearing on their mantle origin. Neues Jahrbuch Fur Mineralogie-Abhandlugen. (150) 273-306.

Bellieni, G., Comin-Chiramonti, P., Marques, L.S., Melfi, A.J., Nardy, A.J.R., Papatrechas, C., Piccirillo, E.M. &Rosemberg, A. (1986). Petrogenetic aspect of acid and basaltic lavas from Paraná plateau (Brazil): geological, mineralogical and petrochemical relationships. Journal of Petrology. (27) 915-944.

Bühn, B., Pimentel, M.M., Matteini, M., Dantas, E.L. (2009). High spatial resolution analysis of Pb and U isotopes for geochronology by laser ablation multi-collector inductively coupled plasma mass spectrometry (LA-MC-IC-MS). Anais da Academia Brasileira de Ciências. (81 (1)) 1–16.

Carlson, R.W., Hart, W.K. (1987). Crustal genesis on the Oregon Plateau. Journal of Geophysical Research. (92) 6191-6206.

Calegari, S.S., Neves, M., A., Guadagnin, F., França, G., S., Vincentelli, M., G., C. (2016). The Alegre Lineament and its role over the tectonic evolution of the Campos Basin and adjacent continental margin, Southeastern Brazil. Journal of South American Earth Sciences. (69) 226-242.

Chang, H.K., Kowsman, R.O., Figueiredo, A.M.F.& Bender, A.A. (1992). Tectonics and stratigraphy of the East Brazil Rift System – Na overview. Tectonophysics. (213) 97-138.

Corval, A. (2005). Petrogênese das suítes basálticas toleíticas do Enxame de Diques da Serra do Mar nos setores central e norte do estado do Rio de Janeiro. Dissertação de Mestrado, UERJ, 92p.

Corval, A. (2009). Petrogênese e Contexto Geodinâmico das Suítes Basálticas Toleíticas (de alto-TiO2 e baixo-TiO2) do Cretáceo Inferior da Porção Centro-oriental do Enxame de Diques da Serra do Mar. Phd Thesis, Universidade do Estado do Rio de Janeiro, Brazil, 189 p.

Courtillot, V.E., Renne, P.R. (2003). On the Ages of Flood Basalt Events. C. R. Geoscience. (335) 113–14

Coutinho, J.M.V. (2008). Dyke swarms of the Paraná triple junction, Southern Brazil. Geologia USP: Série Científica. (8 (2)) 29–52.

Cox, K.G., Bell, J.D., Pankhurst, R.J. (1979). The interpretation of igneous rocks. George Allen & Unwin, London, 450 p.

De Campos C.M., Mendes J.C., Ludka I.P., Medeiros S.R., Moura J.C., Wallfass C. (2004). A review of the Brasiliano magmatism in southern Espírito Santo, Brazil, with emphasis on post-collisional magmatism. Journal of the Virtual Explorer, 17 (http://virtualexplorer.com.au/journal/ 2004/17/campos).

De Campos, C.P., Medeiros, S.R., Mendes, J. C., c, Pedrosa-Soares, A. C., Dussin I., Ludka, I.P., Dantas, E.L. (2016). Cambro-Ordovician magmatism in the Araçuaí Belt (SE Brazil): Snapshots from a post-collisional event. Journal of South American Earth Sciences. (68) 248-268.

Deckart, K., Gilbert, F., Marques, L.S., Hervé, B. (1998). New time constraints on dyke swarms related to the Paraná-Etendeka magmatic province, and subsequent South Atlantic opening, southeastern Brazil. Journal of Volcanology and Geothermal Research. (80) 67-83.

Deer W.A., Howie R. A., Zussman J. (1992). An introduction to the rock-forming minerals. London: Longman.

Deer, W.A., Howie, R.A., Zussman, J. (2003). An Introduction to the Rock-Forming Minerals. Longman Scientific and Technical, New York.

DePaolo, D.J. (1981). Neodymium isotopes in the Colorado front range and crust-mantle evolution in the Proterozoic. Nature. (291) 193–196.

Eisele, J., Sharma, M., Galer, S.J.G., Blichert-Toft, J., Devey, C.W., Hofmann, A.W. (2002). The role of sediment recycling in EM-1 inferred from Os, Pb, Hf, Nd, Sr isotope and trace element systematics of the Pitcairn hotspot. Earth and Planetary Science Letters. (196) 197-212.

Ernst, R. (2014). Large Igneous Provinces. Cambridge University Press, p. 653.

Ewart, A.J., Marsh, J.S., Duncan, A.R., Miller, R.M., Hawkesworth, C.J., Betton, P.J., Rex, D.C. (1984). Geochemistry and petrogenesis of the Etendeka volcanic rocks from SWA/Namibia. In: Erlank, A.J. (Ed.), Petrogenesis of Volcanic Rocks of the Karoo Province. Geological Society of South Africa Special Publication 13, Johannesburg, pp. 195-245.

Florisbal, L.M. Heaman, L.M., Janasi., V.A., Bitencourt, M.F. (2014). Tectonic significance of the Florianópolis Dyke Swarm, Paraná–Etendeka Magmatic Province: A reappraisal based on precise U–Pb dating. Journal of Volcanology and Geothermal Research. (289) 140–150.

Gibson, S.A., Thompson, R.N., Day, J.D. (2006). Time scales mechanism of plume lithosphere interaction 40Ar/39Ar geochronology and geochemistry of alkaline igneous rocks from Parana-Etendeka large igneous Province. Earth Planet. Sci. Lett. (251) 1-17.

Gioia, S.M.C.L., Pimentel, M.M. (2000). The Sm–Nd isotopic method in the Geochronology Laboratory of the University of Brasília. Anais da Academia Brasileira de Ciências. (72 (2)). 219–245.

Gradim C., Roncato J., Pedrosa-Soares A.C., Cordani U., Dussin I., Alkmim F.F. (2014). The hot back-arc zone of the Araçuaí orogen, Eastern Brazil: from sedimentation to granite generation. Brazilian Journal of Geology. (44(1)) 155-180.

Gomes, I.R., Neves, M.A., Serri, M., Pinto, W.M.. Araujo, D.R. (2016). Métodos magnetométricos aplicados ao estudo de diques máficos no sul do estado do Espírito Santo. In: 48º Congresso Brasileiro de Geologia, 2016, Porto Alegre. Anais, 2016

Guedes, E., Heilbron, M., Vasconcelos, P.M., Valeriano, C.M., Almeida, J.C.H., Teixeira, W., Thomaz Filho, A. (2005). K-Ar and 40Ar/39Ar ages of dikes emplaced in the onshore basement of Santos Basin, Resende area, SE Brazil: implications for the South Atlantic opening and Tertiary reactivation. J. S. Am. Earth Sci. (18) 371-382.

Guedes, E., Heilbron, M., Valeriano, C., M., Almeida, J., C., H., Peter, S. (2016). Evidence of Gondwana early rifting process recorded by Resende-Ilha Grande Dike Swarm, southern Rio de Janeiro, Brazil. Journal of South American Earth Sciences. (67) 11-24

Hart, W.K., Carlson, R.W., Shirey, S.B. (1997). Radiogenic Os in primitive basalts from the northwestern U.S.A.: implications for petrogenesis. Earth and Planetary Science Letters. (150) 103-116.

Hawkesworth, C.J., Gallager, K., Kelley, S., Mantovani, M.S.M., Peate, D.H., Regelous, M., Rogers, N. (1992). Parana magmatism and the opening of the south atlantic. In: Storey, B., Alabaster, A., Pankhurst, R. (Eds.), Magmatism and the Causes of Continental Breakup. Geological Society, London, pp. 221-240 special publication 68.

Heilbron, M.L., Pedrosa-Soares, A.C., Campos Neto, M.C., Silva, L.C., Trouw, R., Janasi, V.A. (2004). Província Mantiqueira. In: V.M. Mantesso-Neto, A. Bartorelli, C.D.R. Carneiro & Brito-Neves, B.B. (orgs.). Geologia do Continente Sul-Americano. São Paulo, Editora Beca, p. 203-234.

Hoskin, P.W.O. & Schaltegger, U. (2003). The composition of zircon and igneous and metamorphic petrogenesis. In: Hanchar, J. M. & Hoskin, P.W.O. (eds) Zircon. Reviews in Mineralogy and Geochemistry (53) 27–62.

Irvine, T.N. &Baragar, W.R.A. (1971). A guide to the chemical classification of the common volcanic rocks. Canadian Journal of Earth Sciences (8) 523–548.

Janasi, V.A., Freitas, V.A., Heaman, L.H. (2011). The onset of flood basalt volcanism, Northern Parana Basin, Brazil: a precise Ub/Pb baddeleyite/zircon age for a Chapecó-type dacite. Earth Planet. Sci. Lett. (302) 147-153.

Leake, B.E., Woolley, A.R., Arps, C.E.S., Birch, W.D., Gilbert, M.C., Grice, J.D., Hawthorne, F.C., Kato, A., Kisch, H.J., Krivovichev, V.G., Linthout, K., Laird, J., Mandarino, J.A., Maresch, W.V., Nickel, E.H., Rock, N.M.S., Schumacher, J.C., Smith, D.C., Stephenson, N.C.N., Ungaretti, L., Whittaker, E.J.W., Guo, Y. (1997). Nomenclature of amphiboles: Report of the subcommittee on amphiboles of the International Mineralogical Association Commission. Zamerican Mineralogist. (V.82) pag.1019-1037.

Le Bas, M.J., Le Maitre, R.W., Streckeisen, A., Zanettin, B. (1986). A chemical classification of volcanic rocks based on the total alkali–silica diagram. Journal of Petrology. (27) 745-750.

Lindsley, D.H. (1983). Pyroxene thermometry. American Mineralogist. (68 (5-6)) 477-493

Liu, S., Hu, R., Gao, S., Feng, C., Qi, L., Zhong, H., Xiao, T., Qi, Y., Wang, T., Coulson, I.M. (2008). Zircon U–Pb geochronology and major, trace elemental and Sr–Nd–Pb isotopic geochemistry of mafic dykes in western Shandong Province, east China: Constrains on their petrogenesis and geodynamic significance. Chemical Geology (255) 329–345

Ludwig, K.R. (2008). User's manual for Isoplot 3.6. A geochronological toolkit for Microsoft Excel. Special Publication, No. 4. Berkeley Geochronologic Center, Berkeley, USA.

Lourenço, F.S., Alkmim, F.F., Araújo, M.N.C., Romeiro, M.A.T., Matos G.C., Crósta,. A.P., (2016). The Piúma lineament, southern Espirito Santo: structural expression and tectonic significance. Brazilian Journal of Geology (46(4)) 531-546.

Marques, L.S., Bellieni, G., DeMin, A., Piccirillo, E.M. (1993). O Enxame de Diques da Ilha de Santa Catarina: resultados geoquímicos preliminaries. Boletim de Resumos Expandidos do 4° Congresso Brasileiro de Geoquímica, Brasília. 3-4.

Marques, L.S., Dupré, B., Piccirillo, E.M. (1999). Mantle source compositions of the Paraná Magmatic Province (southern Brazil): evidence from trace element and Sr-Nd-Pb isotope geochemistry. Journal of Geodynamics. (28(4-5)) 439-458.

Marques, L.S. (2001). Geoquímica dos diques toleíticos da costa sul-sudeste do Brasil: contribuição ao conhecimento da Província Magmática do Paraná. (Livre-Docência Thesis) Universidade de São Paulo, São Paulo.

Marques, L.S., Babinski, M., Ruiz, I.R. (2003). Lead isotopes of Early Cretaceous coastal dykes of Paraná Magmatic Province (Florianópolis Swarm): preliminary results. IV Simpósio Sul-americano de Geologia Isotópica. Short Papers, Salvador, Brazil, pp. 605–608.

Marques, L.S., Ernesto, M. (2004). O magmatismo Toleítico da Bacia do Paraná. In: Mantesso-Neto, V., Bartorelli, A., Carneiro, C.D.R., Brito-Neves, B.B., eds., Geologia do Continente Sul-Americano: Evolução da obra de Fernando Flávio Marques de Almeida. São Paulo, Editora Beca, 647p.

Mantovani, M.S.M., Marques, L.S., Souza, M.A., Civetta, L., Atalla, L., Innocenti, F. (1985). Trace element and strontium isotope constraints on the origin and evolution of Paraná continental flood basalts of Santa Catarina state (Southern Brazil). Journal of Petrology. (26) 187-209.

McCullouch, M.T., Gamble, J.A. (1991). Geochemical and geodynamical constraints on subduction zone magmatism. Earth and Planetary Science Letters (102) 358-374.

Milner, S.C., Duncan, A.R., Ewart, A., Marsh, J.S. (1994). Promotion of the Etendeka Formation to group status: a new integrated stratigraphy. Commun. Geol. Surv. Namib. (9) 5-11.

Mohriak, W. U., Rosendahl, B.R., Turner, J. P., and Valente, S. C. (2002) Crustal architecture of South Atlantic volcanic margins, in, Volcanic rifted margins, eds,1 ed.Boulder : Geological Society of America. (v.362) p. 159-202.

Monteiro, H.L.J. & Valente, S.C. (2003). Estudo Petrológico comparativo das suítes de baixo-TiO2 do Enxame de Diques da Serra do Mar: Jornada de Iniciação Científica, UFRuralRJ, Seropédica, p. 54-55.

Muzio, R., Scaglia, F., Masquelin, H. (2012). Petrochemistry of mesozoic mafic intrusions related to the Parana magmatic province, Uruguay. Int. Geol. Rev. (54) 844-860.

Neal, C.R., Mahoney, J.J., Chazey III, W.J. (2002). Mantle sources and the highly variable role of continental lithosphere in basalt petrogenesis of the Kergulen Plateau and Broken Ridge LIP: results from ODP Leg 183. J. Petrol. (43) 1177-1205.

Ngonge E. D., Hollanda M. H. B. M., Archanjo C. J., Oliveira D. C., Vasconcelos P. M. P., Muñoz P. R. M. (2016). Petrology of continental tholeiitic magmas forming a 350-km-long Mesozoic dyke swarm in NE Brazil: Constraints of geochemical and isotopic data. Lithos (258–259) 228–252.

Northfleet, A.A., Medeiros, R.A. & Mühlmann, H. (1969). Reavaliação dos dados geológicos da Bacia do Paraná. Boletim Técnico da Petrobrás. (12 (3)) 291- 346.

Novais, L.C.C., Teixera, L.B., Neves, M.T., Rodarte, J.B.M., Almeida, J.C.H., Valeriano, C.M. (2004). Novas ocorrências de diques de diabásio na faixa Colatina-ES: estruturas rútpeis associadas e implicações tectônicas para as bacias de Campos e do Espírito Santo. Boletim de Geociências Petrobras 1(2(1)) 191-194

Pankhurst, R.J. and O'Nions, R.K. (1973). Determination of Rb/Sr and $^{87}Sr/^{86}Sr$ ratios of some standard rocks and evaluation of X-ray fluorescence spectrometry in Rb-Sr geochemistry: Chem. Geol. (12) 127-136.

Pearce, J.A. (2008). Geochemical fingerprinting of oceanic basalts with applications to ophiolite classification and the search for Archean oceanic crust. Lithos 100, 14-48.

Peate, D.W., Hawkesworth, C.J., Mantovani, M.S.M., 1992. Chemical stratigraphy of the Paraná Lavas (South América): classification of magma types and their spatial distribution. Bulletin of Volcanol. (55 (1)) 119-139.

Peate, D.W., Hawkesworth, C.J. (1996). Lithospheric to asthenospheric transition in Low-Ti flood basalts from southern Paraná Brazil. Chem. Geol. (127) 1-24.

Peate, D.W. (1997). The Paraná magmatic province. In: Mahoney, J.J., Coffin, M.F. (Eds.), Large Igneous Provinces: Continental, Oceanic and Planetary Flood Volcanism, Geophysical Monograph. (100) 217-245.

Pedrosa-Soares, A.C., Wiedemann-Leonardos, C.M. (2000). Evolution of the Araçuaí Belt and its connection to the Ribeira Belt, Eastern Brazil. In: Cordani, U., Milani, E.J., Thomaz-Filho, A., Campos, D.A. (Eds.), Tectonic Evolution of South America. Sociedade Brasileira de Geologia, São Paulo, pp. 265-285.

Pedrosa-soares A. C., Noce C. M., Alkmim F. F., Silva L. C., Babinski M., Cordani U., Castañeda C. (2007). Orógeno Araçuaí: Síntese do Conhecimento 30 anos após Almeida 1977. Geonomos. (15) 1-16.

Pedrosa-Soares, A.C., Campos, C.P., Noce, C.M., Silva, L.C., Novo, T., Roncato, J., Medeiros, S., Castañeda, C., Queiroga, G., Dantas, E., Dussin, I., Alkmim, F. (2011). Late-Neoproterozoic-Cambrian granitic magmatism in the Araçuaí orogen (Brazil), the Eastern Brazilian Pegmatite Province and related mineral resources. Geological Society, London, Special Publications. (350) 25-51.

Piccirillo, E.M., Melfi, A.J. (1988). The Mesozoic Flood Volcanism of the Paraná Basin. Petrogenetic and Geophysical Aspects. São Paulo: Instituto Astronômico e Geofísico, Universidade de São Paulo, SP, Brazil.

Piccirillo, E.M., Bellieni, G., Cavazzini, G., Comin-Chiaramonti, P., Petrini, R., Melfi, A.J., Pinesi, J.P.P., Zantadeschi, P., and DeMin, A. (1990). Lower Cretaceous tholeiitic dyke swarms from the Ponta Grossa (southeast Brazil): Petrology, Sr-Nd isotopes and genetic relationships with the Paraná flood volcanics. Chemical Geology (89) 19-48.

Pinto, V.M., Hartmann, L.A., Orestes S.J., McNaughton, N.J., Wildner, W. (2011). Zircon U-Pb geochronology from the Paraná bimodal volcanic province support a brief eruptive cycle at ~135Ma. Chemical Geology (281) 93-102.

Puchtel, I.S., Arndt, N.T., Hofmann, A.W., et al. (1998). Petrology of mafic lavas within the Onega plateau, central Karelia: evidence for 2.0 Ga plume-related continental crustal growth in the Baltic Shield. Contributions to Mineralogy and Petrology (130) 134-153.

Raposo, M.I.B., Ernesto, M., and Renne, P.R. (1998). Paleomagnetism and 40Ar/39Ar dating of the Early Cretaceous Florianópolis Dyke Swarm (Santa Catarina Island), Southern Brazil. Physics of the Earth and Planetary Interiors (108) 275-290.

Renne, P.R., Ernesto, M., Pacca, I.G., Coe, R.S., Glen, J.M., Prevot, M., Perrin, M. (1992). The age of Parana flood volcanism, rifting of Gondwanaland, and the Jurassic-Cretaceous boundary. Science (258) 975-979.

Renne, P. R., Deckart, K., Ernesto, M., Féraud, G.,Piccirillo, E. M. (1996). Age of the Ponta Grossa dike swarm (Brazil), and implications to Paraná flood volcanism. Earth and Planetary Science Letters (144) 199-211.

Rocha-Júnior, E.R.V., Marques, L.S., Babinski, M., Nardy, A.J.R., Figueiredo, A.M.G., Machado, F.B. (2013). Sr–Nd–Pb isotopic constraints on the nature of the mantle sources involved in the genesis of the high-Ti tholeiites from northern Paraná continental flood basalts (Brazil). Journal of South American Earth Sciences 46, 9–25.

Rubatto, D. 2002. Zircon trace element geochemistry: partitioning with garnet and the link between U–Pb ages and metamorphism. Chemical Geology (184) 123-138

Sarmento, C.C.T., Sommer, C.A., Lima, E.F., Lima, E.F. (2017). Mafic subvolcanic intrusions and their petrologic relation with the volcanism in the south hinge Torres Syncline, Paraná-Etendeka Igneous Province, southern Brazil. Journal of South American Earth Sciences (77) 70-91

Silva, J. N. (1993). Mapa litológico da Folha Cachoeiro de Itapemirim SF.24-V-A, escala 1:250.000, Estado do Espírito Santo. Brasília: CPRM – Serviço Geológico do Brasil.

Silva, M.A., Camozzato, E., Paes, V.J.C., Junqueira, P.A., Ramgrab, G.E. (2004). Folha SF.24-Vitoria. In: Schobbenhaus, C., Gonçalves, J.H., Santos, J.O.S., Abram, M.B., Le~ao Neto, R., Matos, G.M.M., Vidotti, R.M., Ramos, M.A.B., Jesus, J.D.A. de (Eds.), Carta Geologica do Brasil ao Milionesimo, Sistema de Informações Geográficas. Programa Geologia do Brasil. CPRM, Brasília (CD-ROM).

Srivastava R,K.(eds.). (2011). Dyke Swarms: Keys for Geodynamic Interpretation. Springer, 605 p.

Söllner, F.; Lammerer, B. and Weber-Diefenbach, K. (1991). Die Krustenentwicklung in der Küstenregion nördlich von Rio de Janeiro/Brasilien Münchener Geowissenschaftliche Hefte 11, München, Friedrich Pfeil Verlag (4) 100 pp.

Sun, S.S. and McDonough, W.F. (1989). Chemical and isotopic systematics of oceanic basalts; implications for mantle composition and processes. In: Magmatism in the ocean basins. Saunders, A.D. and Norry, M.J. (Editors), Geological Society of London, London. (42) 313-345.

Teixeira, L. B., Rodarte, J. B. M. (2003). Datações de Diques de Diabásios na Faixa Colatina. Rio de Janeiro: Petrobras, Internal Report.

Thiede, D.S., Vasconcelos, P.M. (2010). Paraná flood basalts: rapid extrusion hypothesis confirmed by new 40Ar–39Ar results. Geology (38) 747–750.

Thirwall, M.F., Upton, B.G.J., Jenkins, C. (1994). Interaction between continental lithosphere and the Iceland plume-Sr-Nd-Pb isotopic geochemistry of tertiary basalts, NE Greenland. Journal of Petrology (35) 839–879.

Thompson, R. N., Morrison, M. A., Hendry, G. L., Parry, S. J., Simpson, P. R., Hutchison, R., & O'Hara, M. J. (1984). An Assessment of the Relative Roles of Crust and Mantle

in Magma Genesis: An Elemental Approach [and Discussion]. Philosophical Transactions of the Royal Society of London A: Mathematical, Physical and Engineering Sciences (310(1514)) 549-590.

Tomazzoli, E.R., Lima, E.F. (2006). Magmatismo ácido na Ilha do Arvoredo-SC. Rev. Bras. Geosci. (36) 57–76.

Turner, S., Peate, D., Hawkesworth, C., Mantovani, M. (1999). Chemical stratigraphy of the Paraná basalt succession in western Uruguay: further evidence for the diachronous nature of the Parana magma types. J. Geodyn. (28 (4)) 459-469.

Valente, S.C.; Ellam, R.L.; Meighan, I.G.; Fallick, A.E. (1998). Geoquímica isotópica, modelo geodinâmico e petrogênese dos diabásios do Cretácio Inferior no Enxame de Diques Máficos da Serra do Mar (EDSM) na área do Rio de Janeiro, RJ. Boletim de Resumos do 40º Congresso Brasileiro de Geologia, Belo Horizonte, SBG, 1998, p. 471.

Valente, S.C.; Corval, A.; Duarte, B.P.; Ellam, R.B.; Fallick, A.E.; Dutra, T. (2007). Tectonic boundaries, crustal weakness zones and plume-subcontinental lithospheric mantle interactions in the Serra do Mar Dyke Swarm, SE Brazil. Revista Brasileira de Geociências (37) 194-201.

Valente, S.C., Dutra, T., Heilbron, M., Corval, A., Szatmari, P. (2009). Litogeoquímica de Diques de Diabásio da Faixa Colatina, ES. Geochimica Brasiliensis (23(2)) 177-192.

Vieira, V.S., Silva, M.A., Corrêa, T.R., Lopes, M.H.B. (2014). Mapa Geologico do Espírito Santo e Escala 1:400.000. In: VI Simexmin and Simposio Brasileiro de Exploração Mineral, Ouro Preto, Anais.

Watson, E.B., Harrison, T.M. (1983). Zircon saturation revisited: temperature and composition effects in a variety of crustal magma types. Earth Planet. Sci. Lett. (64) 295–304.

SUPPLEMENTARY MATERIAL

Mineral chemistry data (olivine, pyroxene, plagioclase) of the mafic dykes in the southern Espírito Santo state.

Sample		Olivine chemical compositions												
		SiO_2	TiO_2	Al_2O_3	FeO	MgO	MnO	CaO	Na_2O	Cr_2O_3	K_2O	Total	Fo	Fa
Cobiça dyke	Core	38.40	0.01	0.03	22.02	38.91	0.34	0.35	0.14	0.02	0.01	100.23	0.76	0.24
Cobiça dyke	Core	38.29	0.02	0.03	20.90	39.53	0.30	0.28	0.04	0.02	0.01	99.41	0.77	0.23
Cobiça dyke	Core	38.49	0.01	0.05	20.23	40.43	0.32	0.30	0.06	0.00	0.02	99.91	0.78	0.22
Cobiça dyke	Core	38.66	0.04	0.04	20.38	40.21	0.24	0.31	0.07	0.01	0.01	99.98	0.78	0.22
Cobiça dyke	Core	38.97	0.00	0.05	20.57	40.44	0.30	0.27	0.07	0.03	0.00	100.71	0.78	0.22
Cobiça dyke	Core	38.67	0.00	0.08	20.46	40.19	0.28	0.31	0.05	0.01	0.02	100.07	0.78	0.22
Cobiça dyke	Rim	35.73	0.02	0.06	37.13	27.00	0.53	0.36	0.02	0.00	0.01	100.85	0.56	0.44
Cobiça dyke	Core	38.51	0.01	0.00	20.70	39.66	0.29	0.33	0.06	0.00	0.02	99.59	0.77	0.23
Cobiça dyke	Core	38.70	0.00	0.07	20.19	40.23	0.34	0.24	0.09	0.02	0.01	99.89	0.78	0.22
Cobiça dyke	Core	38.34	0.02	0.07	20.52	40.51	0.29	0.30	0.04	0.02	0.01	100.14	0.78	0.22
Cobiça dyke	Core	38.48	0.01	0.04	20.68	39.62	0.31	0.31	0.07	0.00	0.02	99.54	0.77	0.23
Cobiça dyke	Core	37.21	0.00	0.03	25.50	35.80	0.36	0.29	0.03	0.00	0.00	99.23	0.71	0.29
Cobiça dyke	Rim	36.34	0.00	0.03	33.08	30.11	0.39	0.36	0.04	0.00	0.00	100.36	0.62	0.38
Cobiça dyke	Rim	36.17	0.02	0.01	35.26	28.42	0.48	0.31	0.07	0.00	0.02	100.74	0.59	0.41
Cobiça dyke	Core	38.40	0.15	0.08	22.89	38.02	0.38	0.32	0.04	0.03	0.02	100.32	0.75	0.25
Cobiça dyke	Core	38.07	0.00	0.06	23.53	38.03	0.34	0.31	0.13	0.03	0.01	100.49	0.74	0.26
Cobiça dyke	Core	38.60	0.00	0.03	20.23	40.20	0.29	0.27	0.09	0.00	0.02	99.74	0.78	0.22
Cobiça dyke	Core	38.68	0.06	0.04	21.04	39.55	0.29	0.29	0.07	0.01	0.00	100.03	0.77	0.23
Cobiça dyke	Core	39.39	0.06	0.10	24.45	35.72	0.30	0.29	0.14	0.02	0.03	100.49	0.72	0.28
Cobiça dyke	Core	38.82	0.00	0.03	22.63	39.12	0.30	0.33	0.01	0.02	0.01	101.28	0.75	0.25
Cobiça dyke	Core	38.89	0.00	0.04	20.72	40.21	0.37	0.32	0.12	0.01	0.04	100.72	0.78	0.22
Cobiça dyke	Core	38.57	0.00	0.05	22.61	39.23	0.31	0.32	0.00	0.01	0.02	101.13	0.76	0.24
Cobiça dyke	Core	38.85	0.05	0.11	23.40	38.55	0.35	0.31	0.04	0.02	0.00	101.68	0.75	0.25

Sample	Pyroxene chemical compositions												
	SiO_2	TiO_2	Al_2O_3	FeO	MgO	MnO	CaO	Na_2O	K_2O	Total	En	Fs	Wo

Cobiça dyke	Rim	51.27	0.70	1.63	19.36	15.99	0.42	10.06	0.21	0.05	99.68	0.47	0.32	0.21
Cobiça dyke	Core	53.99	0.30	1.24	11.49	19.87	0.35	13.13	0.15	0.01	100.53	0.56	0.18	0.26
Cobiça dyke	Rim	52.83	0.32	2.38	7.50	18.03	0.20	18.33	0.26	0.01	99.85	0.51	0.12	0.37
Cobiça dyke	Core	51.86	0.34	3.27	7.22	17.65	0.18	18.63	0.25	0.02	99.41	0.50	0.12	0.38
Cobiça dyke	Rim	53.80	0.27	1.49	8.83	18.77	0.28	16.44	0.17	0.00	100.05	0.53	0.14	0.33
Cobiça dyke	Rim	52.61	0.36	1.30	13.71	17.83	0.41	13.43	0.19	0.02	99.86	0.51	0.22	0.27
Cobiça dyke	Rim	51.72	0.46	0.90	21.49	16.85	0.55	7.95	0.17	0.02	100.11	0.49	0.35	0.17
Cobiça dyke	Core	51.75	0.58	2.52	10.29	16.46	0.28	17.67	0.22	0.02	99.80	0.47	0.17	0.36
Cobiça dyke	Rim	52.38	0.48	2.05	12.56	18.11	0.38	13.97	0.20	0.00	100.14	0.51	0.20	0.29
Cobiça dyke	Rim	51.19	0.84	2.32	12.13	14.48	0.31	18.80	0.37	0.03	100.47	0.42	0.20	0.39
Cobiça dyke	Rim	49.27	1.20	2.15	18.75	11.57	0.47	15.49	0.28	0.02	99.21	0.35	0.32	0.34
Cobiça dyke	Core	52.37	0.65	2.58	9.14	17.36	0.26	17.57	0.21	0.01	100.16	0.49	0.15	0.36
Cobiça dyke	Core	52.02	0.55	3.67	7.28	16.97	0.17	19.00	0.23	0.01	99.88	0.49	0.12	0.39
Cobiça dyke	Core	51.75	0.57	2.43	11.05	16.08	0.31	17.54	0.19	0.01	99.93	0.46	0.18	0.36
Cobiça dyke	Rim	50.01	0.89	1.75	20.40	13.61	0.44	12.37	0.21	0.02	99.69	0.40	0.34	0.26
Cobiça dyke	Rim	52.56	0.60	2.20	12.95	17.59	0.39	14.60	0.20	0.01	101.08	0.50	0.21	0.30
Cobiça dyke	Core	53.03	0.44	2.42	9.14	18.45	0.26	17.10	0.18	0.01	101.04	0.51	0.14	0.34
Cobiça dyke	Core	53.16	0.31	2.48	7.13	18.00	0.21	18.56	0.24	0.02	100.09	0.51	0.11	0.38
Cobiça dyke	Core	52.68	0.34	3.48	7.42	17.69	0.19	18.20	0.26	0.01	100.28	0.51	0.12	0.37
Cobiça dyke	Core	52.05	0.37	4.24	8.17	16.77	0.20	17.77	0.42	0.02	100.00	0.49	0.13	0.37
Cobiça dyke	Core	53.25	0.39	2.03	7.59	17.99	0.18	18.78	0.26	0.03	100.50	0.50	0.12	0.38
Cobiça dyke	Core	53.10	0.41	2.58	7.35	18.07	0.18	18.93	0.28	0.01	100.89	0.50	0.12	0.38
Cobiça dyke	Rim	52.92	0.47	2.39	10.38	17.51	0.29	16.67	0.40	0.02	101.04	0.50	0.16	0.34
Cobiça dyke	Rim	53.14	0.38	1.23	14.23	18.44	0.34	13.16	0.17	0.01	101.10	0.51	0.22	0.26
Cobiça dyke	Core	53.32	0.33	2.09	7.36	17.75	0.18	19.28	0.24	0.01	100.55	0.50	0.12	0.39
Cobiça dyke	Core	52.13	0.32	2.78	8.25	17.45	0.15	18.39	0.32	0.06	99.86	0.49	0.13	0.37
Cobiça dyke	Core	53.46	0.31	2.28	7.02	17.98	0.23	18.85	0.23	0.02	100.37	0.51	0.11	0.38
Cobiça dyke	Core	53.84	0.30	2.06	6.78	18.35	0.16	18.99	0.22	0.01	100.71	0.51	0.11	0.38
Cobiça dyke	Core	53.29	0.36	2.48	6.88	17.80	0.18	19.69	0.23	0.00	100.93	0.50	0.11	0.40
Cobiça dyke	Core	53.68	0.33	1.80	7.80	18.54	0.21	17.90	0.23	0.00	100.49	0.52	0.12	0.36

Cobiça dyke	Rim	52.76	0.49	1.38	17.64	18.60	0.42	9.76	0.10	0.01	101.15	0.52	0.28	0.20
Cobiça dyke	Core	53.87	0.30	1.57	10.11	19.55	0.29	15.18	0.16	0.00	101.02	0.54	0.16	0.30
Cobiça dyke	Core	54.19	0.28	1.51	7.82	18.65	0.19	17.97	0.14	0.00	100.74	0.52	0.12	0.36
Cobiça dyke	Core	52.87	0.51	2.54	9.38	17.66	0.27	17.51	0.21	0.00	100.95	0.50	0.15	0.35
Cobiça dyke	Rim	50.97	0.76	2.34	14.58	14.60	0.39	16.46	0.21	0.01	100.32	0.42	0.24	0.34
Cobiça dyke	Rim	51.76	0.68	1.32	21.82	16.42	0.53	8.76	0.14	0.01	101.45	0.47	0.35	0.18
Cobiça dyke	Core	51.09	0.73	2.51	12.85	15.40	0.36	16.62	0.21	0.01	99.77	0.45	0.21	0.35
Cobiça dyke	Core	52.34	0.57	2.65	8.97	17.21	0.31	17.83	0.17	0.01	100.07	0.49	0.14	0.37
Cobiça dyke	Core	53.18	0.40	1.54	12.11	18.77	0.29	14.47	0.16	0.00	100.93	0.52	0.19	0.29
Cobiça dyke	Rim	50.97	0.66	1.42	17.65	14.99	0.43	12.72	0.24	0.03	99.10	0.44	0.29	0.27
Lajinha dyke	Rim	50.22	0.92	1.80	20.72	12.55	0.54	14.15	0.21	0.00	101.10	0.37	0.34	0.30
Lajinha dyke	Rim	50.48	0.85	1.77	20.35	13.31	0.38	13.39	0.23	0.01	100.76	0.39	0.33	0.28
Lajinha dyke	Core	52.45	0.49	3.11	8.43	17.53	0.26	18.28	0.20	0.00	100.75	0.50	0.13	0.37
Lajinha dyke	Rim	53.52	0.32	1.20	11.06	18.97	0.33	14.55	0.20	0.01	100.15	0.53	0.17	0.29
Lajinha dyke	Rim	50.63	0.82	1.54	20.47	12.14	0.45	14.76	0.19	0.01	101.00	0.35	0.34	0.31
Lajinha dyke	Core	53.60	0.32	1.57	10.00	18.67	0.27	16.01	0.13	0.02	100.58	0.52	0.16	0.32
Lajinha dyke	Core	52.76	0.41	2.26	8.50	18.00	0.29	17.81	0.21	0.00	100.23	0.51	0.13	0.36
Lajinha dyke	Rim	51.88	0.41	4.47	8.26	17.59	0.18	16.98	0.26	0.03	100.06	0.51	0.13	0.35
Lajinha dyke	Core	51.56	0.58	4.33	7.34	17.30	0.23	18.17	0.28	0.02	99.80	0.50	0.12	0.38
Lajinha dyke	Rim	51.92	0.58	2.55	11.25	16.46	0.25	17.29	0.25	0.03	100.58	0.47	0.18	0.35
Lajinha dyke	Rim	50.21	0.99	1.88	18.15	11.75	0.45	16.79	0.21	0.01	100.43	0.35	0.30	0.35
Lajinha dyke	Core	51.39	0.64	1.26	18.36	14.53	0.46	13.75	0.17	0.01	100.56	0.42	0.30	0.28
Lajinha dyke	Rim	53.56	0.37	1.21	12.69	18.70	0.31	14.32	0.19	0.01	101.36	0.52	0.20	0.29
Lajinha dyke	Core	53.66	0.29	1.68	7.65	18.45	0.26	18.30	0.21	0.02	100.52	0.51	0.12	0.37
Lajinha dyke	Core	53.43	0.30	2.11	6.93	18.01	0.17	19.07	0.25	0.01	100.28	0.51	0.11	0.38
Lajinha dyke	Rim	52.75	0.42	1.98	13.82	18.31	0.39	13.19	0.16	0.01	101.02	0.52	0.22	0.27
Lajinha dyke	Rim	53.15	0.35	1.56	10.99	18.68	0.29	15.29	0.14	0.01	100.44	0.52	0.17	0.31
Lajinha dyke	Rim	53.40	0.34	1.45	10.60	18.96	0.32	15.49	0.16	0.01	100.72	0.53	0.17	0.31
Lajinha dyke	Core	54.57	0.28	1.23	10.46	20.10	0.32	14.29	0.15	0.01	101.41	0.55	0.16	0.28
Lajinha dyke	Core	53.33	0.34	1.42	11.53	18.32	0.35	15.10	0.19	0.02	100.61	0.51	0.18	0.30

Lajinha dyke	Rim	52.64	0.40	1.24	15.10	18.15	0.36	12.04	0.14	0.02	100.08	0.51	0.24	0.25
Lajinha dyke	Rim	53.42	0.41	1.43	11.67	18.20	0.37	15.58	0.18	0.01	101.29	0.51	0.18	0.31
Lajinha dyke	Core	53.64	0.34	1.62	9.57	19.23	0.28	15.76	0.20	0.02	100.66	0.54	0.15	0.32
Lajinha dyke	Core	52.81	0.51	1.91	14.15	18.50	0.36	12.54	0.18	0.00	100.96	0.52	0.22	0.25
Lajinha dyke	Core	51.27	0.72	1.69	19.22	15.47	0.52	11.33	0.12	0.00	100.34	0.45	0.31	0.24
Lajinha dyke	Rim	50.25	0.86	1.76	21.85	13.09	0.42	12.41	0.15	0.01	100.80	0.38	0.36	0.26
Lajinha dyke	Rim	50.79	0.67	1.86	19.39	15.37	0.42	11.56	0.19	0.00	100.25	0.44	0.31	0.24
Lajinha dyke	Core	52.18	0.55	2.63	8.51	17.00	0.23	18.77	0.20	0.00	100.06	0.48	0.14	0.38
Lajinha dyke	Core	51.07	0.32	3.22	7.30	17.02	0.21	19.05	0.25	0.09	98.53	0.49	0.12	0.39
Lajinha dyke	Core	53.17	0.31	2.27	6.98	17.95	0.15	19.18	0.21	0.01	100.23	0.50	0.11	0.39
Lajinha dyke	Core	54.19	0.30	1.78	6.89	18.58	0.21	18.92	0.23	0.01	101.11	0.52	0.11	0.38
Lajinha dyke	Core	53.38	0.36	2.13	7.80	18.27	0.22	18.36	0.24	0.01	100.77	0.51	0.12	0.37
Lajinha dyke	Core	52.77	0.43	2.65	7.65	17.47	0.18	19.37	0.22	0.01	100.74	0.49	0.12	0.39
Lajinha dyke	Core	53.84	0.28	1.49	8.77	18.70	0.21	16.93	0.19	0.01	100.40	0.52	0.14	0.34
Santa Angélica dyke	Core	52.80	0.06	0.85	10.55	12.42	0.50	23.22	0.32	0.01	100.72	0.35	0.17	0.48
Santa Angélica dyke	Core	52.98	0.10	0.73	10.85	12.26	0.43	22.74	0.31	0.01	100.41	0.35	0.18	0.47
Santa Angélica dyke	Core	52.19	0.19	1.34	10.43	12.51	0.36	22.76	0.35	0.07	100.20	0.36	0.17	0.47
Santa Angélica dyke	Core	51.26	0.39	3.50	11.91	12.33	0.33	19.74	0.45	0.30	100.21	0.37	0.20	0.43
Santa Angélica dyke		51.38	0.48	3.68	12.26	13.01	0.28	17.25	0.44	0.30	99.08	0.40	0.21	0.38
Santa Angélica dyke		51.26	0.48	3.66	11.84	11.97	0.31	18.71	0.56	0.35	99.14	0.37	0.21	0.42
Santa Angélica dyke		52.47	0.23	1.83	10.49	12.33	0.39	22.33	0.36	0.12	100.55	0.36	0.17	0.47
Santa Angélica dyke		51.98	0.30	2.40	10.71	12.69	0.39	21.19	0.42	0.18	100.25	0.37	0.18	0.45
Santa Angélica dyke		52.28	0.14	2.09	9.87	12.59	0.40	22.79	0.53	0.16	100.84	0.36	0.16	0.47
Santa Angélica dyke	Rim	53.01	0.08	0.87	10.75	12.62	0.50	22.71	0.37	0.02	100.92	0.36	0.17	0.47
Santa Angélica dyke	Rim	52.82	0.12	0.80	10.30	12.46	0.46	23.54	0.36	0.02	100.87	0.35	0.16	0.48
Santa Angélica dyke	Rim	53.23	0.13	0.91	10.75	12.24	0.49	23.06	0.35	0.02	101.17	0.35	0.17	0.48
Santa Angélica dyke	Rim	53.35	0.08	0.74	9.93	12.76	0.53	23.23	0.31	0.02	100.95	0.36	0.16	0.48
Santa Angélica dyke	Core	53.41	0.11	0.73	10.46	12.74	0.49	22.84	0.30	0.01	101.08	0.36	0.17	0.47
Santa Angélica dyke	Rim	53.40	0.05	0.73	10.57	12.60	0.47	23.23	0.35	0.02	101.42	0.36	0.17	0.47
Santa Angélica dyke	Core	53.25	0.15	0.77	10.02	12.54	0.47	23.79	0.30	0.02	101.31	0.36	0.16	0.48

Santa Angélica dyke	Core	53.34	0.06	0.58	10.18	12.80	0.53	23.44	0.42	0.01	101.36	0.36	0.16	0.48
Santa Angélica dyke	Core	53.16	0.11	0.68	10.27	12.54	0.52	23.31	0.32	0.01	100.91	0.36	0.16	0.48
Santa Angélica dyke	Rim	53.38	0.08	0.73	10.41	12.65	0.50	22.82	0.34	0.01	100.92	0.36	0.17	0.47
Santa Angélica dyke	Rim	53.18	0.06	0.76	10.41	12.55	0.48	23.26	0.31	0.01	101.01	0.36	0.17	0.48
Santa Angélica dyke	Core	53.33	0.06	0.76	10.50	12.80	0.51	22.93	0.36	0.00	101.25	0.36	0.17	0.47
Santa Angélica dyke	Core	53.42	0.09	0.76	10.49	12.54	0.49	22.85	0.34	0.01	100.96	0.36	0.17	0.47
Santa Angélica dyke	Rim	53.39	0.07	0.73	10.38	12.42	0.52	22.99	0.34	0.01	100.85	0.36	0.17	0.48
Santa Angélica dyke	Core	53.08	0.10	0.74	10.35	12.68	0.44	22.85	0.33	0.02	100.60	0.36	0.17	0.47
Santa Angélica dyke	Core	52.98	0.09	0.63	10.52	13.04	0.49	22.56	0.35	0.02	100.69	0.37	0.17	0.46
Santa Angélica dyke	Rim	53.61	0.08	0.74	10.36	12.85	0.47	22.85	0.34	0.00	101.28	0.37	0.17	0.47
Santa Angélica dyke	Rim	53.34	0.07	0.70	10.20	12.63	0.43	23.63	0.28	0.01	101.29	0.36	0.16	0.48
Santa Angélica dyke	Core	53.52	0.04	0.65	9.78	12.78	0.44	23.89	0.28	0.01	101.39	0.36	0.15	0.48
Santa Angélica dyke	Rim	53.32	0.14	0.69	10.37	12.71	0.52	23.03	0.33	0.02	101.12	0.36	0.17	0.47
Santa Angélica dyke	Core	49.49	0.65	5.54	12.78	12.05	0.39	16.84	0.65	0.51	98.91	0.38	0.23	0.39
Santa Angélica dyke	Core	49.88	0.68	5.26	12.89	12.25	0.33	16.85	0.75	0.49	99.38	0.39	0.23	0.38
Santa Angélica dyke	Core	50.85	0.36	3.74	11.42	12.38	0.30	19.18	0.60	0.35	99.19	0.38	0.20	0.42
Santa Angélica dyke	Core	50.37	0.49	4.52	11.96	12.49	0.33	18.25	0.62	0.39	99.40	0.39	0.21	0.41
Santa Angélica dyke	Core	51.76	0.25	2.52	10.78	12.70	0.39	21.03	0.40	0.20	100.02	0.37	0.18	0.45
Santa Angélica dyke	Core	50.75	0.34	3.68	11.56	12.49	0.28	18.92	0.52	0.33	98.88	0.38	0.20	0.42

Sample		**Plagioclase chemical compositions**									
		SiO2	**Al2O3**	**FeO**	**CaO**	**Na2O**	**K2O**	**Total**	**An**	**Ab**	**Or**
Cobiça dyke	Rim	53.18	28.29	0.89	12.72	4.06	0.32	99.46	62.20	35.95	1.85
Cobiça dyke	Core	52.29	28.38	0.91	12.82	3.77	0.28	98.43	64.22	34.13	1.65
Cobiça dyke	Core	52.53	28.55	0.89	13.03	3.74	0.29	99.03	64.70	33.56	1.74
Cobiça dyke	Core	52.98	28.29	1.08	12.60	4.17	0.34	99.45	61.34	36.71	1.95
Cobiça dyke	Rim	52.65	28.25	0.96	12.71	3.96	0.30	98.83	62.81	35.41	1.78
Cobiça dyke	Rim	52.58	28.66	0.78	12.85	3.84	0.29	99.00	63.78	34.51	1.71
Cobiça dyke	Rim	53.18	28.33	0.85	12.79	3.98	0.32	99.45	62.79	35.35	1.86

Cobiça dyke	Core	51.97	29.11	0.77	13.49	3.57	0.26	99.17	66.60	31.88	1.53
Cobiça dyke	Core	51.65	29.61	0.70	13.56	3.36	0.23	99.12	68.11	30.51	1.38
Cobiça dyke	Core	51.93	29.63	0.78	13.91	3.33	0.23	99.80	68.82	29.85	1.33
Cobiça dyke	Rim	53.48	28.49	0.89	12.47	3.98	0.36	99.66	62.04	35.85	2.11
Cobiça dyke	Core	52.94	29.24	0.42	13.43	3.71	0.29	100.03	65.56	32.73	1.71
Cobiça dyke	Core	53.57	28.61	0.47	12.79	4.05	0.32	99.81	62.43	35.73	1.85
Cobiça dyke	Core	52.03	29.70	0.54	13.77	3.47	0.25	99.74	67.68	30.85	1.46
Cobiça dyke	Core	51.86	29.45	0.50	13.50	3.50	0.29	99.10	66.95	31.37	1.68
Cobiça dyke	Rim	51.06	30.28	0.59	14.19	3.17	0.22	99.51	70.28	28.40	1.32
Cobiça dyke	Rim	52.65	28.28	0.86	12.74	4.43	0.36	99.31	60.15	37.83	2.02
Cobiça dyke	Core	52.25	28.51	1.30	13.03	3.40	0.25	98.75	66.89	31.57	1.54
Cobiça dyke	Core	53.35	28.67	0.82	12.85	4.00	0.31	100.00	62.82	35.39	1.79
Cobiça dyke	Core	53.83	28.34	0.89	12.27	4.24	0.35	99.92	60.25	37.70	2.06
Cobiça dyke	Rim	54.33	27.89	0.94	11.89	4.35	0.37	99.76	58.86	38.99	2.15
Cobiça dyke	Rim	51.01	30.72	0.85	14.16	3.12	0.21	100.06	70.65	28.14	1.22
Cobiça dyke	Rim	51.68	30.44	0.49	14.19	3.45	0.24	100.49	68.50	30.13	1.37
Cobiça dyke	Rim	50.99	30.39	0.48	14.47	3.22	0.25	99.79	70.26	28.31	1.42
Cobiça dyke	Rim	52.17	30.13	0.86	13.82	3.34	0.28	100.59	68.46	29.92	1.62
Cobiça dyke	Core	51.68	29.70	1.01	14.05	3.36	0.22	100.02	68.92	29.80	1.28
Cobiça dyke	Core	51.90	30.33	0.66	14.13	3.35	0.21	100.57	69.15	29.64	1.21
Cobiça dyke	Core	51.61	29.88	1.12	13.53	3.42	0.24	99.80	67.66	30.93	1.41
Cobiça dyke	Rim	52.06	29.62	0.81	13.57	3.48	0.29	99.82	67.17	31.14	1.69
Cobiça dyke	Rim	52.14	29.88	0.89	13.48	3.48	0.23	100.09	67.25	31.38	1.38
Cobiça dyke	Rim	51.17	30.44	0.64	14.77	3.05	0.20	100.28	71.96	26.87	1.17
Cobiça dyke	Core	48.92	32.21	0.55	16.57	2.14	0.14	100.51	80.43	18.78	0.79
Cobiça dyke	Core	50.16	31.22	0.60	15.41	2.56	0.17	100.11	76.14	22.87	0.99
Cobiça dyke	Core	49.04	31.82	0.64	15.82	2.36	0.15	99.82	78.07	21.06	0.87
Cobiça dyke	Core	48.31	32.63	0.59	16.78	1.87	0.11	100.29	82.65	16.70	0.66
Cobiça dyke	Rim	52.11	30.14	0.63	13.91	3.39	0.22	100.40	68.51	30.19	1.30
Cobiça dyke	Rim	55.80	27.32	0.99	10.64	4.94	0.49	100.18	52.76	44.34	2.90

Cobiça dyke	Rim	53.07	29.36	0.83	13.03	3.88	0.29	100.46	63.91	34.38	1.71
Cobiça dyke	Core	55.22	27.71	1.26	11.28	4.66	0.44	100.57	55.74	41.66	2.60
Cobiça dyke	Core	54.14	26.15	2.55	10.67	4.78	0.51	98.79	53.56	43.38	3.07
Lajinha dyke	Rim	54.36	28.19	0.80	11.77	4.37	0.39	99.88	58.42	39.28	2.29
Lajinha dyke	Core	48.71	32.10	0.52	16.23	2.14	0.12	99.81	80.20	19.11	0.69
Lajinha dyke	Core	48.25	32.55	0.56	16.59	1.96	0.10	100.01	81.86	17.53	0.61
Lajinha dyke	Core	48.67	32.48	0.44	16.42	2.01	0.13	100.15	81.23	18.01	0.76
Lajinha dyke	Core	48.51	32.09	0.55	16.24	2.10	0.12	99.60	80.48	18.83	0.68
Lajinha dyke	Rim	51.70	29.96	0.73	14.00	3.42	0.22	100.03	68.47	30.26	1.26
Lajinha dyke	Rim	54.93	27.46	0.95	10.87	4.86	0.47	99.54	53.75	43.47	2.79
Lajinha dyke	Core	53.79	28.89	0.95	12.63	4.10	0.33	100.70	61.76	36.31	1.94
Lajinha dyke	Core	52.79	28.86	0.81	12.87	3.97	0.30	99.60	63.01	35.22	1.77
Lajinha dyke	Core	52.82	28.97	0.88	12.87	3.86	0.31	99.71	63.64	34.55	1.81
Lajinha dyke	Rim	53.31	28.90	0.87	12.68	4.09	0.31	100.18	61.98	36.20	1.83
Lajinha dyke	Rim	50.74	29.19	1.37	13.60	3.16	0.24	98.30	69.40	29.16	1.43
Lajinha dyke	Core	50.81	30.36	0.65	14.35	3.14	0.21	99.51	70.76	28.01	1.23
Lajinha dyke	Core	52.00	30.02	0.65	13.96	3.44	0.25	100.32	68.14	30.40	1.46
Lajinha dyke	Core	50.63	31.30	0.60	14.88	2.90	0.18	100.49	73.15	25.82	1.02
Lajinha dyke	Rim	51.56	30.17	0.66	14.01	3.31	0.25	99.96	69.04	29.47	1.48
Lajinha dyke	Rim	53.95	28.15	1.05	12.06	4.30	0.39	99.90	59.37	38.34	2.29
Lajinha dyke	Rim	51.81	30.02	0.83	13.65	3.49	0.25	100.05	67.34	31.18	1.47
Lajinha dyke	Rim	50.85	30.70	0.68	14.60	3.03	0.20	100.05	71.86	26.97	1.17
Lajinha dyke	Rim	49.54	30.00	2.08	14.33	2.75	0.21	98.91	73.27	25.47	1.26
Lajinha dyke	Rim	53.76	29.40	0.73	12.76	4.10	0.33	101.09	62.01	36.05	1.93
Lajinha dyke	Core	51.65	30.38	0.38	13.99	3.31	0.24	99.94	69.07	29.54	1.40
Lajinha dyke	Core	48.06	32.88	0.46	16.88	1.91	0.11	100.30	82.49	16.86	0.65
Lajinha dyke	Core	53.60	29.30	0.43	12.80	4.18	0.32	100.63	61.69	36.48	1.83
Lajinha dyke	Rim	53.63	29.08	0.35	12.50	4.01	0.34	99.90	61.99	36.02	1.98
Lajinha dyke	Rim	51.78	29.64	0.71	13.20	3.57	0.26	99.16	66.13	32.35	1.52
Lajinha dyke	Rim	52.50	29.29	0.85	12.99	3.74	0.30	99.66	64.56	33.64	1.80

Lajinha dyke	Core	50.72	30.72	0.62	14.59	3.02	0.19	99.87	71.95	26.95	1.10
Lajinha dyke	Core	53.20	29.29	0.40	12.68	3.92	0.31	99.79	62.98	35.20	1.82
Lajinha dyke	Core	51.35	30.31	0.62	14.29	3.15	0.20	99.92	70.62	28.19	1.19
Lajinha dyke	Core	51.09	30.26	0.80	14.07	3.14	0.21	99.57	70.31	28.42	1.27
Lajinha dyke	Rim	51.01	30.95	0.45	14.53	3.13	0.20	100.28	71.10	27.71	1.19
Lajinha dyke	Rim	52.16	28.89	1.29	13.07	3.69	0.30	99.40	65.02	33.20	1.78
Lajinha dyke	Core	52.03	29.43	1.02	13.48	3.61	0.28	99.84	66.28	32.10	1.62
Lajinha dyke	Core	53.77	28.91	0.87	12.58	3.93	0.33	100.39	62.63	35.44	1.93
Lajinha dyke	Rim	52.45	28.81	0.90	12.84	3.82	0.30	99.13	63.83	34.37	1.80
Santa Angélica dyke	Rim	55.70	27.57	0.09	10.25	5.77	0.10	99.49	49.24	50.18	0.58
Santa Angélica dyke	Core	55.72	27.18	0.24	9.70	5.77	0.14	98.74	47.79	51.39	0.82
Santa Angélica dyke	Core	56.10	27.12	0.23	9.63	5.89	0.14	99.11	47.08	52.11	0.81
Santa Angélica dyke	Core	55.53	27.39	0.30	10.01	5.64	0.29	99.17	48.67	49.63	1.70
Santa Angélica dyke	Core	54.98	27.55	0.35	10.11	5.57	0.32	98.88	49.14	49.00	1.85
Santa Angélica dyke	Core	55.66	27.76	0.01	10.27	5.50	0.13	99.33	50.41	48.81	0.78
Santa Angélica dyke	Core	55.54	27.99	0.09	10.54	5.47	0.13	99.75	51.19	48.07	0.74
Santa Angélica dyke	Rim	57.23	26.54	0.14	8.78	6.40	0.12	99.21	42.82	56.47	0.70
Santa Angélica dyke	Rim	59.08	25.40	0.08	7.32	7.20	0.11	99.19	35.75	63.63	0.63
Santa Angélica dyke	Core	55.99	27.71	0.08	9.85	5.39	0.51	99.53	48.74	48.24	3.02
Santa Angélica dyke	Core	55.95	27.67	0.04	8.75	6.26	0.16	98.82	43.18	55.89	0.92
Santa Angélica dyke	Core	55.97	27.46	0.22	10.09	5.78	0.12	99.64	48.74	50.55	0.71
Santa Angélica dyke	Core	55.04	27.98	0.06	10.69	5.27	0.10	99.15	52.52	46.87	0.61
Santa Angélica dyke	Rim	58.36	25.58	0.16	7.86	6.96	0.12	99.04	38.15	61.18	0.67
Santa Angélica dyke	Rim	58.79	25.78	0.10	7.80	7.01	0.13	99.60	37.80	61.46	0.74
Santa Angélica dyke	Core	56.55	26.85	0.33	9.28	6.24	0.16	99.41	44.71	54.38	0.91
Santa Angélica dyke	Core	57.83	27.00	0.07	8.49	6.60	0.15	100.14	41.22	57.93	0.85
Santa Angélica dyke	Core	56.95	26.81	0.03	9.16	6.15	0.14	99.22	44.79	54.41	0.80
Santa Angélica dyke	Rim	58.41	25.70	0.14	8.17	6.75	0.19	99.36	39.64	59.29	1.07
Santa Angélica dyke	Rim	59.13	24.86	0.10	7.60	7.39	0.12	99.20	35.97	63.34	0.69
Santa Angélica dyke	Rim	58.58	26.24	0.13	7.93	6.83	0.11	99.81	38.83	60.52	0.65

Santa Angélica dyke	Rim	58.19	26.69	0.16	8.56	6.55	0.12	100.27	41.62	57.66	0.72
Santa Angélica dyke	Core	55.44	26.58	0.07	8.75	6.40	0.15	97.39	42.69	56.46	0.84
Santa Angélica dyke	Core	57.71	25.95	0.11	8.23	6.39	0.48	98.87	40.41	56.78	2.81
Santa Angélica dyke	Core	58.58	26.27	0.11	7.91	6.92	0.17	99.95	38.34	60.67	0.99
Santa Angélica dyke	Core	58.81	25.62	0.23	7.54	7.02	0.12	99.34	36.98	62.32	0.70
Santa Angélica dyke	Rim	59.46	25.31	0.31	7.23	7.25	0.11	99.68	35.31	64.03	0.66
Santa Angélica dyke	Rim	58.29	25.96	0.09	8.16	6.73	0.14	99.36	39.80	59.40	0.80
Santa Angélica dyke	Rim	58.76	25.47	0.06	7.79	7.01	0.12	99.20	37.78	61.53	0.69
Santa Angélica dyke	Core	55.25	26.23	0.12	8.82	7.46	0.60	98.48	38.32	58.59	3.09
Santa Angélica dyke	Core	57.27	26.08	0.08	8.38	6.60	0.21	98.61	40.74	58.02	1.24
Santa Angélica dyke	Core	57.53	26.22	0.06	8.19	6.74	0.26	99.00	39.56	58.94	1.50
Santa Angélica dyke	Rim	59.58	25.38	0.14	7.30	7.37	0.09	99.86	35.18	64.29	0.53
Santa Angélica dyke	Rim	57.39	26.33	0.09	8.43	6.60	0.14	98.98	41.03	58.17	0.80
Santa Angélica dyke	Core	58.47	25.88	0.06	7.94	6.83	0.14	99.33	38.78	60.41	0.80
Santa Angélica dyke	Core	57.96	26.08	0.11	8.08	6.77	0.15	99.15	39.38	59.74	0.88
Santa Angélica dyke	Rim	59.18	25.09	0.11	7.12	7.49	0.29	99.28	33.88	64.47	1.65
Santa Angélica dyke	Rim	58.62	25.38	0.38	7.30	7.23	0.14	99.06	35.51	63.66	0.82
Santa Angélica dyke	Core	58.79	25.65	0.11	7.51	7.30	0.18	99.54	35.87	63.09	1.04
Santa Angélica dyke	Core	58.47	26.17	0.13	8.12	6.83	0.14	99.86	39.34	59.87	0.79
Santa Angélica dyke	Core	57.05	26.72	0.27	8.64	6.31	0.13	99.11	42.74	56.47	0.78
Santa Angélica dyke	Rim	58.93	25.68	0.10	7.67	7.19	0.14	99.70	36.81	62.41	0.77